# Corrosion Detection in Oil and Gas Pipeline Using 3-D Bluetooth Enabled Printed Microsensor

By

Stephen Ato Appiah

Submitted in Partial Fulfillment of the Requirements

for the Degree of

Master of Science Engineering

in the

Chemical Engineering

YOUNGSTOWN STATE UNIVERSITY

December 2023

**Corrosion Detection In Oil And Gas Pipeline Using 3-D Bluetooth Enabled Printed Microsensor**

Stephen Ato Appiah

I hereby release this thesis to the public. I understand that this thesis will be made available from the OhioLINK ETD Center and the Maag Library Circulation Desk for public access. I also authorize the University or other individuals to make copies of this thesis as needed for scholarly research.

Signature:

_____

*Stephen Ato Appiah,* Student Date

Approvals:

_____

*Dr. Holly Martin*, Thesis Advisor Date

_____

*Dr. Pedro Cortes*, Committee Member Date

_____

*Dr. Vamsi Borra*, Committee Member Date

_____

*Dr. Salvatore A. Sanders*, Dean of Graduate Studies Date

**Abstract**

Corrosion is a huge economic and environmental concern for metal applications. Detecting and monitoring corrosion are imperative to prolong material life span, decrease the life-cycle cost, and reduce environmental impact. There are various methodologies for corrosion detection and monitoring which include, but are not limited to, ultrasonic, fiber optics, acoustics, and thermal imaging. These corrosion detection techniques exploit changes in structural, chemical, mechanical, thermal, electrical, and magnetic properties of metals to detect corrosion and calculate corrosion rate. This project focuses on developing a 3-D printed Bluetooth microsensor to detect corrosion in steels used for oil and gas pipeline. In this thesis, AD5941 microsensor was used to detect the changes in impedance of the metal caused by corrosion. This microsensor would later be modified to YSUTag microcontroller. The study also considered the effect of metal size and orientation on impedance reading. The investigation revealed that the difference in sizes and orientation of metal had little to no impact of the impedance reading. Through the use of the microsensor, both uniform and localized corrosion can be detected, allowing for the understanding of the life-span and prevention of environmental damages.

## Acknowledgments

I am exceptionally grateful and appreciative to the following people who have helped me through this journey.

Funding for the project provided by
*Dr. Pedro Cortes*

Thesis advisor for golden opportunity to do these amazing projects
*Dr. Holly J. Martin*

Project also advised by
*Dr. Vamsi Borra*

Impedance measurement and data analysis supported by
*Brendan M Kuzior and Josh Porter*

Special Thanks
*To my parents for their support, my brothers, for being by my side through tough times, and my friends for standing in me and supporting my aspirations.*

**Table of Content**

**List of Figures**

**List of Tables**

# 1 Chapter 1 Introduction

Corrosion is “the deterioration of materials when they interact with their environment”. Corrosion is a global phenomenon because the losses caused by corrosion are enormous, and it has a negative impact on the economies of organizations, in particular, and countries, in general [1]. Metallic pipes carrying water, oil, or gas are vulnerable to corrosion, which causes degradation, leaks or bursts, and failures. A good corrosion prevention strategy can keep these metallic pipelines from corroding, especially in harsh settings and corrosive soils [2]. Extensive research has been conducted to bring out solutions to control and mitigate corrosion and its effects. The various methodologies for corrosion detection and monitoring may include ultrasonic, fiber optics, acoustics, or thermal imaging. However, there are challenges with the method of application of these techniques, the metal geometry, the metal thickness, and employee’s time consumption, which are also other concerns for using these applications [3], [4], [5]. Therefore, to effectively control corrosion, modern devices should possess the ability to detect corrosion at early stages, without being limited by the challenges listed above. This chapter introduces the fundamentals of oil and gas pipeline corrosion, discusses the major corrosion techniques and challenges, highlights the main contribution of the study conducted in this thesis, outlines the thesis organization, and concludes with closing remarks.

## 1.1 Corrosion of Metal pipeline

This section introduces the fundamentals of corrosion. First, a definition and factors that influence corrosion is examined. Second, the various classifications of corrosion and how they occur are provided. Third, corrosion of oil and gas pipelines and its effect is also presented. Forth, types of corrosion monitoring and detection technique and their limitations are covered.

### 1.1.1 What is corrosion?

Corrosion is the erosion of material qualities caused by interactions with their surroundings, and corrosion of most metals (and many other materials) is unavoidable. All material types are subject to corrosion, even though the deterioration is most commonly associated with metallic materials. For example, besides metals, there is the deterioration of polymeric insulating coating on wiring of aged aircraft. Also, there is the degradation of ceramics through selective dissolution. Occurrence and progression of corrosion is due to the randomness of its process. Nature permits materials to remain in their lowest possible energy state (or most stable state), hence most metals/alloys corrode (combine with water/oxygen present in the environment) to achieve this lowest energy condition [4]. The basic reason or driving force behind all corrosion is a decrease in a system's Gibbs energy. In practical terms, all metals (and metal-based engineering components) are produced by adding energy to the system. As a result of this uphill thermodynamic fight, the metal feels compelled to revert to its native, low energy oxide state [5]. Even though the return to the native oxide state of the metal is unavoidable, significant impediments (corrosion management strategies) can be applied to delay its progress toward the

equilibrium state. As a result, the rate of approach to equilibrium is frequently of importance. This rate is determined not just by the nature of the metal surface, but also by the nature of the environment and how both evolve [6].

Most corrosion processes require at least two electrochemical reactions to occur (one anodic and one cathodic). A deteriorating surface can be compared to a short-circuited battery; the dissolution reaction at the anode generates electrons for the reduction reaction at the cathode. A short circuit is an electrical connection created by a conductor between two physical locations that are frequently separated by relatively short distances [6]. Thus, electrochemists investigating batteries, fuel cells, and physical and analytical electrochemistry employ many of the same methods to analyze corrosion processes. Wagner and Traud originally presented the application of mixed potential theory to corrosion, which was then discussed later by Petroceli in the Electrochemical Society. The shape of polarization curves were then theoretically analyzed by Stern and Geary, in 1957, creating the basis of the primary experimental technique , known as electrochemical polarization, currently used in electrochemical studies of corrosion [6].

*Figure 1.1. Example of corroded surfaces [103]*

### 1.1.2 The Chemistry of Corrosion

Corrosion is characterized as the degradation of a component stemming from its interactive reactivity with the surrounding environment (Figure 1.1). Upon metal encountering a corrosive liquid, an electrochemical process initiates, involving electron movement across the interface of metal and liquid. The conservation of energy is evident as metals revert to their initial state, with the energy driven corrosion originating from the transformation of ores into metals. This transformational energy is termed as Gibb's free energy. As an atom departs from a metal's crystal arrangement, it surpasses the binding forces uniting atoms within the crystal structure. Surface atoms encounter weaker attractive forces than those deeper within the material. Large temperature elevation can prompt surface atoms to depart from the structure, relinquishing their electrons [7]. This accounts for why, in a corrosive media, there is rapid corrosion when temperature increases. The equation of an oxidation reaction is:

$$M_{(s)} \rightarrow M^{n+} + ne^{-}$$

Where 'M' is metal and 'n' is the number of electrons left by the metal atom on the bulk metal.

Atoms instantly transform into ions in liquid after leaving the metal surface. As other metal atoms dissolve subsequently, converting into ions, the overall weight of the material decreases. The metal ion engages with the dissolved oxygen within the liquid, resulting in the creation of metal oxide. Frequently, the corrosive environment remains static, allowing the oxide product to accumulate on the corroded surface. In the case of iron, the oxide produced is commonly referred to as 'rust', which is specifically $Fe_2O_3$ [8]. The oxidation and reduction process is depicted in Figure 2. Although corrosion might appear to follow a standard pattern, various corrosion forms

emerge due to localization, the corrosive environment's nature, and the metal's inherent chemistry. Corrosion is not confined to specific electrodes, as it can manifest on a micro scale. Multiple anodic and cathodic sites often emerge on a single surface, where oxidation and reduction reactions occur [8].

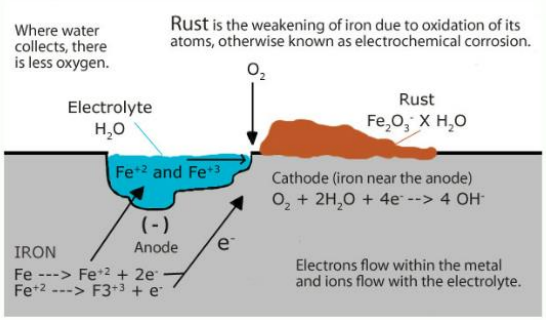


*Figure 1.2. Mechanism of iron corrosion to produce rust [104].*

### 1.1.3 Effects of Corrosion

Corrosion is harmful to structural materials and, from time to time, even causes catastrophic failures, resulting in enormous monetary loss, as well as loss of lives. Researchers all over the world have conducted substantial research to better understand the process of corrosion phenomena, as well as the corrosion resistant qualities of various metals and alloys, in order to employ them for various applications [1]. They have made concurrent efforts to control corrosion by producing superior alloys, adjusting the microstructure of the alloys, applying corrosion resistant coatings, and/or changing the surroundings. Their ultimate goal is to extend the service life of materials as much as possible. All of these measures are targeted at reducing the impact of corrosion. Some of the major harmful effects of corrosion are as follows:

- Serious injuries or fatalities as a result of structural collapse or breakdown (e.g., aircraft, automobiles, bridges, etc.).
- Metal thickness reduction, leading to mechanical integrity loss and structural failure or disintegration of metallic components.
- Additional spending on corroded component maintenance and redesigning corrosion-resistant equipment.
- Financial losses as a result of industrial plant shutdowns and economic losses as a result of fluid pollution caused by vessel deterioration.
- Metal surface qualities (electrical conductivity, surface reflectance, ease of fluid movement on the surface, and so on) are lost.
- Pipeline leakage resulting in the release of harmful chemicals into the environment.

According to National Association of Corrosion Engineers (NACE) International Measures of Prevention Application, and Economics of Corrosion Technology (IMPACT) report, the global cost of corrosion has climbed to $2.5 trillion, or 3.4% of global GDP. The global cost of corrosion statistics published by NACE is shown in Table 1.1.

***Table 1.1 Global corrosion costs (in billions of dollars) (© NACE International)*** *[copied from 9].*

| Economic Regions | Agriculture CoC US $ Billions | Industry CoC US $ Billions | Services CoC US $ Billions | Total CoC US $ Billions | Total GDP US $ Billions | CoC % GDP |
|---|---|---|---|---|---|---|
| United States | 2.0 | 303.2 | 146.0 | 451.3 | 16,720 | 2.7% |
| India | 17.7 | 20.3 | 32.3 | 70.3 | 1,670 | 4.2% |
| European Region | 3.5 | 401 | 297 | 701.5 | 18,331 | 3.8% |
| Arab countries | 13.3 | 34.2 | 92.6 | 140.1 | 2,789 | 5.0% |
| China | 56.2 | 192.5 | 146.2 | 394.9 | 9,330 | 4.2% |
| Russia | 5.4 | 37.2 | 41.9 | 84.5 | 2,113 | 4.0% |
| Japan | 0.6 | 45.9 | 5.1 | 51.6 | 5,002 | 1.0% |
| Four Asian Tigers + Macau | 1.5 | 29.9 | 27.3 | 58.6 | 2,302 | 2.5% |
| Rest of the World | 52.4 | 382.5 | 117.6 | 552.5 | 16,057 | 3.4% |
| Global | 152.7 | 1,446.7 | 906.0 | 2,505.4 | 74,314 | 3.4% |

From the Table 1.1, it could be deduced that immense industrial growth is the reason behind the huge economic losses due to corrosion in regions like the United States, the European Region, China, and other countries. The biggest expense is usually due to structural component damage in industries, as shown in Figure 1.3, regular replacement of damaged metallic components, and industrial downtime, among other things. Other indirect economic losses caused by corrosion include loss of efficiency, pollution, ejection or unwanted failure of machinery, and loss of production during plant downtime. Additionally, human lives lost in incidents induced by corrosion, such as pipeline damage or burst boilers, are always beyond interpretation in terms of

money [9]. Corrosion costs India, which has a GDP of around $2 trillion, up to $100 billion every year. Listed are some recent unfortunate incidents around the world that occurred due to corrosion.

*Figure 1.3. Typical examples of corrosion [105][106][107][108].*

On 20 April 2010, the Deepwater Horizon exploded after oil leaked for about 87 days, 11 people were believed to have died and 17 people treated for injuries. Investigation revealed that pitting corrosion was the main cause of the leakage [10][11]. A 50-foot-tall high-pressure crystal production vessel exploded in 2009 at the NDK Crystal manufacturing factory in Belvidere, Illinois, wounding bystanders and killing a trucker at a nearby petrol station. This incident occurred as a result of stress corrosion cracking in the wall. The Donghuang II oil pipeline exploded near Qingdao, eastern China, on November 22, 2013, and was caused by pitting corrosion. On May 20, 2000, while hundreds of NASCAR spectators were leaving a stock car race and crossing a pedestrian bridge out of the Charlotte motor speedway, an 80-foot portion of the concrete and steel walkway snapped in half. Pedestrians plummeted 17 feet to the freeway below, with 107

persons injured. This was resulted from a stress corrosion cracking of the concrete. El Paso Natural Gas's 30-inch natural gas pipeline exploded on August 19, 2000, causing an 86-foot-long, 46-foot-wide, and 20-foot-deep crater. This was caused by the internal corrosion of the pipeline. The 1,200-degree fireball killed twelve people. These incidents demonstrate unequivocally that corrosion has proven to be catastrophic on numerous occasions, claiming human lives. All of these catastrophes were caused by pipeline or structural failure due to corrosion.

### 1.1.4 Classification of Corrosion

Corrosion is categorized in several ways, including low-temperature corrosion and high-temperature corrosion. It is further divided into two types: wet corrosion and dry corrosion [1]. Uniform or general corrosion is the most common type of corrosion. Uniform corrosion is a type of corrosion that happens equally across the surface of a metal substrate. When a protective coating or barrier film on a metal structure fails, uniform corrosion occurs. Corrosion has traditionally been categorized into eight types based on the morphology of the attack, as well as the type of environment to which the material is exposed [12]. Uniform corrosion causes metal thinning as a result of chemical or electrochemical processes on the metal surface. It initially affects the surface, eventually causing it to fail. Because it is a type of corrosion that is predictable, controllable, and avoidable, it is frequently seen as a safe form of corrosion. Uniform corrosion is the most common types of corrosion. It can be protected using methods such as cathodic protection, anodic protection, and paint application.

Localized corrosion is an unsafe form of corrosion because it is very difficult to spot and happens usually without any warning. Localized corrosion usually happens at selective sites on the metal substrate. Compared to uniform corrosion, it causes severe deterioration of metal. Corrosion activity at localized areas is influenced by a variety of elements such as exposure time, defects in barrier coatings, and electrolyte change. The following types of localized corrosion have been identified.

#### *1.1.4.1 Uniform corrosion*

Uniform corrosion is normally distinguished by a chemical or electrochemical reaction, which spreads uniformly over the entire surface exposed. On a tonnage basis, uniform attack or general over-all corrosion characterizes the greatest destruction of metal. The metal becomes thinner and eventually fails. From the technical standpoint, this form of corrosion is not of too great a concern, because the life of equipment can be precisely calculated based on comparatively simple tests or experience [13].

#### *1.1.4.2 Pitting corrosion*

Pitting is probably the most damaging and insidious form of corrosion; containers fail due to perforation, but only a small amount of metal is lost in the total structure. Due to the small size of the pits, as shown in Figure 1.4, it is quite problematic to forecast and, sometimes, corrosion

products may cover the pits. Pitting causes modest weight loss in the metal substrate but can lead to the structure failing completely.

*Figure 1.4. Pitting corrosion [108].*

#### *1.1.4.3 Crevice corrosion*

Crevice corrosion normally occurs adjacent to the space or crevice between two metal surfaces joining. It usually happens in engineering structures like below flanges, as shown in Figure 1.5, in between bolts or nuts, or under rivets, but can also occur under deposits, such as sand or dirt [1]. It is considered a special type of pitting, with the geometry of the crevice. It results when shielded portions on the metal surface are exposed to corrosive environment. The shielded portion has a narrow opening, just enough to allow entering of the solution, but prevents the escape of the solution. Factors like pH, constituent's concentration, and variation of oxygen concentration affect initiate crevice corrosion.

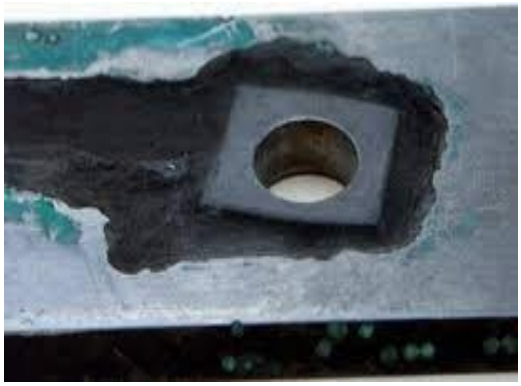

*Figure 1.5. crevice corrosion [109]*

#### *1.1.4.4 Erosion Corrosion*

Accelerated corrosion of metals and alloys due to the movement of corrosive fluids against the surface of the metal or alloy is referred to as erosion corrosion. When the fluid flows turbulently, it can lead to the removal of material from the inner surface of pipes or tubes, as Shown in Figure 1.6, causing erosion that may eventually result in leakage. This corrosion attack may happen due to poor internal design of component. Protruding inclusions can cause laminar flow to be perturbed. Consequentially, localized regions on the inner surface being hit by high-velocity fluid can start erosion corrosion [14].

*Figure 1.6. Erosion Corrosion on Inner Surface of an Elbow Pipe [110].*

### 1.1.4.5 Galvanic Corrosion

Galvanic corrosion occurs when two metals with distinct electrochemical properties are in close proximity, as shown in Figure 1.7, establishing an electrical connection, and then both metals are also in contact with an electrolyte. The driving force behind this form of corrosion arises from the potential difference generated between these dissimilar metals. The more active metal becomes the anode and corrodes faster. The less active, or noble, substrate acts as the cathode and corrodes slower. The ions are transferred from anode to cathode via the electrolyte. Most of the bimetallic corrosion takes place in marine environments, primarily because saltwater functions effectively as an electrolyte in these cases. Galvanic corrosion is influenced by the placement of the metal on the galvanic series. Therefore, opting for metals positioned closely to each other within the galvanic series can reduce the impact of galvanic corrosion [15].

*Figure 1.7. Galvanic corrosion of two dissimilar metal [111].*

### 1.1.4.6 Selective Leaching

Selective leaching involves the corrosion-driven removal of a specific element from a solid alloy. An illustrative instance is the preferential elimination of zinc from brass alloys, a phenomenon

termed dezincification. Comparable processes are observed in diverse alloy systems, including the extraction of aluminum, iron, cobalt, and chromium. Employing the term "selective leaching" encompasses these procedures, negating the need for designations like dealuminumification or decobaltification [13].

#### *1.1.4.7 Intergranular Corrosion*

Intergranular corrosion represents a distinct type of corrosion typically observed along the edges of grains or adjacent to these boundaries, as shown in Figure 1.8. Intergranular corrosion primarily arises due to the development of precipitates and the separation of materials within the particular zone near grain boundaries [13]. Intergranular corrosion is typically limited to a small region; however, in certain instances, it can lead to the complete detachment of the entire grain due to the complete breakdown of boundaries. This corrosion significantly impacts the mechanical characteristics of the metal substrates. An illustrative instance of intergranular corrosion involves the sensitization of stainless steels or the decay of welded joints [13].

*Figure 1.8. Intergranular corrosion of two dissimilar metal [112]*

#### *1.1.4.8 Stress Corrosion*

Stress corrosion cracking emerges from the synergistic impact of corrosive surroundings and tensile stress, as shown in Figure 1.9. This form of cracking can be prompted by either external or internal stresses [13]. Its frequently manifests in regions subjected to elevated stress levels, including pressure vessels, bends in pipelines, and subterranean reactors. Besides metals, materials such as ceramics, pristine substances, and polymers are prone to stress-induced cracking in specific corrosive settings. Corrosive environments triggering such cracking primarily involve highly reactive corrosive ions like chloride ions ($Cl^-$) and ammonia ($NH_3^-$) in the medium [1].

*Figure 1.9. Stress corrosion cracking [103]*

## 1.2 Objectives

All the various forms of localized corrosion can be difficult to detect, resulting in potentially catastrophic failure. The purpose of this study is to create a 3-D printed Bluetooth microsensor to detect corrosion in steels used for oil and gas pipelines. The microsensor will detect the changes in electric properties of the metal caused by corrosion, including resistance, impedance, magnetic permeability, and magnetorestriction. The microsensor could also be used to measure

environmental conditions, like temperature and humidity. Through the use of the microsensor, both uniform and localized corrosion can be detected, allowing for the understanding of the lifespan of the metal and the prevention of environmental damages. The objective of this corrosion study is to determine how the microsensor performs. Two different phases were created. The first used two different thicknesses of metal, with the metal exposed to four different corrosive environments. From there, the two most corrosive environments were utilized to determine how the geometry of the metal affects the detection of corrosion behavior. For this study, only impedance was considered when using the microsensor. Weight loss and surface analysis with a Keyence microscope where also considered to detect the presence of corrosion. The project steps are simplified as follows:

- Weight measurement of 4140 stainless steel metal specimen
- Using Keyence Profilometer V-5000, surface analysis of each specimen is performed before corrosion.
- With the help of epoxy, copper wire lead is connected to the metal specimen, the lead makes it easy to measure impedance with the microsensor.
- Initial impedance is measured and then specimen is exposed to the corrosive environment.
- Every week, the impedance of each sample is measured to monitor the presence of corrosion. The process is repeated for eight weeks.

## 1.3 Organization

The thesis is divided into several chapters, including:

- Chapter 1, this chapter, provides a brief introduction to the project, objective, and scope of this project.
- Chapter 2 contains the similar research related to different approach in detecting or monitoring the presence of corrosion in oil and gas pipeline.
- Chapter 3 discusses the materials and methods used.
- Chapter 4 presents the results obtained and the corresponding discussion.
- Chapter 5 summarizes the conclusion and provides future recommendations.

## 1.4 Scope of work

The aim of this project is to test if the impedance measurement with the sensor is affected by metal thickness or orientation. To test this, 4140 steel was corroded in four different environments, namely under a NaCl solution, immersed in a NaCl solution then dried, placed over a NaCl solution, and buried under wet dirt. All environments were then covered to prevent evaporation. The outside environment was in the lab setting, at room temperature. Several tests were conducted to make comparisons, and a suitable frequency for consistent impedance measurement was chosen. Impedance measured with the sensor was displayed on Sensopal. After choosing the two most corrosive environments, three pipe samples were used for each selected environment at a time, and the specimens were again covered to prevent water loss.

Initial and final weights of the samples were recorded and compared to detect metal loss as evidence of corrosion. Also, initial and final imaging from the Keyence profilometer was used for surface analysis as evidence of corrosion.

# 2 Chapter 2 Literature Review

## 2.1 Corrosion of Oil and Gas Pipeline

Corrosion increases in watery environments, which can exist in a variety of complex situations during oil and gas production and processing. These conditions can also be seen in pipeline systems and transportation facilities. Three important components make up the corrosion process [16]. First, there is the anode, which depicts the position where the metal corroded. Second, the electrolyte, which is often a corrosive substance, is responsible for transferring electrons from the anodic to the cathodic sites [16]. The third component is the cathode, which is an electrical conductor that is not consumed throughout the corrosion process.

There are severe corrosion-related consequences that continue to plague the worldwide oil and gas industry. Natural gas and crude oil typically include a high concentration of corrosive contaminants. These contaminants in the oil and gas industry may include free water, hydrogen sulfide ($H_2S$), and carbon dioxide ($CO_2$). Internal surfaces of oil and gas pipelines exposed to water, $H_2S$, and $CO_2$ are prone to corrosion [16]. Furthermore, fittings and lines may degrade as a result of changing fluid compositions and operating conditions, such as temperature and pressure. Metal deterioration is frequently followed by a loss of mechanical qualities, such as ductility and strength. As a result, materials and thicknesses deplete and eventually fail [16].

Mild steel is often utilized for the building of pipelines used in the natural gas sector for economic reasons, as it is cheaper to produce. However, when compared to other forms of steel, this type of steel often has a lower corrosion resistance. Natural gas extracted from a reservoir may be contaminated with organic acids, oil, hydrogen sulfide ($H_2S$), carbon dioxide ($CO_2$), and water.

These ingredients generate an extremely hostile environment that induces corrosion, increasing mild steel corrosion rates, causing it to deteriorate faster [17].

Corrosion is currently one of the most difficult unresolved challenges in many sectors. Corrosion has caused billions of dollars in losses in several industrial disasters. According to research from around the world, some oil pipelines ruptured due to corrosion, resulting in an oil spill and environmental degradation [17]. This was associated with resource depletion, costly oil clean-up, and widespread environmental harm. All industrial designs must address the consequences of corrosion on the equipment's lifespan. Because of the repercussions of corrosion, mechanical, chemical, and petroleum engineers have begun to evaluate the corrosion influence on the chemistry of their chosen processes, as corrosion can disrupt any reaction and its products [17].

Oil product contamination by corrosion products occurs in oil refineries as refineries age. Pipelines carrying refined and crude oil that include sulfur compounds are similarly vulnerable to corrosion, as shown in Figures 2.1 and 2.2. Oil reservoirs and containers are also vulnerable to corrosive effects, due to pressure and heat exchange variations in petroleum products. To prevent localized corrosion in oil and gas pipelines, it is critical to identify and comprehend the mechanisms and conditions that govern the initiation and progression of this form of corrosion [19].

*Figure 2.1. Internal corrosion of pipeline [120].*

*Figure 2.2. External corrosion of pipeline [121].*

## 2.2 Internal Corrosion of Pipeline.

Carbon dioxide corrosion, often known as sweet ($CO_2$) corrosion, is a kind of corrosion that commonly occurs on the inside surfaces of oil and gas pipelines. This type of corrosion may also occur in the presence of corrosive hydrogen sulfide ($H_2S$), also known as sour corrosion, and organic acids. $CO_2$ corrosion is caused by an electrochemical interaction between carbon steel and aqueous $CO_2$.

### 2.2.1 Mechanism of sweet (CO2) corrosion.

There are three major steps of the sweet corrosion mechanism, as shown in Table 2.1. The first step is the hydration of carbon dioxide gas. The second step is a cathodic reduction, which involves non-scaling and scaling. The third step is anodic oxidation [20,21]. The anodic process dissolves the iron, while the cathodic reaction produces hydrogen. The reaction leads to the formation of $FeCO_3$ scales. Depending on the conditions of the habitat in which the scales are generated, these scales may be protective or non-protective to the surface. The primary anodic and cathodic reactions that occur on steel surface due to $CO_2$ corrosion is shown in Table 2.1.

**Table 2.1. Major anodic and cathodic reaction mechanism of $CO_2$ corrosion occurring on steel surface [120].**

| **Name** | **Reaction** | **Eq.** |
|---|---|---|
| Hydration of $CO_2$(g) | $CO_{2(g)} + H_2O_{(l)} \leftrightarrow H_2CO_{2(aq)}$ | 1 |
| Cathodic reduction non-scaling | $2H^+_{(aq)} + 2e^- \rightarrow H_{2(g)}; (pH < 4)$<br>$2H_2CO_{3(aq)} + 2e^- \rightarrow H_{2(g)} + 2HCO^-_{3(aq)}; (pH4 - 6)$ | 2-a<br>2-b |
| Cathodic reduction scaling | $2HCO^-_{3(aq)} + 2e^- \rightarrow H_{2(g)} + 2CO_{2(g)}; (pH \geq 6)$ | 2-c |
| Anodic oxidation | $Fe_{(s)} \rightarrow Fe^{2+}_{(aq)} + 2e^-$ | 3 |

Many studies have been conducted on the factors that influence the rate of sweet corrosion in oil and gas pipelines [22-24]. Several factors, including physical, environmental, and metallurgical, influence the underlying mechanism of sweet corrosion, which is a multiple step process [25]. The most common factors, such as the effect of oxygen concentration [26,27], $CO_2$

partial pressure [28], iron content [29], temperature effect [30], pH of the environment [31], and the effect of flow [32], are listed and briefly discussed.

### 2.2.2 Mechanism of sour corrosion

Hydrogen sulfide ($H_2S$) corrosion, also known as sour corrosion, is a common type of corrosion that occurs on the inside surfaces of oil and gas pipelines. When hydrogen sulfide ($H_2S$) dissolves in water, this type of corrosion develops. According to the oil and gas sector, more than 950,000 wells, or up to one-third of all oil wells, are sour [33]. The first occurrence of sour corrosion was documented in oil wells in Louisiana and Texas in 1940 [34]. Since then, sour corrosion has been an issue in various oil fields across the world.

The mechanism of sour corrosion on steel surfaces consists of two major processes: (i) anodic corrosion on the steel surface and (ii) cathodic reduction reaction of aqueous $H_2S$, as shown in Table 2.2. The development of FeS scales is the end result of the sour corrosion mechanism. Depending on the concentration of $H_2S$, temperature, and pressure of the solution, these scales take on varied shapes and morphologies. Under the deposits, corrosion can occur as a result of the sort of scales created by iron sulfide. This is a sort of localized corrosion in an oil and gas well's internal pipeline [35].

**Table 2.2. Major cathodic and anodic reaction mechanism of sour corrosion occurring on steel surface [120].**

| Name | Reaction | Eq. |
|---|---|---|
| Cathodic reduction | $H_2S_{(g)} + e^- \leftrightarrow H^+{}_{(aq)} + HS^-{}_{(aq)}$ | 4-a |
| | $HS^-{}_{(aq)} + e^- \rightarrow H^+{}_{(aq)} + s^{-2}{}_{(aq)}$ | 4-b |
| Anodic oxidation | $Fe_{(s)} \rightarrow Fe^{2+}{}_{(aq)} + 2e^-$ | 5 |
| Overall Reaction | $Fe_{(s)} + H_2S_{(g)} \rightarrow FeH_{(s)} + H_{2(g)}$ | 6-a |
| | $Fe_{(s)} + H_2S_{(g)} \rightarrow FeS_{1\_x(s)} + H_{2(g)}$ | 6-b |

Several elements have been identified as influencing the pace and behavior of sour corrosion in oil and gas pipelines [34]. Temperature, pressure, hydrogen sulfide concentration and dissociation, nature of metal surface deposits (wax, scales, and corrosion products), duration, steel types, flow velocity, oxygen access, ethanoic acid and sodium chloride, and fluid chemistry (water cut, pH, oil wettability, phase ratios, and organic acid) are among these factors, as shown in Table 2.3. All of these variables have an effect on sour corrosion. However, it is thought impossible to comprehend the impact of each individual element on $H_2S$ corrosion. More details on the elements influencing sour corrosion can be found elsewhere [36].

**Table 2.3. The factors affecting sour corrosion [copied from 120].**

| Factors | Remarks | Reference |
|---|---|---|
| Oxygen Concentration | A high level of oxygen (< than 40 ppb) leads to oxidizing ferrous ions ($Fe^{2+}$) to ferric ions ($Fe^{3+}$) because it interrupts the stability of the $FeCO_3$ layer. The rate of cathodic reaction increases with oxygen, since it is a strong oxidizer in the aerobic condition and the $FeCO_3$ layer is not stable. | 26,27 |
| Effect of $CO_2$ Partial Pressure | Increasing carbon dioxide partial pressure increases the rate of corrosion. On the contrary, carbonate layer formation decreases the rate of the corrosion. Higher $CO_2$ partial pressure means more $CO_2$ and consequently, the carbonic acid concentration in the solution is increased. | 28 |
| Iron content | The solubility limit of ferrous ion ($Fe^{2+}$) and carbonate ion ($CO_3^{2-}$) play a major role in the formation of the film of $FeCO_3$. | 29 |
| Temperature Effect | Higher temperature increases $CO_2$ partial pressure, which in turn increases the rate of corrosion. Higher $CO_2$ partial pressure means more $CO_2$ and consequently, the carbonic acid concentration in the solution is increased. | 30 |
| pH of the Environment | In general, increase in the pH decreases the rate of sour corrosion and vice versa. The reason for the decrease on the corrosion rate is due to formation of $FeCO_3$ with increase pH. | 31 |
| Effect of Flow | Increase in flow rate during sour corrosion leads to the removal of protective $FeCO_3$ layer. Enhanced mass transfer of reactants near the metal surface during sour corrosion leads to increase in the corrosion rate as a result of increase in flow rate. | 32 |

## 2.3 Corrosion mitigation in the oil and gas industry

Technical options for corrosion control and prevention in the oil and gas industry include cathodic and anodic protection, material selection, chemical dosing, and the application of internal and external coatings. It is well acknowledged in the oil and gas industry that good corrosion management contributes to asset integrity and the optimization of mitigation, monitoring, and inspection costs [37]. There are various methods that have been discussed to help capture these events, and are classified as [38]:

- Selection of appropriate materials
- Use of inhibitors
- Use of protective coatings
- Cathodic protection techniques
- Frequent corrosion monitoring and inspection

### 2.3.1 Selection of appropriate material

When it is discovered that the existing building materials are corrodible, it is usually resolved to replace the materials of construction and select substitute materials to meet the specific purpose [20]. Stainless steels are a diverse group of alloys, each with its own unique mix of corrosion resistance and mechanical qualities. Many of these stainless steel grades are employed in oil and gas applications, depending on the demands of the specific service environment [39]. Smith [40] proposed a 13% Chromium, Super 13% Chromium, 22% Chromium duplex, 25% Chromium

duplex, 28% Chromium stainless steel, 825 nickel alloy, 625 nickel alloy, 2550 nickel alloy, or C276 nickel alloy as corrosion-resistant alloys for the oil and gas industry.

Table 2. 5 [41] below summarizes the chemical composition, mechanical qualities, and results of testing for the approved steels and alloys used in the oil and gas industries. Table 2.5 [39] also shows the results of 720 hours of sulfide stress cracking (SSC) testing of the stainless steels recommended by Johansson et al. [46] in NACE solution (5% NaCl, pH 3, 1 bar pH2S).

Based on a thorough examination of process and operating circumstances, Nali [38] offered some of the most widely utilized materials (shown in Table 2.4) in the hydrocarbon and oil and gas industries. Before selecting a specific metal for the application, he indicated that a careful research of flow conditions, corrosion mechanisms involved, and the estimated life of a material is required. Mannan et al. [42] created a novel high-strength corrosion resistant alloy 945 for oil and gas applications with the nominal composition Fe-47Ni-20.5Cr-3Mo-2Cu-3Nb1.5Ti in their study. The alloy was designed to have a minimum yield strength of 125 ksi and a great mix of ductility and impact strength. Craig [43] proposed various alloys (given in Table 2.6) that have important applications in the oil and gas business in the absence of oxygen.

**Table 2.4. Recommended materials in the oil and gas industry [copied from 122].**

| Material specification | Oil and gas applications |
|---|---|
| Carbon steels | Bulk fluids, crude pipelines, flow lines, water and steam injection lines, production and test separators, KO drums, storage tanks |
| Low- and medium-alloy steels | Well head items, chokes, manifolds and well components with sour and high-temperature applications |
| Straight chromium steels (chromium 12% to 18%) | Christmas trees, well heads, downhole rods, valves and casing pipes |
| Chromium-nickel steels (chromium >18%, nickel >8% | Valve trims, instruments and materials of separators and tanks, low-chloride levels |
| Nickel steels (2.5%, 3.5%, 9% nickel) | Rarely used in oil and gas sectors, LNG storage tanks, piping and pumps |
| Duplex stainless steels (22% chromium duplex, 25% chromium super, duplex) | Piping, vessel, and tank internals where a very high level of chlorides is present |
| Nickel-chrome (inconels) Ni-Cr-Fe alloys | Well head and flow lines, manifolds with high sour and temperature applications |
| Nickel-iron (incolys) Ni-Fe-Cr alloys | Well head and flow lines, manifolds with high sour and temperature applications |

**Table 2.5. Chemical composition and mechanical properties of recommended stainless steels [copied from 122].**

| Grade | Typical chemical composition (wt.%) | | | | | | PRE | Microstructure | $R_{po}$ (MPA) | $R_m$ (MPA) | $A_3$ (%) | CPT ASTM G 150 | CPT ASTM G48 F | CCT ASTM G48 F |
|---|---|---|---|---|---|---|---|---|---|---|---|---|---|---|
| | Cr | Ni | Mo | C | N | other | | | | | | | | |
| DX 2101 | 21.5 | 1.5 | 0.3 | 0.03 | 0.22 | 5 Mn | 26 | Duplex | 450 | 650 | 30 | 17 | 15 | <0 |
| 254 SMO | 20 | 18 | 6.1 | 0.01 | 0.20 | Cu | 43 | Austentic | 300 | 650 | 40 | 87 | 65 | 35 |
| 654 SMO | 24 | 22 | 7.3 | 0.01 | 0.50 | Mn, Cu | 56 | Austentic | 430 | 750 | 40 | >90 | >bp | 60 |

**Table 2.6. Drop evaporation and sulfide stress cracking tests for recommended stainless steels in oil and gas industry [copied from 122].**

| Grade | Drop evaporation test | | | | | SSC testing | | | |
|---|---|---|---|---|---|---|---|---|---|
| | Wick test | 40% CaCl2, 100°C | 25% NaCl, bp | DET (%) | | Cold work (%) | Stress (% of YS) | Temperature (°C) | Result |
| LDX 2101 | No cracks | No cracks | No cracks | - | | - | - | Rt | - |
| 54 SMO | No cracks | - | - | 80 | | 40 to 80 | 90 | 25 | No cracks |
| 54 SMO | - | - | - | 100 | | 0 to 80 | 100 | 25 | No cracks |

### 2.3.2 Use of corrosion inhibitors

Corrosion inhibitors are chemical substances that are introduced to a medium in small amounts to prevent or reduce corrosion. Corrosion inhibitors protect metals from corrosion when metal is stored or transported, in addition to corrosion caused by hostile species [44]. The inhibitors' active components included long-chain amines, fatty amides, imidazolines, fatty acids, and their salts [44]. Miksic et al. [44] investigated numerous types of corrosion inhibitors for the petroleum industry under different flow conditions. Inhibitors were tested in the electrolyte and electrolyte/hydrocarbon mixture in the presence of $CO_2$ and $H_2S$ in static and dynamic settings at concentrations ranging from 50 to 200 ppm. These inhibitor containing solutions offered very high levels of protection for steel against corrosive attack and flow limitations caused by moisture, condensation, oxygen, carbon dioxide, hydrogen sulfide, and other corrosive contaminants. In contrast to traditional approaches, such as film-forming amine-based corrosion inhibitors, injecting a volatile corrosion inhibitor (VpCI)-based substance into any section of the system immediately activates the VpCI with a self-replenishing mono-molecular protective layer [45].

A physical bond is formed on the metal surface due to VpCIs, which create a barrier layer against hostile ions. The barrier heals and replenishes itself, and it can be paired with other functional features to provide further protection. Pipelines, oil and gas wells, refinery units, and fuels are all areas where this technology is used. Anti-corrosion additives based on VpCI have been engineered to operate well in multiphase flow systems in conjunction with various drag reducers. These various combinations of corrosion inhibitors and drag reducers provide improved water flow and corrosion protection for pipes transporting water or a hydrocarbon-water mixture. All

of these additions result in energy savings in oil production and an increase in total recoverable reserves. Figure 2.3 is a pie chart that shows the world consumption of corrosion inhibitors on a value basis. When adopting an inhibitor for oil and gas business, it is important to consider how environmentally safe or less toxic the inhibitor is. Also considering the readiness and cost is a key factor. Choosing organic corrosion inhibitors over inorganic chemicals helps in protecting steels in acidic environments [120].

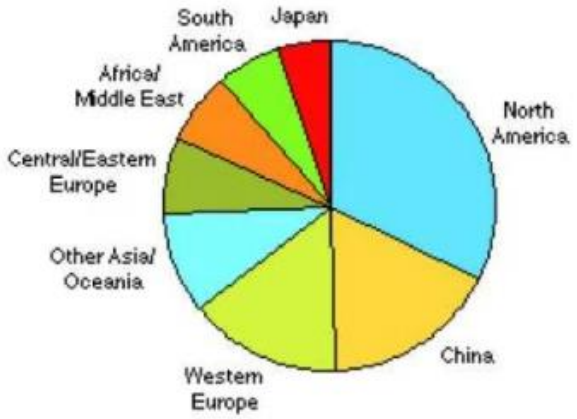


*Figure 2.3. Pie chart of world consumption of corrosion inhibitor [122]*

According to a survey of the literature on high-temperature acid corrosion inhibitors, efficient corrosion inhibitors for oil well acidization include acetylene alcohols, quaternary ammonium salts, aldehydes, amines, and others [46]. A list of inhibitors indicated by earlier researchers, as well as their potential use in the oil and gas industries are shown in Table 2.7.

**Table 2.7 Different types of inhibitors used for Oil and gas pipeline applications [copied from 122].**

| Inhibitors | Oil and gas applications |
|---|---|
| 3-Phenyl-2-propyn-1-ol | API J55 oil field tubing in HCl solutions over a wide range of conditions [51] |
| Hydrazides and thiosemicarbazides of fatty acids with 11, 12, and 18 carbon atoms | Mild steel and oil well steel (N80) in boiling 15% hydrochloric acid solution [52] |
| Mixture of ketones, quinolinium salts, and formic acid | Oil field tubular goods to temperatures as high as 400°F (204°C) in hydrochloric [53] |
| 2-Undecane-5-mercapto-1-oxa-3, 4-diazole | Mild steel in 15% HCl at 105 ± 2°C and N80 steel in 15% HCl containing 5,000 ppm of 2-undecane-5-mercapto-1-oxa-3, 4-diazole [54] |
| 2-Heptadecene-5-mercapto-1-oxa-3, 4-diazole | |
| 2-Decene-5-mercapto-1-oxa-3, 4-diazole | |
| Dibenzylidene acetone | N80 steel and mild steel in HCl [55] |
| Di-N-dimethylaminobenzylidene acetone | |
| Methoxy phenol and nonyl phenol | N80 steel in 15% HCl at different exposure periods (6 to 24 h) and temperatures (30°C to 110°C) [56] |
| N-(5,6-diphenyl-4,5-dihydro-[1,2,4] triazin-3-yl)-guanidine | Mild steel in 1 M hydrochloric acid and 0.5 M sulfuric acid [57] |
| 6-Benzylaminopurine | Cold rolled steel in 1.0 to 7.0 M H2SO4 at 25°C to 50°C [58] |
| Mixture of synthetic magnetite and ferrous gluconate | Oil well steel (N80) in 50 mg/l sulfide concentration at various pH (5.5 to 11.5) and at high-temperature pressure conditions [59] |
| Rosin amide imidazoline | N80 and P110 carbon steels in CO2-saturated simulated formation water [60] |

### 2.3.3 Use of protective coating and lining

Utilizing protective layers or coatings are popular methods to protect pipelines used for oil and gas transmission from corrosion. Liners and coatings are put on pipeline internal walls to avoid internal corrosion [47]. Coatings are also placed externally on the surface of steel pipelines to protect them from corrosion-causing air influences. This helps avoid direct contact of the material and the process media, thereby enhancing the lifespan of the material and equipment [47]. Temperature, humidity, and other environmental parameters are used to select effective coatings. Protective coatings should be adaptable, extremely sticky, disbandment resistant, and environmentally friendly. They should be able to endure normal storage, handling, and degradation, while maintaining the requisite electrical resistivity [47]. Coatings must have good electrical insulation and be effective moisture barriers [47]. The protective layer can be paint, a lining, or a coating, as well as a metallic lining or sheets. Non-metallic linings, such as fiber glass flake, epoxy, glass, and rubber are also commonly used on equipment, such as knock-out drums, separators, and storage tanks. Certain components, such as flanges and bolts, benefit from nickel, zinc, and cadmium coatings [38].

Pipeline coating solutions with several purposes, in addition to corrosion protection, include liquid epoxies, polysiloxanes, fusion bonded epoxies (FBE), 3-Layer polyethylene/polypropylene (3LPE/3LPP), asphalt, and others. FBE and 3LPE/3LPP are currently the most regularly utilized pipeline coatings in the oil and gas industry. FBE coatings are quite successful at preventing pipeline corrosion [49]. Figure 2.4 [50] shows an example of FBE coating used to protect oil and gas pipes from corrosion. A global leader in pipe coating solutions, Bredero Shaw, presented

several unique advanced and proven pipeline coating technologies and services designed to protect pipelines for onshore and offshore applications [51].

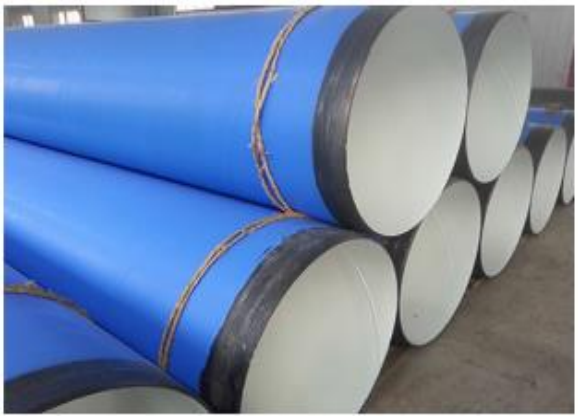

*Figure 2.4. FBE coating for oil and gas pipeline protection from corrosion [120].*

## 2.4 Cathodic Protection

Sir Humphrey Davy [52] is credited with the first application of cathodic protection in 1824, decades before its theoretical underpinning was established. Cathodic protection is a way of reducing corrosion by limiting the potential difference between the anode and the cathode. This is accomplished by passing a current through the structure being protected (such as a pipeline) from an outside source. When enough current is delivered, the entire structure will be at one potential, eliminating the need for anode and cathode locations [53]. It is typically used in conjunction with coatings and is a secondary corrosion control approach. The cathodic protection system can be configured to prevent both oxygen-controlled corrosion and microbiological corrosion [54].

Cathodic protection (CP) was developed to prevent corrosion on external pipeline surfaces. The deployment of a sacrificial anode or an impressed current is required for CP systems. A metal, such as Mg or Zn, is linked to the pipeline in the sacrificial-anode system. Under protection, this metal corrodes and discharges a current into the pipeline. The sacrificial CP is frequently used in underground systems that require a low current. This galvanic system is more cost effective and does not require an external power supply. The impressed-current CP (ICCP), on the other hand, requires an external current source to power some anodes. The current passes from the anodes to the pipeline through the earth. As a result, the pipeline's external surface is protected from corrosion. The two methods of applying cathodic protection include [55]

- Sacrificial (or galvanic) anode cathodic protection (SACP), as shown in Figure 2.5
- Impressed current cathodic protection (ICCP), as shown in Figure 2.6

The major disparity between these techniques is that a naturally occurring electrochemical potential difference between different metallic elements to provide protection is used for SACP (Figure 2.6) and an external power source with inert anodes is used for ICCP (Figure 2.6) [56,57].

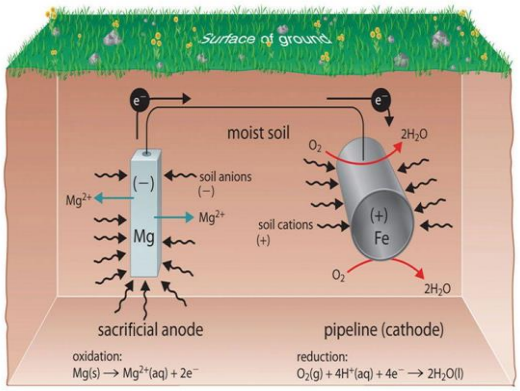


*Figure 2.5. Sacrificial anode cathode protection [123]*

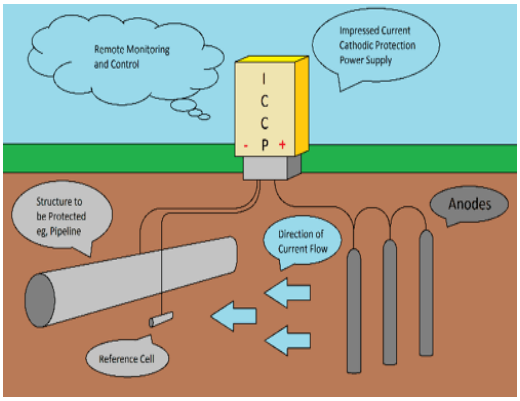


*Figure 2.6. Impressed current cathodic protection (ICCP) [124]*

## 2.5 Frequent corrosion monitoring and inspection

There are various types of corrosion monitoring and inspection. Metal loss/corrosion rate in oil and process systems can be measured directly and online using corrosion monitoring techniques alone [58]. One way is to do on-stream inspections by taking wall thickness measurements on fixed and vulnerable places on equipment, piping, and pipelines on a regular basis to analyze material conditions and corrosion rates [58]. Corrosion inspection can offer compressive snapshots of the corrosion occurring along the pipeline; but, the considerable expenses connected with their use frequently limit their application. These huge expenses are usually the result of labor-intensive procedures, the usage of highly specialized equipment, or losses from pipeline service outages.

In decreasing order of frequency of application, the following paragraphs detail the most widely utilized pipeline inspection procedures [59].

### 2.5.1 Electrical potential surveys techniques

Electrical potential surveys are non-invasive approaches for assessing the risk of pipeline corrosion indirectly. Although these approaches do not quantify corrosion rates or metal loss, they do allow for the detection of coating faults and/or the evaluation of the efficiency of the CP along the pipeline [60]. Closed interval potential survey method considers measuring the potential difference between a pipeline and reference electrode, which is in contact with the soil at regular distance. The survey's goal is to determine whether the pipeline is being polarized in accordance with the CP criteria. Furthermore, these surveys can aid in the identification of stray current pick up and discharge locations, medium to large coating flaws, and unwanted electrical interaction with other metallic structures [61, 62]. Infrared (IR) drop component of the measurements is evaluated by synchronizing the GPS current interrupter, which is systematically switched on and off. However, IR drop produced by stray currents that are not interrupted during the CP-off survey are not accounted for; therefore, stationary data loggers are installed and synchronized.

### 2.5.2 IR coupons

Steel coupons buried adjacent to the pipe and electrically connected to it are also used to test a CP system's operation. Although these coupons can only provide information about the polarization at discrete areas, they provide a more effective technique to reduce IR dips (including those caused by stray currents). By disrupting the electrical link between the coupon and the pipeline (Fig. 2.7 b) [63], accurate IR drop free potential measurements between the coupons and a reference electrode placed close to the coupon may be obtained. They have been used successfully in North America [64, 65] and North Europe [66] since the 1970s.

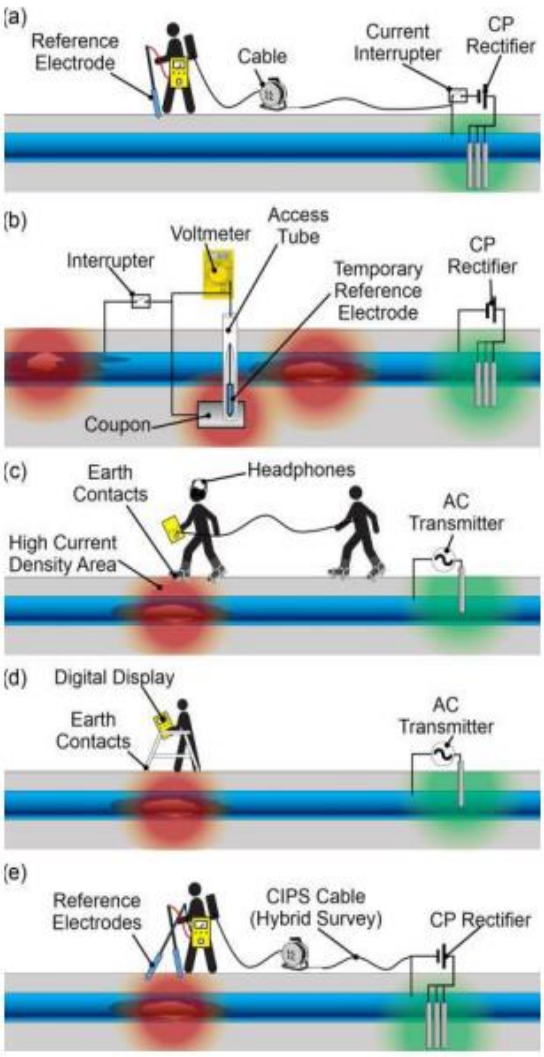


*Figure 2.7 Potential survey methods. a Close interval potential surveys (CIPS), b infrared (IR) coupons, c Pearson, d modern alternating current voltage gradient (ACVG) and e direct current voltage gradient (DCVG) [59]*

### 2.5.3 Alternating current voltage gradient (ACVG) methods

These methods involve sending an alternating current signal to the pipeline via a transmitter unit. This AC signal would leak from the pipe at coating failure locations, where the steel is in direct contact with the soil, creating a zone of high current density. As a result of the high current

density, a potential gradient would form in the extremely resistive soil. The changes in potential difference between two earth connections kept at a fixed distance apart are measured during the survey and utilized to pinpoint coating problems. The Pearson survey (Fig. 2.7e) is founded on ACVG principle and built in the 1940s, becoming the first technique for locating coating breaks at pipelines [67]. For this survey, the impressed AC signal lays in the audible frequency range (typically 1000 Hz). During the survey, the potential gradient is measured between two operators who walk down the pipeline, normally 7 m apart, wearing metal cleats (earth contacts) affixed to their boots. The potential difference is converted into an aural signal by the receiver unit carried by one of the operators for identification of problematic locations [67]. Although alternative survey methods have mostly superseded it, it is still employed on newly constructed pipelines without permanent CP units and in locations with significant stray currents [59].

For recent implementation, an A-shaped frame to support both earth contacts (normally 1m part) is used instead of a second operator using ski poles (Fig. 2.7d). Again, a digital display has been used to substitute the audio output. The digital output has an arrow pinpointing the detective location with added data logging capabilities. More information on this technique can be found in [67].

### 2.5.4 Direct current voltage gradient (DCVG) methods

This technique does not need a transmitter unit like Pearson; it uses the impressed current by the CP units. To obtain coating defects, a single operator using two reference electrodes in contact with the soil at a constant distance measures the voltage gradient (Fig 2.7e) [68]. DCVG

is preferred survey because it has some interesting advantages over the Pearson survey for coating defect detection. One example includes reduced labor during the survey and no installation and repositioning of the transmitter unit [67]. Also, there could be a hybrid survey, where the DCVG survey could be combined with close interval potential (CIPS) due to equipment similarity. While both DCVG and the Pearson technique are quite good in locating coating flaws, there is no overall relationship between the potentials detected and the defect size [67]. Aside from the defect size, numerous additional factors influence the IR drop observed at each location. Another significant shortcoming of these studies is their inability to detect the presence of disbonded coatings. Because disbonded coatings protect the CP current, no potential gradient is formed in the soil around the pipeline. Nonetheless, it has been claimed that a relative comparison of DCVG values acquired under similar conditions for the same pipeline could be useful in determining a repair priority order [69].

### 2.5.5 Inline inspection (ILI) tools

ILI tools (also known as smart pigs) are cylindrical non-destructive testing (NDT) tools that are placed into the pipe to inspect it while it is being carried by the fluid flow. There is a large range of ILI tools available for detecting metal loss, cracks, wax deposition, geometric deformations, and leaks [70,71]. Operational conditions, such as gas corrosivity and temperature, can damage the ILI tool [48].

### 2.5.6 Magnetic flux leakages (MFL)

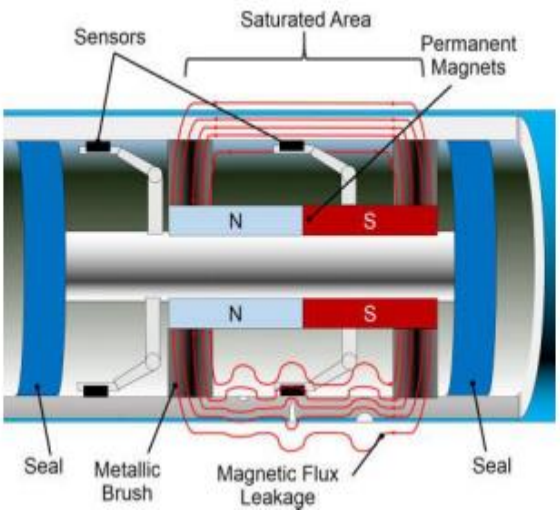


*Figure 2.8 Longitudinal cross-section of a magnetic flux leakages (MFL) inline inspection (ILI)-tool [59]*

As shown in Figure 2.8, two sets of metallic brushes are utilized to ensure that each pole of the permanent magnets is in close contact with the pipe. Hall effect sensors installed in the saturated area are used to detect changes in the strength of the magnetic field. A second set of sensors may be utilized outside of the saturated area to distinguish internal from exterior flaws, where only remnant magnetization affects the pipe and leakages can only be attributed to interior faults [72]. Detection abilities depend on defect orientation with regards to magnetic flux, since maximum detection is at the perpendicular angle. Unfortunately, when the magnetization direction is not parallel to the pipeline, the displacement of the magnetic field as the tool moves creates electrical currents on the pipe, which can have a considerable impact on the readings [73]. MFL tools only measure magnetic flux abnormalities in all circumstances. Because there is no deterministic relationship between magnetic flux variations and metal loss, assessment and quantification of defect size rely on statistical assumptions [73].

## 2.6 Monitoring of Corrosion

Corrosion monitoring seeks to determine whether or not corrosion is already occurring, as well as the rates and patterns of corrosion. Unlike inspection, it does not attempt to determine if a pipeline is fit for operation by examining the current corrosion damage. During the last 30 years, this methodology has been under active development and is still generally based on the use of specially built probes that imitate pipeline surface conditions and measure corrosion rates and patterns. Although several approaches exist for measuring corrosion rates in relatively short periods of time, only a handful of them are compatible with CP systems. The most relevant techniques will be discussed in the following subsections.

### 2.6.1 Electrochemical and Non- electrochemical methods

Corrosion in aquatic environments is an electrochemical process, and many corrosion probes are generally capable of delivering information on instantaneous corrosion rates on an almost continuous basis if the process follows Faraday's law. The presence of CP, a highly resistive soil environment, and coated surfaces, on the other hand, makes reliable electrochemical tests extremely difficult. This could explain why, while electrochemical corrosion monitoring has been widely used in many industrial structures, such as chemical plants, the practical application of existing corrosion monitoring techniques to subterranean infrastructure, such as a steel pipelines, has been limited [74].

Non-electrochemical methods on the other hand, though easier to operate, have low measurement sensitivity because they compare metal losses over time or monitor corrosion

indirectly by monitoring other factors, such as changes in physical qualities, instead of directly measuring the corrosion rate [74].

### 2.6.2 Types of corrosion measuring device

Visual inspection is the traditional method for monitoring the condition of the structure. The measurement methods, such as corrosion potential [75] and Linear Polarization Resistance (LPR) [76] are electrochemical-based methods that map the potential and current of the corrosion activity, which is instantaneous and influenced by environmental factors, such as temperature and humidity, and they cannot monitor and estimate the development of corrosion. The use of X-ray Computer Tomography (XCT) has grown in recent years. This approach has the advantage of increased visibility, which allows for long-term corrosion monitoring [77].

#### *2.6.2.1 Ground Penetrating Radar*

GPR detection of reinforcement corrosion is a novel challenge. Ground-Penetrating Radar (GPR), as shown in Figure 2.9, has been routinely used to find and map steel reinforcements in concrete structures with high speed and precision data gathering [78].

*Figure 2.9 GPR for corrosion detection [125].*

Many researchers have looked into the mechanism of employing GPR for corrosion detection in the laboratory, as well as how to interpret GPR data from field measurements. The most widely utilized method at the moment is based on assessing the measured reflection amplitude at rebars [76,77]. Eisemann et al. [79] published a report on a GPR investigation of a highway bridge. Where significant steel section loss occurred owing to pitting corrosion, unexpectedly low amplitudes of GPR reflected wave of reinforcement were found. However, Parrillo et al. [80] pointed out that a single measurement is insufficient for estimating the level of deterioration. Geophysical Survey Inc. (GSSI) also advised that a single measurement is insufficient for a deck with little deterioration or a deck that is nearly completely destroyed [81]. There are various aspects that can alter the reflection waveform and amplitude that are not caused by deterioration, such as rebar depth fluctuation, diameter, spacing, surface characteristics, structural variation, and surface concrete quality [81].

#### *2.6.2.2 Acoustic Emission Sensor*

During corrosion, cracks propagate, which causes emission of acoustics energy. In normal carbon steel corrosion, 1 mm of steel corrosion results in up to 12 mm of hydrated iron oxide. Multiple micro-fractures and de-laminations of the oxide occur during this expanding phase, resulting in sonic emission. Acoustic emission from corrosion often emits far less energy than emission from crack formation, making it more difficult to detect in the field [82].

*Figure 2.10 Acoustic sound detection for corrosion [126].*

The sensor frequencies employed to detect these signals are governed more by the environmental noise under test conditions than by the emission frequency spectrum. Signals from corrosion can be detected at distances of tens of meters in low noise environments by using monitoring frequencies as low as ten kiloHertz. However, in live process plants, several hundred kiloHertz may be required to get above process noise; in this case, detection distance may be limited to less than half a meter. The quantification of corrosion emission is more difficult and is mostly a function of experience with specific monitoring instrumentation and test techniques (Figure 2.10) [83].

#### *2.6.2.3 Ultrasonic thickness inspection*

When the sites of concern are easily accessible, spot ultrasonic thickness measuring can be used, although, this is rather slow, if a large number of locations must be examined. Guided wave inspection [84] covers huge regions with a single transducer position and is widely used on pipework (Figure 2.11).


*Figure 2.11. Ultrasonic Thickness testing for corrosion [127].*

However, while it reliably detects and locates damaged areas, it does not provide an accurate estimate of the maximum defect depth and is typically limited to detecting defects that remove about 3-5% of the cross-sectional area of the pipe, though this can be reduced in pipes in generally good condition or if the system is permanently installed [10]. Unfortunately, corrosion under pipe supports (CUPS) is a problem for guided wave inspection, because the support itself gives a significant reflection at the low frequencies required to detect gradual wall thinning [85]. Also, the locations of concern are inaccessible for conventional ultrasonic thickness gauging.

## 2.7 Microsensor

Sensors have been created and made using microelectronic manufacturing techniques to directly assess corrosion rates and the performance of corrosion control systems [131]. Microsensors based on corrosion rate measurements via linear polarization, electrical resistance change, and galvanic currents have been developed [131]. The use of sensors is one such approach to solve problems with corrosion. Sensors directly and indirectly assess corrosion damage, or they predict damage by defining the environment. A sensor is a collection of one or more transducer elements used to monitor a system. Transducer elements are devices that convert a system's physical, chemical, and electrochemical properties into electrical signals. Input transducers responsive to relative humidity, temperature of the environment, concentration of hostile species, pH, aeration conditions, electrode potential, and weight change are required for common corrosion applications [131]. A combination of these transducers in any corroding system can be configured to create electrical responses that reflect the corrosive conditions present in the system at any time [132]. A real-time assessment of corrosive conditions is required to initiate corrective feedback and perform corrective actions before major damage occurs [132]. The use of such sensors would thus result in significant cost savings, not only by preventing damage to materials, plant, and equipment, but also by reducing downtime [132].

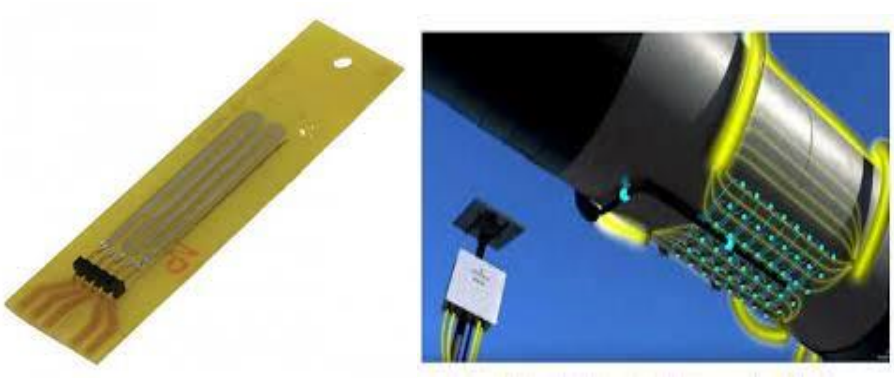

*Figure 2.12. Microsensor used for corrosion detection and Monitoring [128].*

## 2.8 Measuring impedance

An impedance analyzer, such as Agilent E4980A Precision LCR meter [86], Wayne Kerr Precision, and HP 4192A impedance analyzer, are used to measure the lead zinc titanate (PZT). These analyzers can provide the desired characteristics, like impedance (Z), phase-angle, resistance, inductance, capacitance, conductance, and susceptance. Recently, a new way of measuring impedance using a fast Fourier transform (FFT) analyzer and a tiny current measurement circuit was devised [87].

The Electromechanical impedance (EMI) measuring technique has risen to become one of the most significant techniques for structural damage detection, due to its ability to detect damage at an incipient level. The EMI method is based on the concept of discrepancies in the mechanical impedance of the structure due to a change in the properties caused by damage. Many research works have been conducted about EMI in the last two decades, after the first proof of concept was proposed by Liang et al. [90] in 1994. The suitability of an impedance-based method was first

used by G. Park et al. [91] to check the integrity of a bolted civil pipeline structure, based on the dissimilarity of the impedance between an undamaged and damaged structure. The resonant frequency shift variation was used to calculate the corrosion in a metallic beam, and it was observed that the resonant frequency shift increased with an increase in the corrosion of the beam [92]. A wireless impedance measurement device for corrosion detection in metallic structures was also proposed by S. Park et al. [93]. V. Talakokula et al. [94] investigated the quantification of corrosion using extracted equivalent structural parameters for reinforced concrete. A series of experiments were conducted embedding and patching piezo onto a structural surface. The piezo was used to detect and quantify the corrosion for reinforced concrete elements under an accelerated corrosion test method. The extracted equivalent structural parameters, including PZT-identified stiffness and mass losses, were in respectable agreement with the actual stiffness and mass losses of the host structure. The rate of corrosion measured from the PZT-identified mass loss was also in the range of the actual mass loss of the host structure. The equivalent parameters extracted from the admittance signature were also used for the diagnosis of carbonation-induced corrosion [92].

The EMI technique was used by Martowicz et al. [95] to spot a loosened bolt in bolted pipeline connections using the point frequency response function and the transferring frequency response function with outlier analysis to quantify the damage. Zhu et al. [96] also used the Structural Mechanical Impedance (SMI) derived from raw conductance for corrosion detection and quantification using root mean square deviation (RMSD) and peak frequency shift in a steel beam. Wong S.N. [97] used the EMI technique to detect wall thickness loss for a pipeline. The RMSD and resonant frequency were used as a damage indicator for wall thickness reduction. The

loss of wall thickness in a metal structure was also investigated using a probabilistic neural network and re-attachable PZT sensor [98]. Li et al. [99] recommended a corrosion measuring probe based on the EMI principle, which is made from a rounded PZT patch mounted to a metal rod. It was observed that the peak magnitude of the conductance signature decreased as the quantity of corrosion increased. An EMI modification technique was proposed by Zue et al. [100], which considered the influence of the bonding layer between a PZT patch and the host structure using multiple sensors for pipeline crack detection. The damage location and degree were carried out using the RMSD index. A numerical assessment of the EMI signature was conducted in pipe with different degrees of damage by Reddypogu et al. [101]. A pipe with varying corrosion lengths circumferentially, varying corrosion breadth, and depth were examined. The EMI technique was used for steel pipeline erosion identification assessment by S.N. Khunte [102]. J. Raju et al. [103] utilized the concept of equivalent parameters for assessing and quantifying corrosion in a reusable non-bonded configuration for the pipeline.

It is observed from the above that many research efforts have gone into studying the EMI technique for damage detection in structures. However, only a few research works have been reported for corrosion detection, with even fewer reported in pipeline structures.

# 3 Chapter 3. Apparatus and Methodology

## 3.1 Epoxy Binder

Epoxy polymers are named for the presence of at least one epoxy or oxirane ring within their structures. The name "epoxide or epoxy" normally refers to an oxygen-containing ring, the substance, known as epoxy polymer, comprises 1,2-epoxide, which is a ring with three atoms: two carbons and an oxygen. Although the three-dimensional networks are still referred to as epoxy networks, they no longer include any epoxy function [116]. For our experiment, four kinds of epoxy were glued to the 4140 steel and placed under an NaCl solution, to test the adhesion abilities of each. These four epoxies included Permatex 84109 Permapoxy 4 Minute Multi-Metal Epoxy (0.84 oz., grey), J-B Weld 8265s Original Cold-Weld Steel Reinforced Epoxy – 2 oz., Pratley Porcelain Adhesive Repair Kit, and Rhino Glue Gel. As the metal came primed, prior to bonding the epoxy to the steel, the steel was polished with 800 grit silicon sandpaper to remove the primer. After exposure to the NaCl solution, the J-B Weld epoxy was found to keep the wire in place on the metal for the longest time, with the epoxy holding the copper wire leads to the steel for up to 10 weeks. The Permatex epoxy was able to hold the copper wire leads to the steel for about five weeks before peeling off, as shown in Figure 3.1. The Pratley epoxy peeled off after about a week, while the Rhino epoxy did not even stick properly on the dry steel, so it was discarded. Therefore, the J-B Weld epoxy was chosen for the experiment.

a. b. c.

*Figure 3.1. a. Permatex 84109 epoxy came off after 5 weeks, b. Porcelain adhesive came off after a week, c. Rhino epoxy will only hold for a 2days.*

The J-B Weld Original Cold Weld two-part epoxy method provided a strong, long-lasting connection between the metal samples and the copper wire, as shown in Figure 3.2. It made a permanent bond when mixed at a 1:1 ratio and set to a dark grey tint in 4-6 hours at room temperature. The entire cure took 15-24 hours.


*Figure 3.2. J-B weld 8265s epoxy was used for the experiment.*

## 3.2 4140 Alloy steal

4140 alloy steel is composed primarily of iron just like any other steels. It is alloyed with chromium, molybdenum, carbon, and other minor components. Alloying elements of Cr and Mo

gives AISI 4140 steel a high durability and hardenability. AISI 4140 is also known as chromium-molybdenum steel (DIN 42CrMo4). It is ubiquitously steel and typically used in the production of machinery parts, vehicle and aviation components, and oil and gas transport pipelines due to toughness, high fatigue strength, and abrasion and impact resistance [114]. Heat treatment affects the properties of the formed alloy. To improve the surface qualities of AISI 4140 steel, thermal or thermochemical heat treatments are often utilized. The common forms of 4140 alloy are hot rolled bars, annealed bars, or cold drawn bars. Hot rolled treatment procedure is used for flat, round, hex, and square bars. They have a distinct surface quality and are typically weaker than cold-rolled variants. The annealed state is the most common way to buy 4140 steel. This is mainly due to the steel having been annealed in order to be cold formed into bars or plates. In preparation for cold forming, annealing increases the ductility of the steel. The cold drawn is processed at room temperature. Before cold drawing, the steel is treated to generate the softer pearlite microstructure, which increases the material's ductility [115]. For this experiment, annealed steel was chosen because that is what is normally used for oil and gas pipelines.

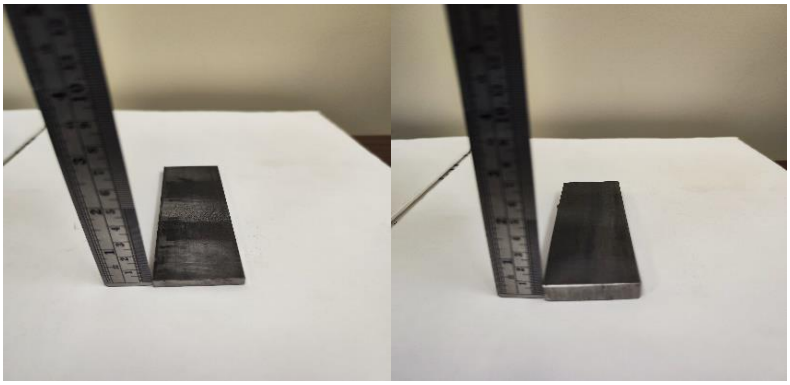

*Figure 3.3 0.25'' and 0.5''4140 steel metal coupon*

To examine the feasibility of the proposed technique in monitoring corrosion of the 4140 annealed steel using AD5941, the experiment was carried out in two phases. Firstly, two 4140

annealed steel of size 0.25 inched and 0.5 inches were used, as shown in Figure 3.3. This difference in size was to determine whether thickness of a metal affected the impedance reading. Each metal piece was purchased from Grainger and came in the form of a plate from the manufacturer. It was taken to the machine shop at YSU and was cut to the dimensions of 5 inches (12.7 cm) x 1.5 inches (3.81 cm) x 0.25 inches (0.635 cm) and 5 inches (12.7 cm) x 1.5 inches (3.81 cm) x 0.5 inches (1.27 cm). Thirteen pieces of the 0.25-inch coupons and five pieces of the 0.5-inch coupons were used. In each of the four different corrosive environments, three specimens of the 0.25-inch coupons and one specimen of the 0.5-inch coupon were placed, and for the control environment, one piece of each thickness was monitored. The three samples were used in each selected corrosive environment, to help to monitor accuracy and consistency of results, while one different thickness was for comparison purposes. After each week of corrosion, it was found that the difference in thickness did not affect the impedance reading using the AD5941. The impedance generally increased as corrosion increased regardless of thickness, which was important to the next phase of the research.

*Figure 3.4. 0.5’’4140 steel metal pipe before corrosion.*

After testing thickness effects, a second set of experiments were performed, to determine if orientation affected corrosion measurement. Therefore, a 4140 annealed steel pipe of thickness 0.5 inches (1.27 cm), with an outer diameter (OD) of 2.5 inches (6.35 cm) and an inner diameter (ID) of 1.5 inches (3.81 cm) was purchased from Online Metals, as shown in Figure 3.4. Since thickness did not matter, as demonstrated with the rectangular specimens, 0.5 inches was chosen as the thickness of the pipe, due to its ready availability, as 0.25 inches was not available for purchase at the time. The 4140 annealed steel pipe came in a length of 70 inches (177.8 cm) when ordered and was taken to the YSU machine shop, where it was cut in length of 5 inches (12.7 cm) a piece.

## 3.3 Copper wire

Electrical wire with a diameter of 26 AWG is a versatile and dependable choice for a wide range of electrical applications. With a diameter of 0.405 mm, this wire is tiny enough to be utilized in small places while remaining strong enough to withstand a wide range of electrical currents, as shown in Figure 3.5. It is often utilized in low-voltage applications, like computers, telecommunications equipment, and automotive wiring. This wire ensures effective electricity conduction with decreased resistance, due to its high conductivity and precision oxygen-free copper. The abrasion-resistant PVC insulation protects the wire and is resistant to sunshine and chemicals [117]. The lead was used to make it easier to connect the sensor to the metal sample.

a. b.

*Figure 3.5. Image showing 26 AWG copper used for the experiment, b shows an end of wire striped to make connections.*

The copper wire was cut into pieces of length 6 inches (15.24 cm) and each end was stripped to exposed 0.5 inches (1.27 cm) of the copper wire (Fig. 3.5b). One end of the copper wire is fixed to the metal sample with the help of the J-B Weld epoxy and the other end is left free to be connected to the sensor. Because the metal was shipped with a surface protective film, sandpaper was used to roughen just the area of the metal where the wire was connected to remove that film before the application of the epoxy to fix the wire. For the initial experiment where metal coupons were used, two strands of the copper wire were connected at the ends of each metal coupon. For the metal pipe used for the second experiment, four wire strands were used. Two of the wires were connected to each end of the pipe and the other two connected across the pipe.

## 3.4 Corrosion environment

The initial experiment used the flat steel coupons placed in five different testing environments. For the five environments, four environments were for the accelerated corrosion testing and one

environment served as a control experiment. The control steel was exposed the ambient conditions of the lab. Three of the four environments utilized a 3.5 wt% sodium chloride (NaCl) solution. In the first environment, steel specimens were fully immersed in the NaCl solution; in the second environment, steel specimens were placed over the NaCl solution; in the third environment, the specimens were initially completely immersed in NaCl and then removed and allowed to dry. The fourth environment placed specimens under wet dirt, using just deionized water, instead of the NaCl solution. The dirt used was collected from the environmental science laboratory, where it had been stored and dried for over three years. A volumetric flask was also used to determine the volume of water to be used.

For the experiments with the metal coupon, four samples were placed in each of the environment. Three of these samples were 0.25-inch in size and one was 0.5-inch in size. Table 3.1 below shows the numbering of samples used in the various environment.

**Table 3.1. Showing samples that were used in each of the four environments**.

| **Sample** | **Environment** |
|---|---|
| Sample 16, Sample 17, Sample 18: 0.25-inch in size<br>Sample 1: 0.5-inch in size | Immersed in NaCl solution |
| Sample 10, Sample 11, Sample 12: 0.25-inch in size<br>Sample 3: 0.5-inch in size | Immersed NaCl solution and dry |
| Sample 13, Sample 14, Sample 15: 0.25-inch in size<br>Sample 5: 0.5-inch in size | Placed over NaCl solution |
| Sample 7, Sample 8, Sample 9: 0.25-inch in size<br>Sample 4: 0.5-inch in size | Buried under wet dirt |
| Sample 1, Sample 4, Sample 6: 0.25-inch in size<br>Sample 2: 0.5-inch in size | Control |

Prior to the corrosion tests, the initial weights of the metal coupons were measured, and those values were recorded. Then, four metal specimens (3 0.25-inches and 1 0.5-inches) were placed in each environment, with the environment changed every 7 days, after taking the EMI reading with the sensor. The environment was chosen to model real life conditions to which pipelines are

exposed. The second phase of the experiment considered only two of the four corrosive environments, specifically the wet dirt environment and the immersed then dried environment were chosen, as these were the most aggressive environments.

## 3.5 Weight Measurement.

Material weight loss measurements is one of the ways to detect the presence of corrosion in a material. To confirm that the corrosion is actually happening in our experiment and that the impedance change measured by the sensor is as a result of corrosion, the weight loss corrosion detection was also employed. To do this, the initial weight of each specimen was recorded prior to corrosion, using a 10,000-gram (10 kg) capacity balance, shown in Figure 3.6. After the 8 weeks corrosion period, each metal was cleaned, to remove the weakly adhered oxide particles and the weight is recorded again; strongly adhered oxides were not chemically removed. The changes in weight represented the degradation of the material.

The weight loss method was only used for the metal coupon experiment. Changes in grams were captured by the balance on the gram scale; however, changes of grams on the kilogram scale were negligible. The weight loss of the materials was not that much, so the kilogram scale would not detect the small changes. The weight of the metal coupon was recorded in grams, while the weight of the steel pipes was heavier and recorded in kilograms. In addition, after the first experiment, it was already established that the sensor could detect the presence of corrosion.


*Figure 3.6. Weight of metal coupons being measured.*

## 3.6 Metal Surface Analysis using Keyence VR-5000 Measurement System

Surface analysis is also one way to tell if corrosion is happening. It is generally done by inspecting a targeted area on a specimen for a period of time to detect surface changes and corrosion traits. A Keyence Wide-Area 3D Measurement System was used to perform the surface analysis, as shown in Figure 3.7. The Keyence System is a non-contact 3D scanner that can swiftly and precisely survey huge regions, providing information on the profile and roughness of the specimen. It is ideal for assessing profile, roughness, flatness, wear volume, or comparing 3D scan data to CAD files to determine the quality of a product. The non-contact 3D measurement can be performed in as little as one second, measuring areas up to 100 mm x 200 mm. The place and press operation eliminates user error [118]. As with the weight loss, only the flat steel specimens could be examined with this method of corrosion detection, to confirm the results from the impedance measurements. The initial surface of a specific area of the metal coupon was captured

and, after 8 weeks of corrosion, the images of the same areas were captured with the V-500 and evidence of corrosion identified.

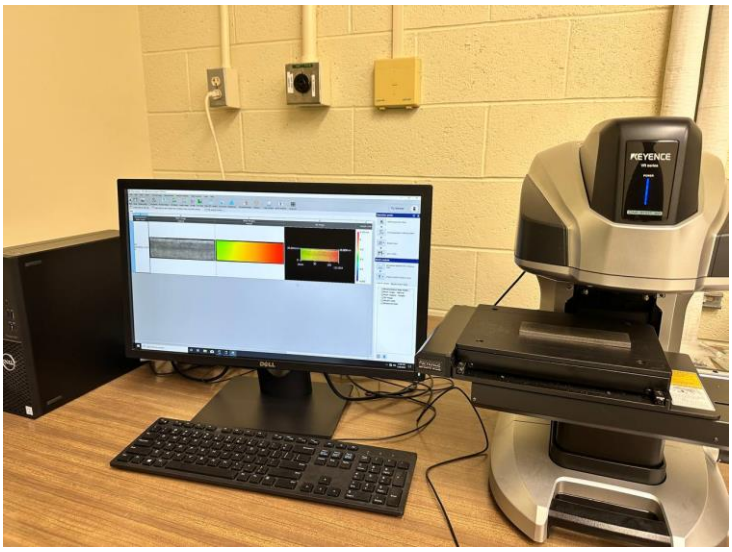


*Figure 3.7 Image show surface of steel metal coupon being captured before corrosion.*

## 3.7 Digital Multimeter

A Digital Multimeter, as shown in Figure 3.8, was used to check the connectivity of the wire to the metal piece before corrosion. It was also used weekly during the experiment, to check if the wire is still connected to the metal piece before the sensor was used to measure the impedance. This was done to ensure correct data was being captured. The measuring resistance range is from 0 Ohms to 2 MOhms, with the following resistance measuring scales of 200 Ohms, 2 kOhms, 20 kOhms, 200 kOhms, and 2 MOhms.

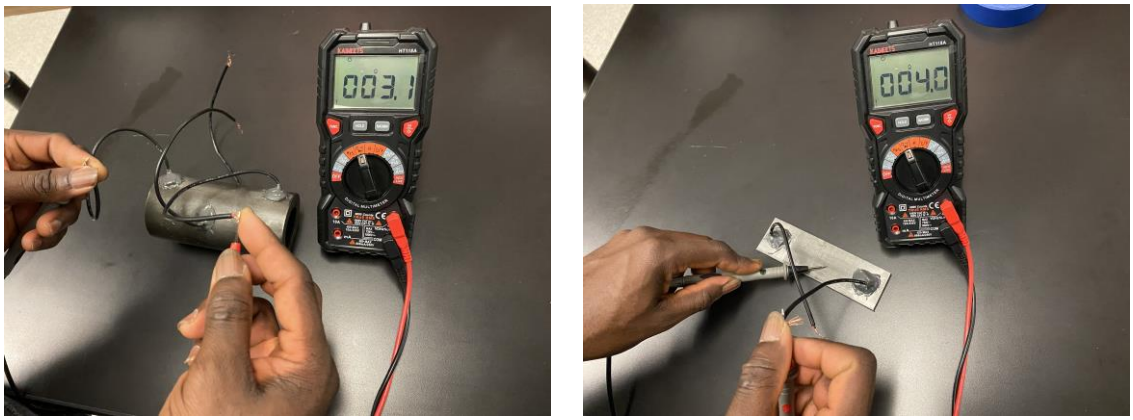


*Figure 3.8 Image showing multimeter used to check wire and metal connectivity.*

To check for continuity of each wire, the multimeter was deployed. First, each wire was tested for conductivity by connecting one terminal of the multimeter to the exposed copper wire, while the other terminal touched the steel metal. The terminals of the multimeter were then connected to the exposed copper wire at each end of the metal to ensure continuity. In the case of the metal pipe, the terminal positions were swapped around, to make sure that regardless of which wires are touched, there is still a continuity. The multimeter beeps when there is connectivity and a measured resistance closer to zero shows connectivity or conductivity. However, during corrosion, resistance values changed, so resistance values closer to zero when checking for continuity were not considered.

## 3.8 Microsensor

The Electromechanical impedance (EMI) measurements were taken every seven days. For specimens immersed in the NaCl solution, EMI was recorded both while in the NaCl solution and

after the specimens were removed from the NaCl solution,. Also, for the specimens in wet dirt, the EMI was recorded while sample were beneath the dirt and then performed again when removed from the dirt. This was to check the EMI variation for the two cases and to determine if the measurements could be taken while being in a potentially conductive environment, like ion-containing water or dirt. The other two environments, which were above the NaCl solution and immersed then dried, and the control were only measured once, as they were not exposed to an environment that could potentially change the reading. The EMI signatures of the corrosion specimen were measured using an impedance analyzer. AD5941 was used to measure the impedance through a frequency response, with the data displayed on SensorPal [119] interface. To obtain the accurate impedance reading, choosing a suitable frequency range was important. Hence, a wide range of frequencies were scanned (1 Hz-100 kHz). The frequency response was observed and then, using a trial-and-error method, a refined frequency range (1-1kHz) was selected, because, in the lower range, more structural dynamics were present, and thus, it is more evident to the presence of corrosion. The highest frequency in the impedance signatures matches to degree of corrosion of the specimen. The range with large peaks usually contains more dynamic interaction, and it is therefore more sensitive to damage [27]. The whole corrosion process and measurements were performed at room temperature varying between 25 °C and 27 °C.

# 4 Chapter 4 Results and Discussion

## 4.1 Results

This section presents the results obtained from the two sets of experiments conducted. Sections 4.1-4.4 firstly considers the experimental data obtained from using the metal coupons. Results from the three analysis methods, which includes corrosion detection using the weight loss approach, surface analysis by visual identification and Keyence V500 series imaging, and lastly, corrosion detection using the microsensor are all presented. Secondly, section 4.5 presents data obtained from the corrosion of the metal pipes using just the microsensor, along with photographic images of the external and internal surface of the pipes.

### 4.1.1 Corrosion detecting using weight loss approach

The tables below show the weights of the various metal coupons used for the four different corrosive environments. As already stated in Chapter 3.3, the initial weight of each specimen used was recorded. After 8 weeks of corrosion, the final weight was also recorded.

**Table 4.1. shows initial and final approx. weight in grams of metal coupons immersed in NaCl solution.**

| Specimen | Initial Weight | Weight after corrosion | Mass loss |
|---|---|---|---|
| **0.5 inches** | | | |
| 1 | 473 | 472 | 1 |
| **0.25 inches** | | | |
| 16 | 273 | 272 | 1 |
| 17 | 286 | 261 | 1 |
| 18 | 259 | 258 | 1 |

From Table 4.1 above, the initial and final weight of each sample used in the immersed and dried environment are shown. The mass loss, which shows the difference between the final and initial weight for each sample, was 1 gram. The scale used to measure the weights did not detect small changes, so the difference in weight was only able to be detected as grams.

**Table 4.2. shows initial and final approx. weight in grams of metal coupons immersed in NaCl solution & dried.**

| Specimen | Initial Weight | Weight after corrosion | Mass loss |
|---|---|---|---|
| **0.5 inches** | | | |
| 3 | 486 | 484 | 2 |
| **0.25 inches** | | | |
| 10 | 237 | 235 | 2 |
| 11 | 235 | 233 | 2 |
| 12 | 241 | 239 | 2 |

From Table 4.2 above, the initial and final weight of each sample used in the immersed and dried environment is shown. The mass loss, which shows the difference between the final and initial

weight for each sample, was 2 grams. The scale used to measure the weights did not detect small changes, so the difference in weight was only able to be detected as grams.

**Table 4.3. shows initial and final approx. weight in grams of metal coupons suspended over NaCl. Solution.**

| Specimen | Initial Weight | Weight after corrosion | Mass loss |
|---|---|---|---|
| **0.5 inches** | | | |
| 4 | 459 | 459 | 0 |
| **0.25 inches** | | | |
| 2 | 246 | 246 | 0 |
| 3 | 237 | 237 | 0 |
| 4 | 237 | 237 | 0 |

From Table 4.3 above, the initial and final weight of each sample placed over NaCl environment is shown. The mass loss, which shows the difference between the final and initial weight for each sample, was 0 grams. Due to the scale used, the small differences likely seen in this environment were not able to be detected.

**Table 4.4. shows initial and final approx. weight in grams of metal coupons buried under wet dirt.**

| Specimen | Initial Weight | Weight after corrosion | Mass loss |
|---|---|---|---|
| **0.5 inches** | | | |
| 5 | 470 | 470 | 0 |
| **0.25 inches** | | | |
| 13 | 245 | 245 | 0 |
| 14 | 238 | 238 | 0 |
| 15 | 240 | 240 | 0 |

From Table 4.4 above, the initial and final weight of each sample used in the immersed and dried environment is shown. The mass loss, which shows the difference between the final and initial weight for each sample, was 0 grams. Due to the scale used, the small differences likely seen in this environment were not able to be detected.

## 4.2 Corrosion detecting using Visual Inspection and Keyence V500 series imaging

### 4.2.1 Visual Inspection

The Figures below in this section show images of the surfaces of the metal coupons and pipes taken before and after exposing the specimens to the various corrosive environments. In this section, we consider the metal coupons results first and then present that of the metal pipe.

*Figure 4.1. above shows image of metal before exposed to corrosion environments.*

Figure 4.1 shows the appearance of an uncorroded sample surface. There grey appearance shows no signs of corrosion. There are slight discolorations across the surface, likely present due to the

coating the steel was shipped with. In addition, near the epoxy-attached wires, one can see a shinier surface, the result of the sanding needed to remove the coating, enabling the epoxy to stay attached to the steel surface.

*Figure 4.2 above shows image of coupons immersed in NaCl solution.*

In Figure 4.2, for the samples that were immersed in the NaCl solution, there is the formation of orange-brown oxide of metal surface, which appeared in powdered form on surfaces when samples were dried. The orange-brown oxide is indicative of rust ($Fe_2O_3$) formation, which was easily dislodged when handling the samples, due to its formation in water.

*Figure 4.3 above shows image of coupons immersed in NaCl solution and dried.*

In Figure 4.3, for the samples that were immersed in the NaCl solution and then dried, a dark reddish-brown surface has formed, which looks completely different from the surface in Figure 4.2. In addition to the difference in color, the oxides that can be seen appear to be thicker, as well as producing flakes, since the oxides towards to the top of the surface were weakly attached to the metal surfaces. As with the immersed in NaCl solution, the oxide is $Fe_2O_3$, although in a different crystalline form.

*Figure 4.4. below shows image of metal coupons placed over NaCl solution.*

In Figure 4.4. which shows the samples placed over the NaCl solution, the surface is mostly still the same color as the pre-corrosion samples (Figure 4.1). The oxides that do form appear to be dark brown with hints of red, along with potentially some black as well. As with the previous two environments, the brown oxides would be $Fe_2O_3$, while the black oxides would be FeO. There is some visual oxide flaking present, indicating that the oxides that did grow were weakly adhered at the top surface of the metal.

*Figure 4.5 below shows image of metal coupons buried in wet dirt.*

In Figure 4.5, which shows the samples buried under wet dirt, the metal pieces are shown as corroded with dirt particles attached on the metal surface. Unlike all of the previous environments, these samples do not contain the reddish-brown color, likely because the dirt is mixing in with the oxide, changing the color. There are distinct locations, especially in the second bar from the left, where the presence of corrosion can clearly be seen, as indicated by the darker colors, where the oxide is forming. There are no oxide flakes, unlike the previous two environments, likely because those came off with the dirt during cleaning.

### 4.2.2 Keyence V500 Imaging

The following section shows the imaging of samples that were used for the experiment. Each figure in Section 4.2.2 reveals four images of samples used in this experiment. The real and surface profile images are both shown for before and after corrosion. On the right sides are the real images and on the left side are the surface profile images. The before corrosion images are

at the top and the after-corrosion images are at the bottom. The after-corrosion images were captured after the loose oxides were cleaned from the metal surface to expose any possible hidden pitting. For all surface profilometry images, red indicates height from the baseline surface, with dark blue indicating depth from the baseline sample. With respect specifically to corrosion, red usually indicates the presence of salt residuals or oxides on the surface, which are built up, while dark blue usually indicates the presence of pitting, which has sunk into the metal surface and removed material to form.

Figure 4.6 through Figure 4.21 shows pre- and post- surface imaging of samples using the Keyence system. Figures 4.6 through 4.9 show samples immersed in NaCl solution. Figures 4.10 through 4.13 show samples immersed in NaCl and dried. Figures 4.14 through 4.17 show samples placed over NaCl solution. Figures 4.19 through 4.21 show samples buried under wet dirt.

#### *4.2.2.1 Samples immersed in NaCl solution*

Figure 4.6 shows four images of Sample 16. Looking at the surfaces before corrosion, evidence of indentation is seen on the profiling image of the uncorroded surface, which are machining defects. These machining defects follow the typical linear pattern. When looking at the corrosion surface, both salt residuals, identified as the white spots in the left image and matching red spots in the right image, and pitting, indicated as the dark blue spots, specifically in the bottom left corner of the bottom images, are present. The green in the bottom right image also matches the profile of the reddish color in the bottom left image, indicating the slight presence of the oxide layer.

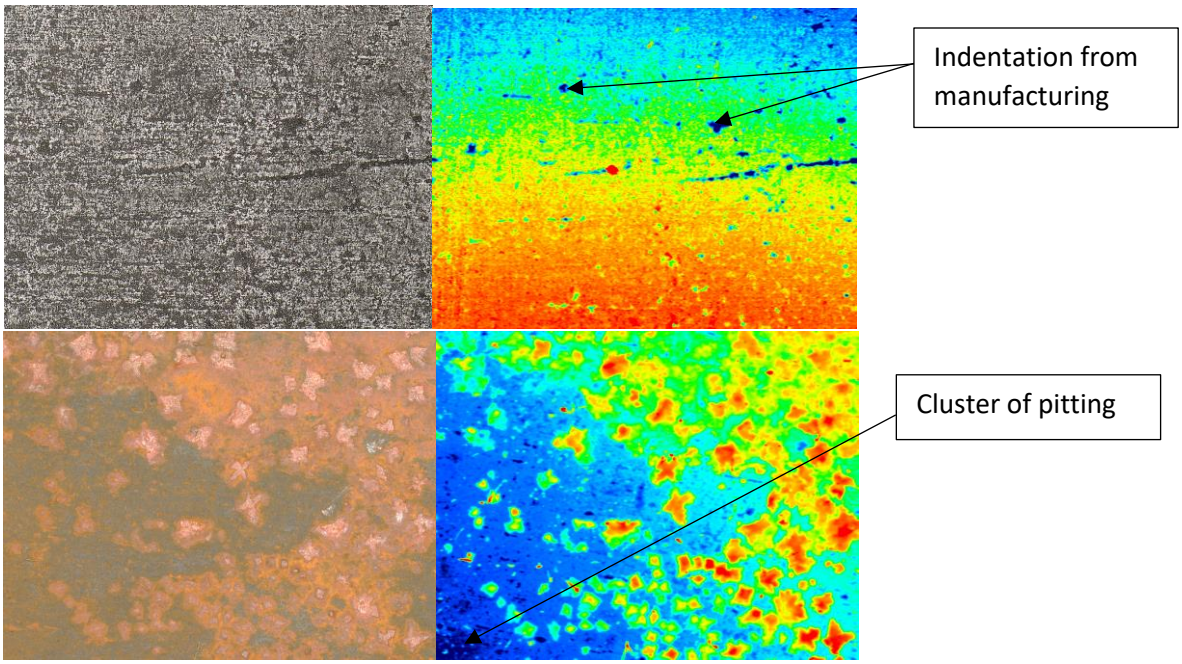


*Figure 4.6 above shows images of sample 16 (0.25-inch size) taken with Keyence measuring system before and after corrosion.*

Figure 4.7 shows four images of Sample 17. As with Sample 16, evidence of machining defects can be seen in both pre-corrosion images, as linear indentations. Unlike Sample 16, minimal pitting is seen on this image, although there is some present in the bottom left corner of the right

image. Most of Sample 17 is covered with the thin oxide layer, with larger pieces of the oxide present in the higher red spots shown in the surface profile image and corresponding with the brighter orange spots on the micrograph.

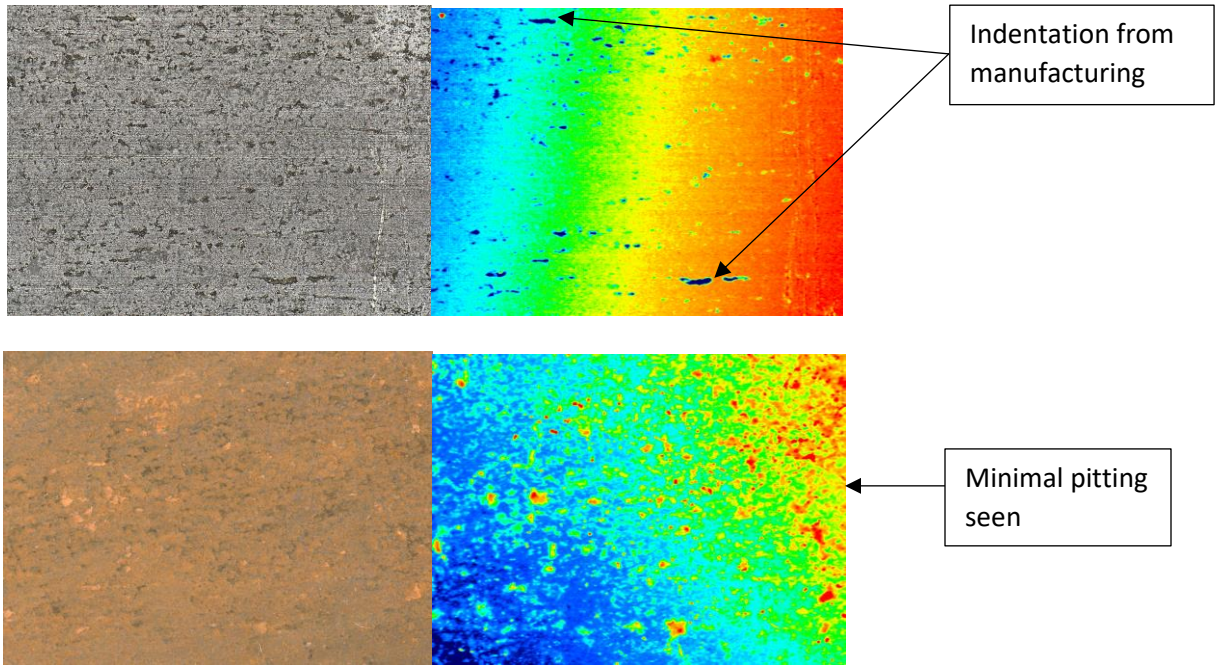


*Figure 4.7. above shows images of sample 17 (0.25-inch size) taken with Keyence measuring system before and after corrosion.*

Figure 4.8 shows four images of Sample 18. As with the previous samples, evidence of machining defects can be seen as linear indentations in the pre-corrosion images. More pitting is seen in this image than the previous images, especially in the bottom left corner of the right image, which match with the darker spots in the bottom left corner of the left image. In addition, the oxide layer is more distinct in the micrograph, with higher oxide spots appearing on the surface profile image.

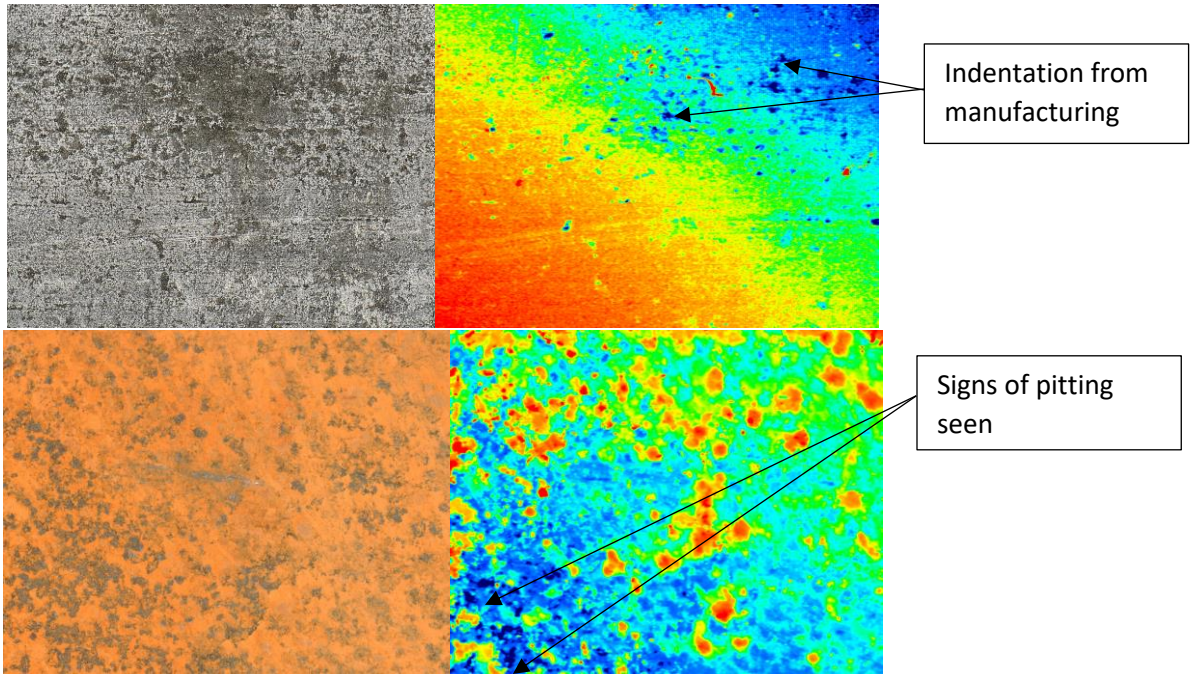


*Figure 4.8 above shows images of sample 18 (0.25-inch size) taken with Keyence measuring system before and after corrosion.*

Figure 4.9 shows four images of Sample 5. Like all previous samples, evidence of machining defects is seen on the profiling image of the uncorroded surface, indicated as dark spots following a more linear pattern. Pitting is seen in this image, especially along the top of the right image, which match with the darker spots on the top of the left image. In addition, the oxide layer is very distinct in the micrograph, with higher oxide spots appearing on the surface profile image. Looking along the same line as the pits, one sees a bright orange spot protruding roughly halfway along the top, which matches a red/orange/yellow spot (indicating height) on the surface profile image. Other spots of oxide also match to the micrograph.

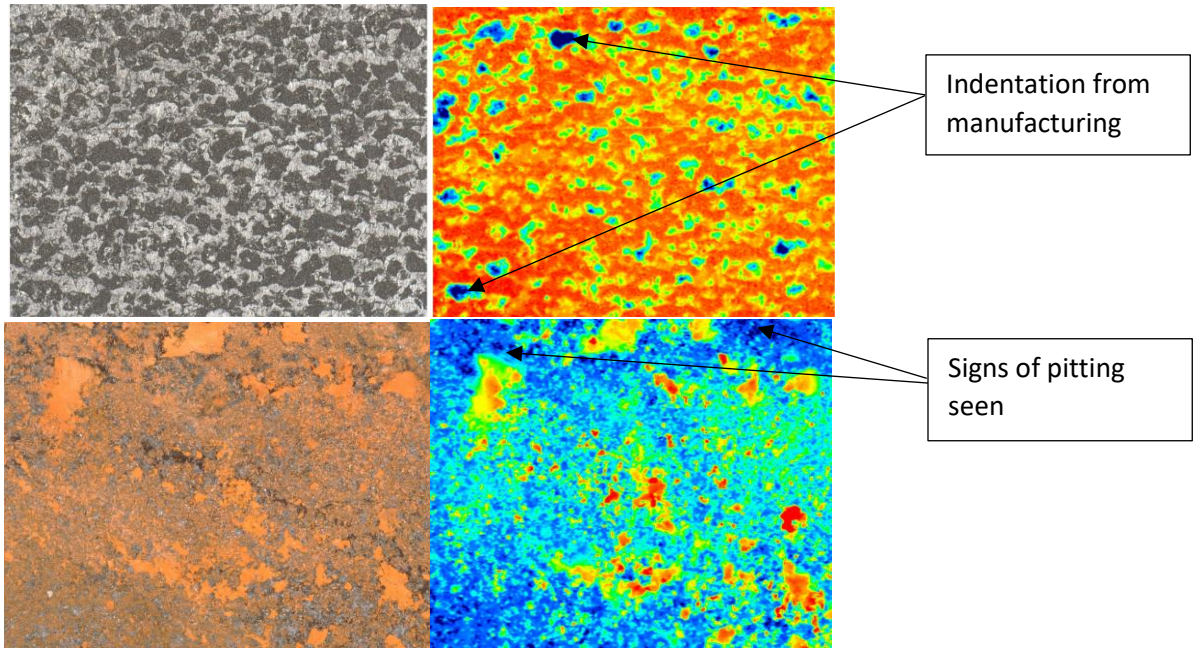


*Figure 4.9 above shows images of sample 5 (0.5-inch size) taken with Keyence measuring system before and after corrosion.*

#### *4.2.2.2 Samples immersed and dried*

Figure 4.10 shows four images of Sample 10. Like the previous samples, evidence of indentation from machining defects is seen on the profiling image of the uncorroded surface, indicated as dark spots following a more linear pattern. As environments were changed, so was the final surface. When looking at the corroded surface, there is a large defect in the bottom right corner of both the micrograph and the surface profile image. In the surface profile image, one can see it is a raised defect (indicated by red, orange, and yellow), that likely indicates the presence of a rust flake still attached the surface. Around the rust flake, in dark blue, one can also see indications of pitting.

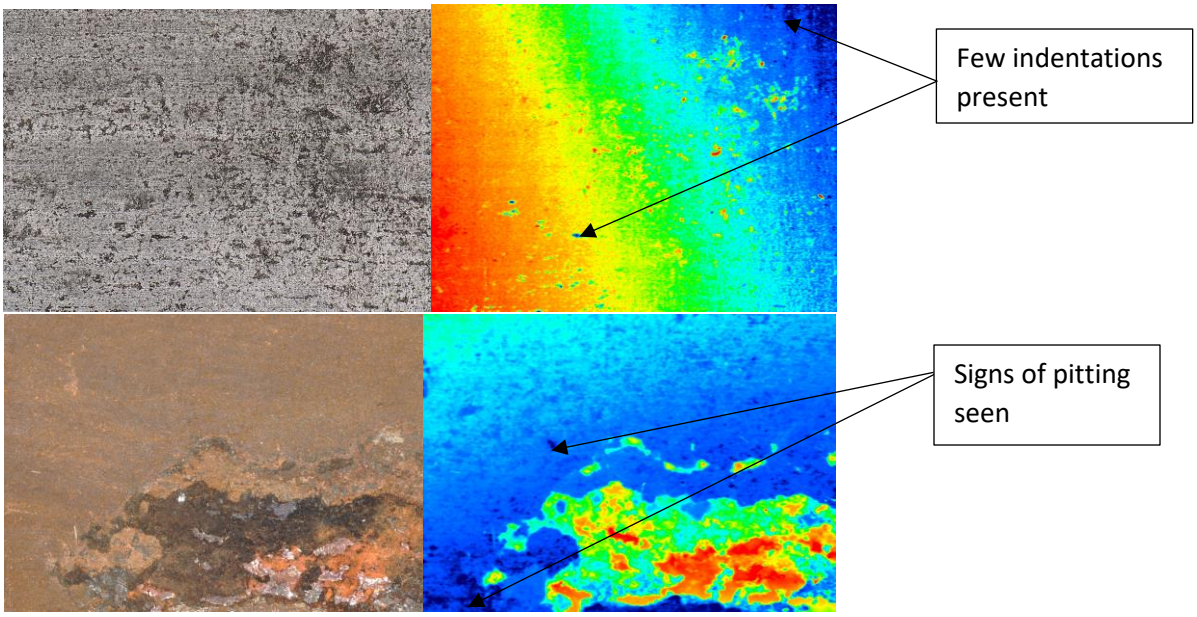


*Figure 4.10 above shows images of sample 10 (0.25-inch size) taken with Keyence measuring system before and after corrosion.*

Figure 4.11 shows four images of Sample 11. Unlike previous samples, not much evidence of machining defects is seen pre-corrosion. When looking at the corroded surface, there is a large defect in the top left corner of both the micrograph and the surface profile image. In the surface profile image, one can see it is a raised defect (indicated by red, orange, and yellow), that likely indicates the presence of a rust flake still attached the surface. Away from the rust flake, and towards the bottom center of the image, in dark blue, one can also see indications of pitting.

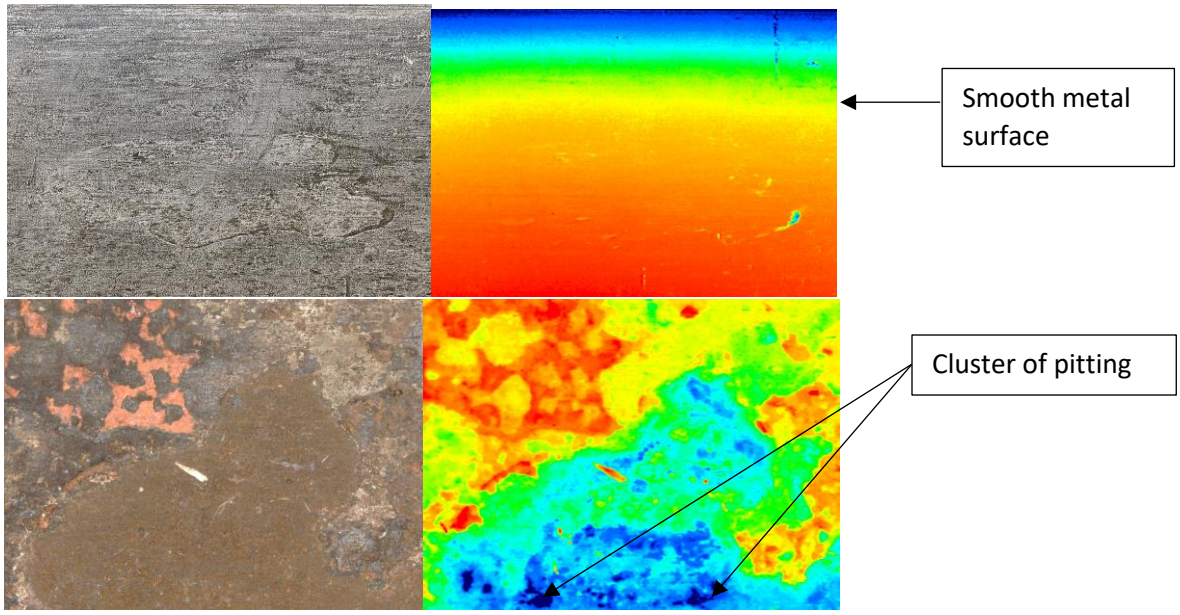


*Figure 4.11. above shows images of sample 11 (0.25-inch size) taken with Keyence measuring system before and after corrosion.*

Figure 4.12 shows four images of Sample 12. In Sample 12, the machining defects are seen, indicated as dark spots following a more linear pattern. Unlike the previous two samples, there are no large distinct defects present when looking at the micrograph. However, when looking at the surface profile image, there is a large indentation, indicated by dark blues, close to the left side of the image post-corrosion. This would be indicative of corrosion, likely pitting corrosion that then coalesced. It could have occurred along, or under, a rust flake, with the rust flake falling off before imaging.

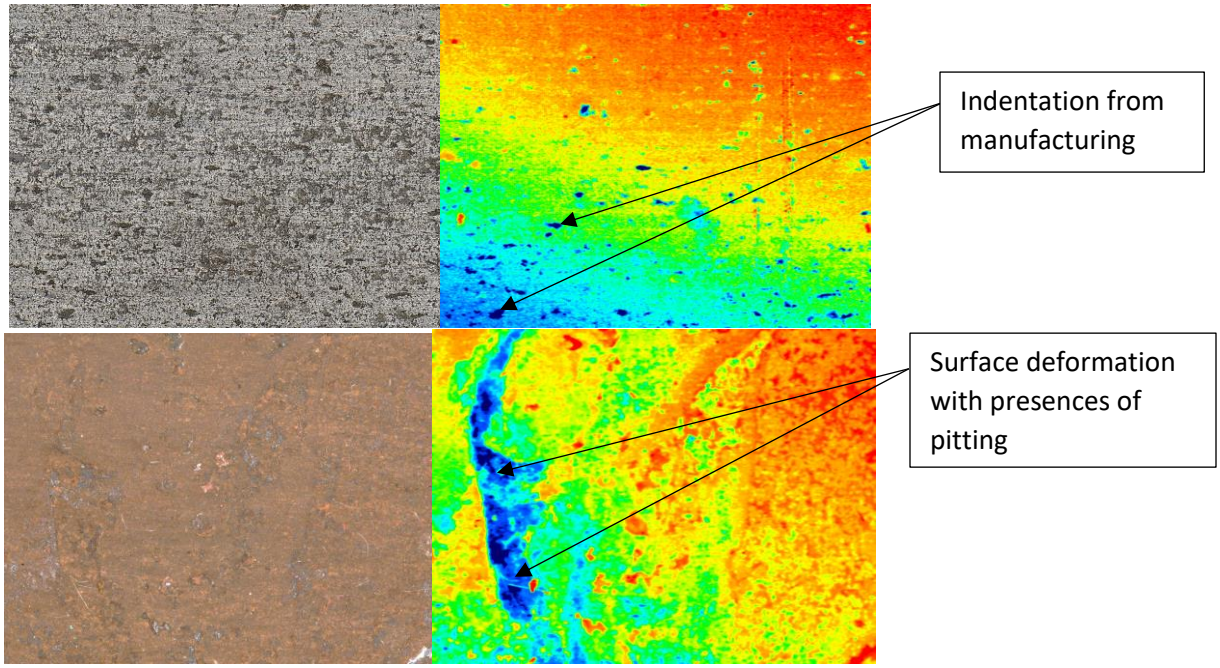


*Figure 4.12. above shows images of sample 12 (0.25-inch size) taken with Keyence measuring system before and after in immersed and dried.*

Figure 4.13 shows four images of Sample 3. Like most previous samples, machining defects are seen in the uncorroded surface, although these do not follow the linear pattern usually present with machining defects. When looking at the surface post-corrosion, one can see multiple medium gray areas on the micrograph, which match with light to medium blue areas in the surface profile image. There is also an area, to the right side of the surface profile image, that is in red, orange, and yellow, indicating height, which matches with a reddish-brown spot, indicative of a rust flake.

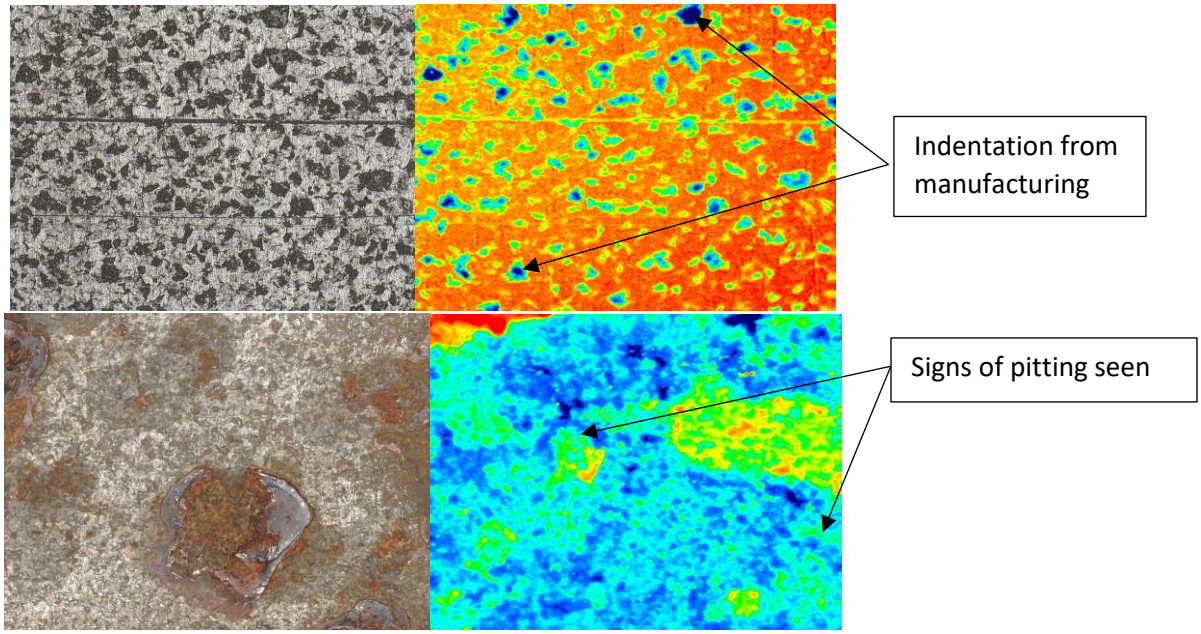


*Figure 4.13 above shows images of sample 3 (0.5-inch size) taken with Keyence measuring system before and after in immersed and dried.*

#### *4.2.2.3 Samples placed over NaCl Solution.*

Figure 4.14 shows four images of Sample 13. The linear defects common to machining defects are present here, like previous samples. Once again, as the environment changed, so did the behavior of the corroded surface. Looking at this surface, there is a reddish-orange spot on the micrograph to left side of the image, which matches with red, orange, and yellow on the surface profile image, indicative of rust formation. There are also signs of pitting around the rust formation, as indicated by the dark blue spots.

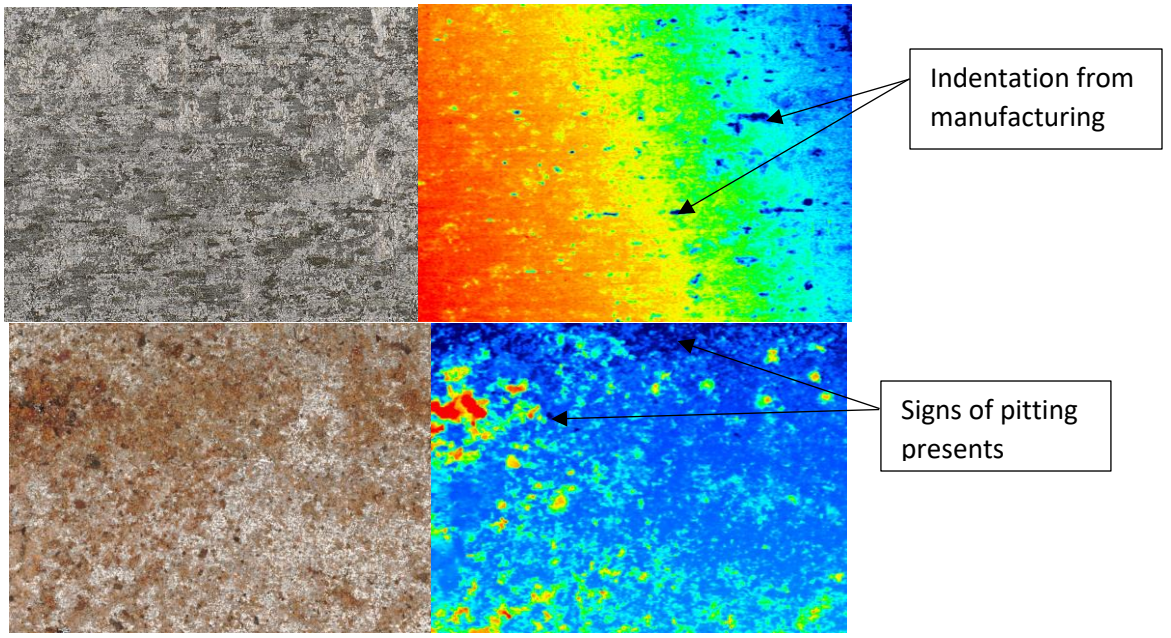


*Figure 4.14. above shows images of sample 13 (0.25-inch size) taken with Keyence measuring system before and after placed over NaCl solution.*

Figure 4.15 shows four images of Sample 14, indentation is seen on the profiling image, indicative of machining defects, on the uncorroded surface. As with the previous surface, there are multiple reddish-orange spots on the micrograph image that match with red, orange, and yellow spots, indicative of rust. There are also multiple dark blue spots, indicative of pitting, that also, surprisingly match up with other reddish-orange spots. This likely means the pits formed, but were wide enough that rust could then form inside.

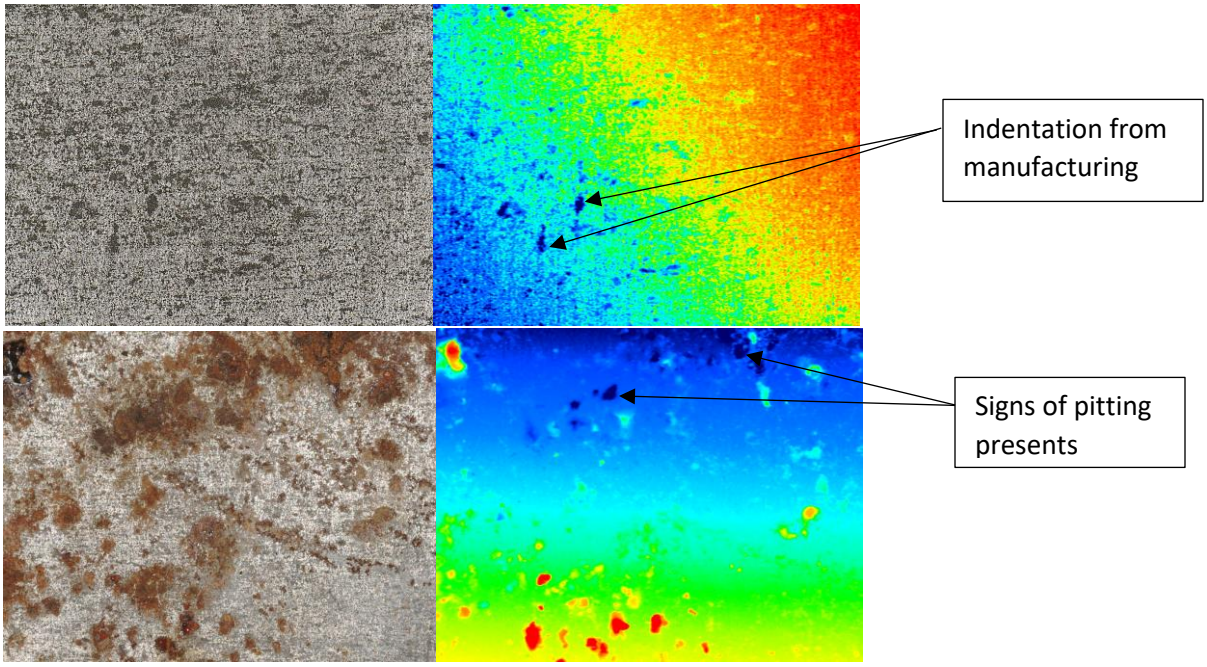


*Figure 4.15 above shows images of sample 14 (0.25-inch size) taken with Keyence measuring system before and after placed over NaCl solution.*

Figure 4.16 shows four images of Sample 15, where machining defects, shown as linear indentations, are seen on the images of the uncorroded surface. More reddish-brown areas are seen on this sample, now matching up with dark blue spots indicating pitting. As with the previous sample, this likely means the pits are very wide and rust could form within the pits.

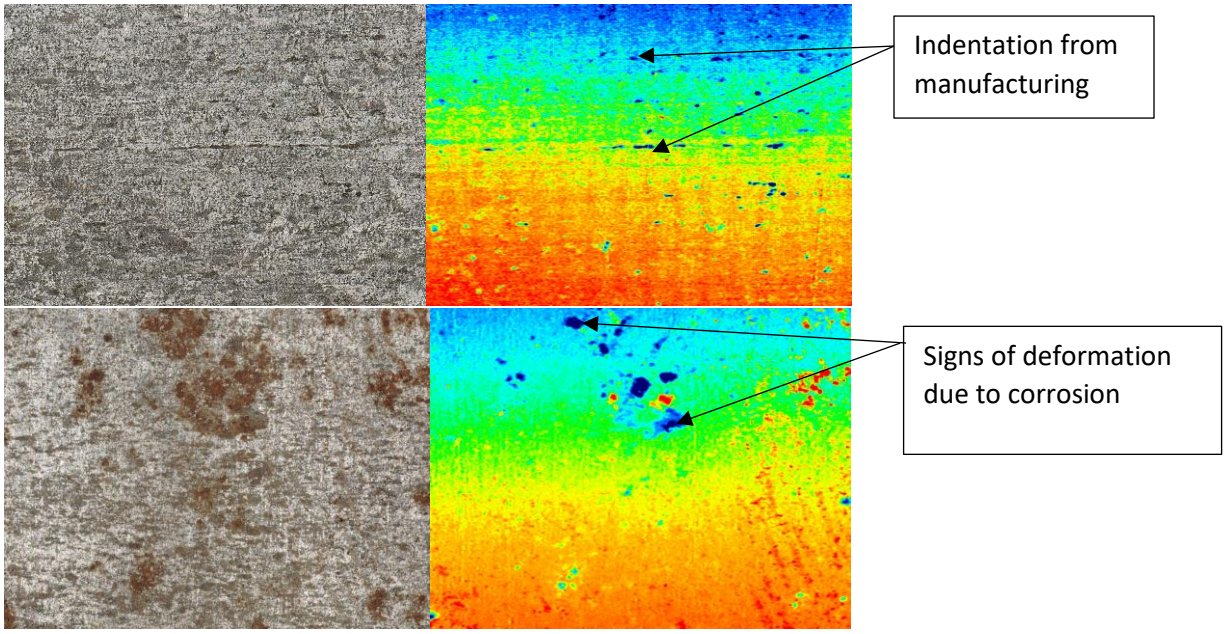


*Figure 4.16. above shows images of sample 15 (0.25-inch size) taken with Keyence measuring system before and after placed over NaCl solution.*

Figure 4.17 shows four images of Sample 5, with machining defects, indicated by linear defects in a dark blue color, are seen in both images of the uncorroded surface. As with the other three samples above the NaCl solution, there are scattered reddish-brown spots. Here, two of the spots matches with the red, orange, and yellow spot in the surface profile image, indicating the formation of a rust flake. The other spots either do not match with anything or match with pits, indicating that corrosion had just begun in these spots and had neither degraded into, nor formed oxides off of, the surface.

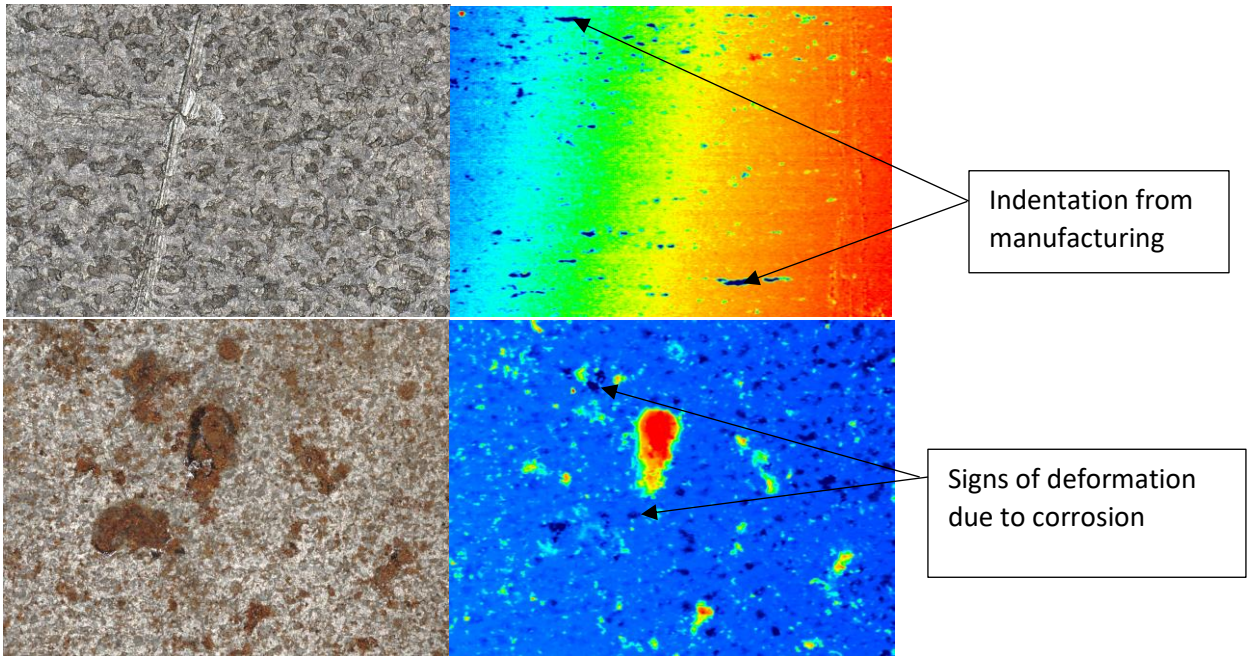


*Figure 4.17. above shows images of sample 5 (0.5-inch size) taken with Keyence measuring system before and after placed over NaCl solution.*

#### *4.2.2.4 Samples placed in wet dirt.*

Figure 4.18 shows four images of Sample 7, evidence of machining defects is seen in the micrograph, but a relatively smooth surface is seen on the profiling image of the uncorroded surface. This is likely due to the unlevelness of the sample, causing the red to blue across an angle. Once again, as the environment changed, so did the behavior of the corroded surface. Under the wet dirt, one can see a reddish-brown color across the entire surface in the micrograph. Looking at the surface profile image, though, one can see evidence of the formation of large pits, especially at the bottom of the image. There are also reds and oranges, which do not specifically match up to any features, and are likely dirt residuals.

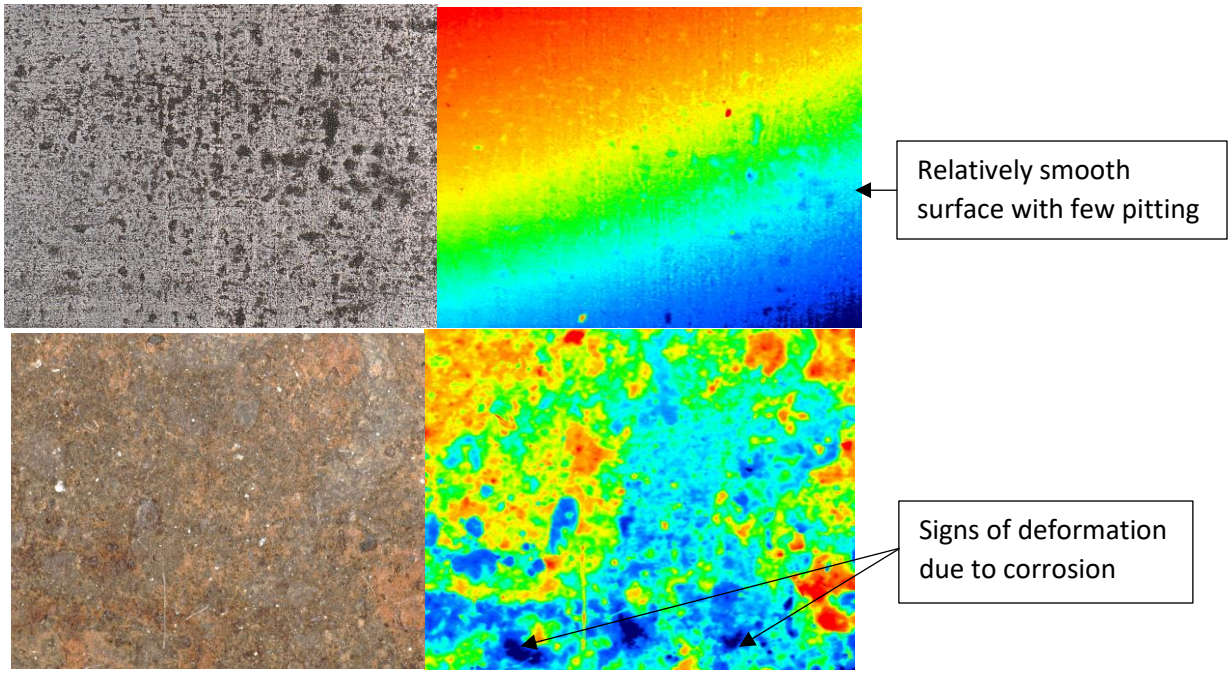


*Figure 4.18. above shows images of sample 7 (0.25-inch size) taken with Keyence measuring system before and after placed in wet dirt.*

Figure 4.19 shows four images of Sample 8, where, as with Sample 7, evidence of machining defects is seen in the micrograph, with only one large indentation seen on the profiling image of the uncorroded surface. Again, the red to blue across an angle occurs, indicating an unlevelness of the sample. As with the previous sample, one can see a reddish-brown color across the entire surface in the micrograph. Looking at the surface profile image, one can see evidence of the formation of large pits, scattered across the entire surface for Sample 8. There are also reds and oranges, which do not specifically match up to any features, and are likely dirt residuals.

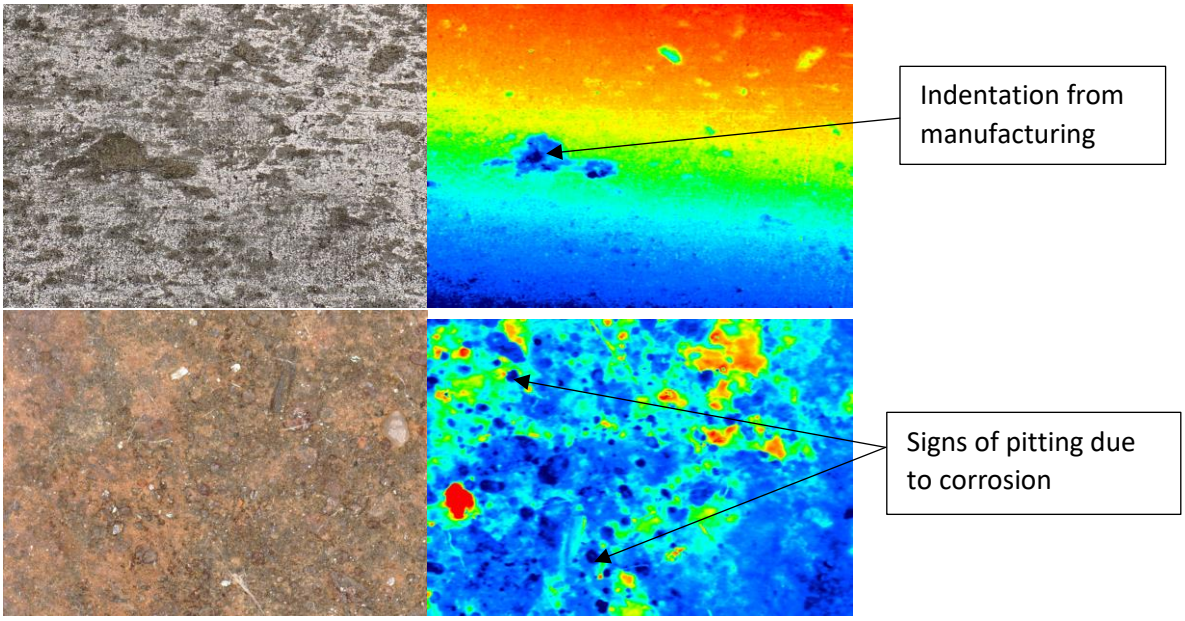


*Figure 4.19. above shows images of sample 8 (0.25-inch size) taken with Keyence measuring system before and after placed in wet dirt.*

Figure 4.20 shows four images of Sample 9, machining defects, in the formation of indentations in a linear formation, are seen on the profiling image of the uncorroded surface. The micrograph of the corroded surface of Sample 9 looks very similar to the micrographs of Samples 7 and 8, with a reddish-brown color across the entire surface. Very large pits, one near the top and one near the bottom, show up on the surface profile image, with the top pit matching with a patch of gray metal. Other pits are scattered across the surface, as are reds and oranges. Like the previous surfaces, the reds and oranges do not specifically match up to any features, and are likely dirt residuals.

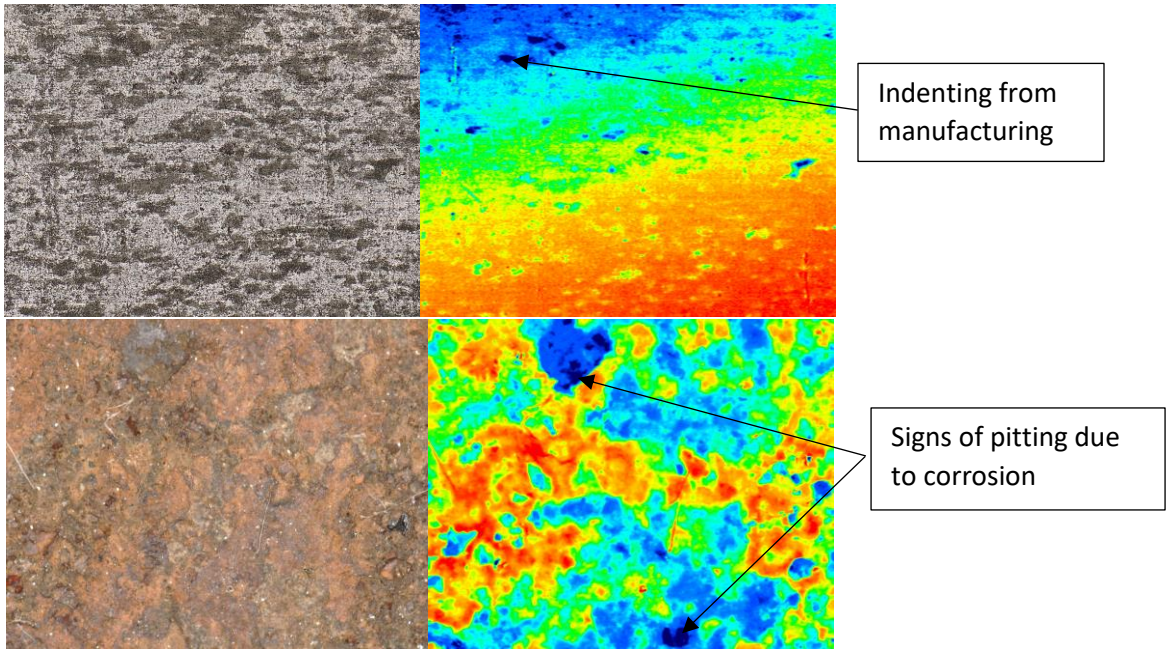


*Figure 4.20. above shows images of sample 9 (0.25-inch size) taken with Keyence measuring system before and after placed in wet dirt.*

Figure 4.21 shows four images of Sample 4, with minimal machining defects present in either the micrograph or the surface profile image of the uncorroded surface. When looking at the corroded surface, unlike Samples 7, 8, and 9, there is more gray present and less of the reddish-brown color. Comparing the micrograph with the surface profile image, one can see that the gray matches the light and dark blues, indicating fresh metal to begin corroding. The darker gray also matches up with the darker blue, indicating the likely formation of pits. Where the reddish-brown color is present, it matches with the reds and oranges present in the surface profile image, indicating the presence of either rust or dirt residuals.

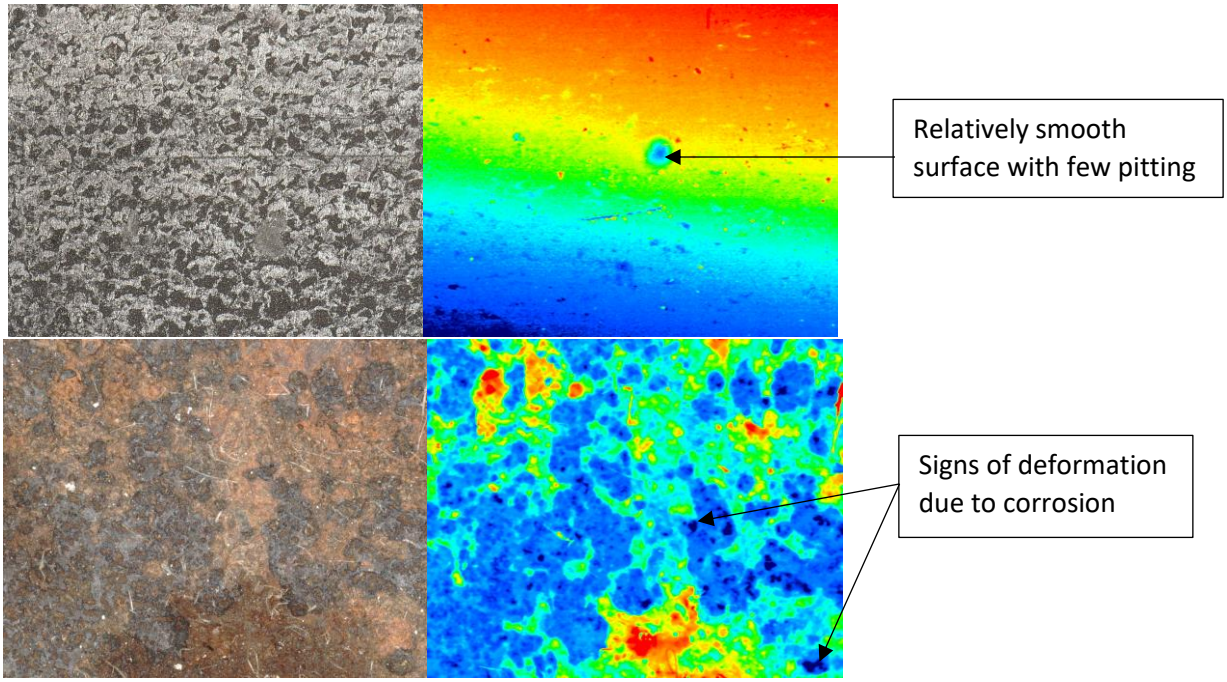


*Figure 4.21. above shows images of sample 4 (0.5-inch size) taken with Keyence measuring system before and after placed in wet dirt.*

## 4.3 Impedance measurement with Microsensor

This section presents the graphical representation of the impedance recorded using the microsensor. The impedance signatures of the corrosion specimen were measured using an impedance analyzer. AD5941 was used to measure the impedance through a frequency response with the data displayed on SensorPal [119] interface. To obtain the accurate impedance reading, choosing a suitable frequency range was significant. Hence, we first scanned a wide range of frequency (1 Hz-100 kHz). We observed the frequency response, and then a refined frequency range (1-1kHz) was selected because in the lower range more structural dynamics were presented and thus it is more evident to the presence of corrosion.

A trial-and-error method were used to refine the frequency range of 1 Hz and 1 kHz. The range was selected because it presents the highest frequency in the impedance signatures matching to the degree of corrosion of the specimen. The range with large peaks usually contains more dynamic interaction, and it is, therefore, more sensitive to damage [27]. Figure 4.22 shows impedance behavior of a frequency range of 0 to 65 Hz. It is revealed that for the metal coupons, the maximum values of impedance were recorded within the frequencies range of 10 to 20 Hz and, also, within 40 to 45 Hz. However, 11.755 Hz was found to be resonance frequency where Z=R (Z=impedance, R= resistance). Figure 4.22 to Figure 4.28 shows the weekly impedance recorded for the various samples in their environment.

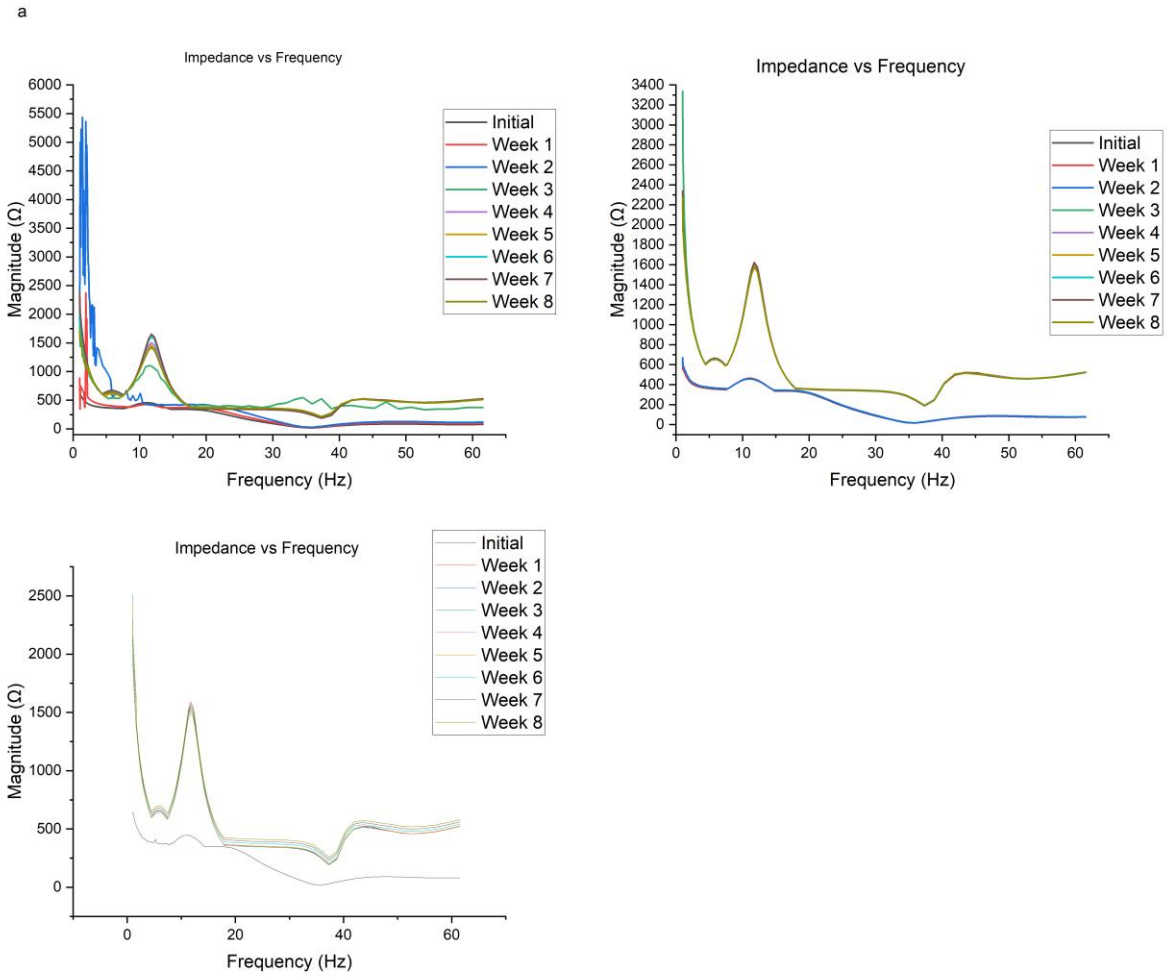


*Figure 4.22. shows impedance behavior of a frequency range of 0 to 65.*

It can be seen that for all three graphs in Figure 4.22 above, the impedance behavior is the same. It appears to increase within 10 Hz to 20Hz, steady from 20Hz until it reduces as it approaches 40Hz, and then increases from 40Hz to about 45Hz, where it finally becomes relatively steady. The same behavior was seen for all samples used for the experiment. The collected data revealed that the maximum impedance is at a resonance frequency of 11.755Hz where Z=R.

## 4.4 Impedance Vs weeks

To determine which week and environment gave the highest corrosion with the impedance measured. The graphs of impedance magnitude were plotted against weeks.

**Table 4.5. Shows impedance value of samples immersed in NaCl solution. Test done with samples in solution.**

| | At 11.755 Hz Frequency | | | | | | | | |
|---|---|---|---|---|---|---|---|---|---|
| | Initial | Week 1 | Week 2 | Week 3 | Week 4 | Week 5 | Week 6 | Week 7 | Week 8 |
| S1 | 453.295 | 406.804 | 430.655 | 1427.654 | 1610.519 | 1223.736 | 1353.323 | 1354.604 | 994.670 |
| S16 | 460.135 | 455.345 | 457.463 | 1417.913 | 1606.373 | 1325.073 | 1632.172 | 1371.648 | 1362.135 |
| S17 | 461.285 | 454.311 | 449.415 | 1609.925 | 1617.834 | 1443.110 | 1469.714 | 1257.945 | 1090.602 |
| S18 | 461.344 | 456.004 | 455.895 | 1405.891 | 1604.828 | 1313.405 | 1634.172 | 1460.343 | 1326.172 |

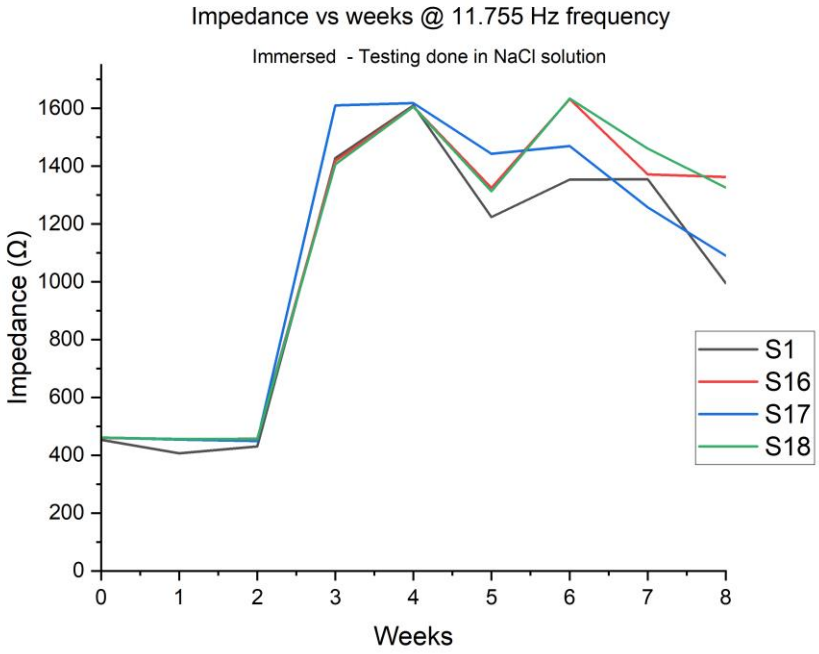


*Figure 4.23. shows impedance value of samples immersed in NaCl solution. Test done with samples in solution.*

For Table 4.5 and Figure 4.23, it is seen that the weekly impedance was recorded while samples were still immersed in the environment at the time of testing. Figure 4.23 shows the impedance on the y-axis and weeks on the x-axis, with each sample represented by a different color. Sample 1 (S1) is black, Sample 16 (S16) is red, Sample 17 (S17) is blue, and Sample 18 (S18) is green. For all samples, there is minimal change in the impedance prior to week two. Between week two

and week three, there is a large increase in the impedance. After week three, the impedance stays high, with some variation week-to-week.

**Table 4.6. Shows impedance value of samples immersed in NaCl. Test done with samples out of solution.**

| | At 11.755 Hz Frequency | | | | | | | | |
|---|---|---|---|---|---|---|---|---|---|
| | Initial | Week 1 | Week 2 | Week 3 | Week 4 | Week 5 | Week 6 | Week 7 | Week 8 |
| S1 | 453.295 | 406.804 | 430.655 | 1127.654 | 1230.519 | 1023.736 | 1353.323 | 1354.604 | 994.670 |
| S16 | 460.153 | 453.218 | 446.435 | 1601.561 | 1617.445 | 1438.871 | 1469.547 | 1267.244 | 1090.660 |
| S17 | 461.285 | 454.311 | 449.415 | 1609.925 | 1617.834 | 1443.110 | 1469.714 | 1257.945 | 1090.602 |
| S18 | 461.344 | 454.922 | 458.655 | 1605.338 | 1610.552 | 1313.532 | 1634.760 | 1392.953 | 1192.976 |

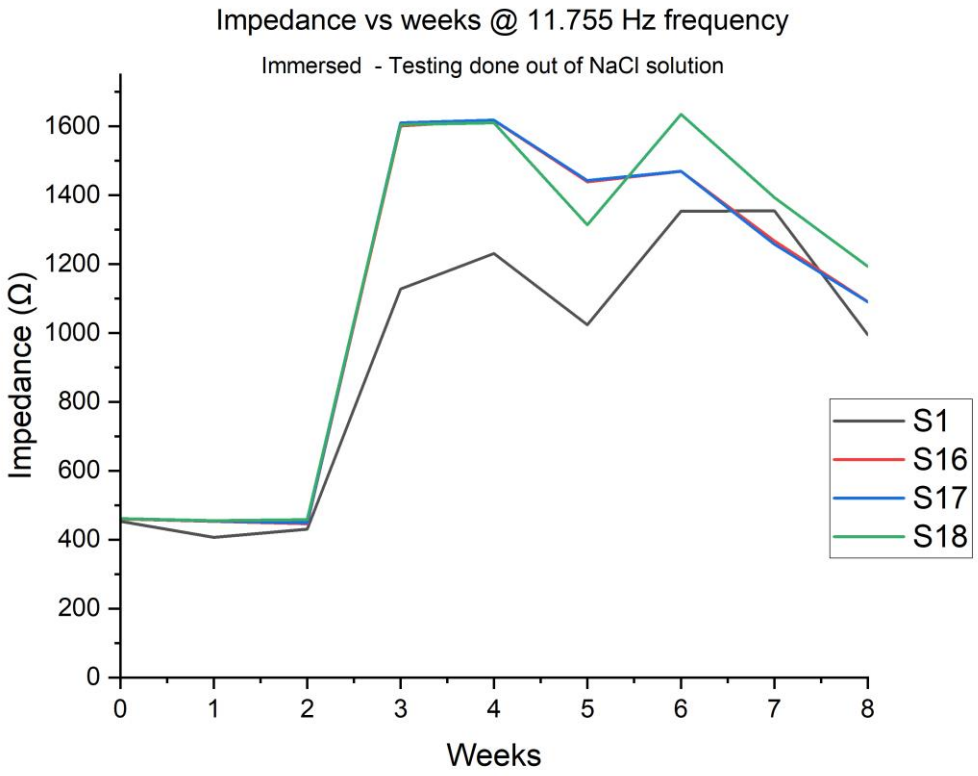


*Figure 4.24. shows impedance value of samples immersed NaCl in solution. Test done with samples out of solution.*

From Table 4.6 and Figure 4.24, it is seen that the weekly impedance was recorded while samples from the immersed environment were exposed to air at the time of testing. This was to account for differences that the presence of the saltwater environment may have on the reading. Figure

4.24 shows the impedance on the y-axis and weeks on the x-axis, with each sample represented by a different color. Sample 1 (S1) is black, Sample 16 (S16) is red, Sample 17 (S17) is blue, and Sample 18 (S18) is green. For all samples, there is minimal change in the impedance prior to week two. Between week two and week three, there is a large increase in the impedance. After week three, the impedance stays high, with some variation week-to-week. The environment does have a slight effect, with the samples in the environment having impedance readings roughly 100 Ω higher than the impedance readings taken in air.

**Table 4.7 Shows impedance value of samples in immersed and dry.**

| | At 11.755 Hz Frequency | | | | | | | | |
|---|---|---|---|---|---|---|---|---|---|
| | Initial | Week 1 | Week 2 | Week 3 | Week 4 | Week 5 | Week 6 | Week 7 | Week 8 |
| S10 | 458.134 | 457.126 | 452.389 | 1624.826 | 1824.666 | 1696.264 | 1576.270 | 1621.547 | 1576.071 |
| S11 | 456.120 | 781.523 | 454.851 | 667.570 | 6835.700 | 2711.013 | 1686.125 | 1400.079 | 1950.006 |
| S12 | 442.115 | 439.849 | 431.130 | 1408.722 | 1894.610 | 1752.958 | 1432.946 | 1402.544 | 1137.970 |
| S3 | 458.010 | 453.987 | 451.826 | 1556.817 | 1807.446 | 1678.722 | 1426.917 | 1621.188 | 1570.764 |

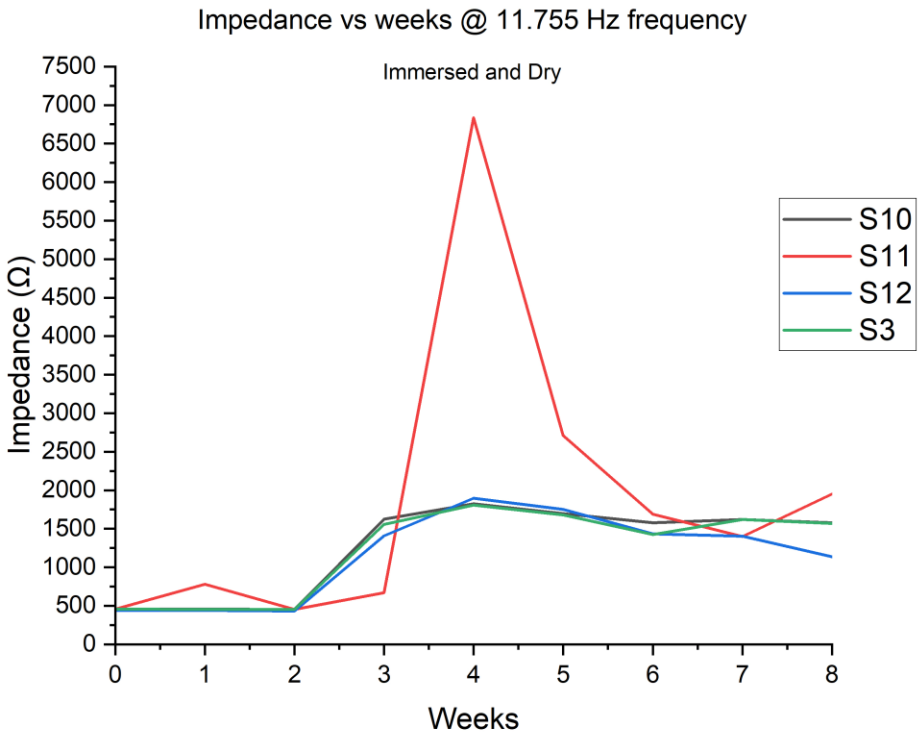


*Figure 4.25. shows impedance value of samples in immersed and dry.*

From Table 4.7 and Figure 4.25, the impedance recorded for the various samples from the immersed and dried environment is shown as recorded for each week. Figure 4.25 shows the impedance on the y-axis and weeks on the x-axis, with each sample represented by a different color. Sample 10 (S10) is black, Sample 11 (S11) is red, Sample 12 (S12) is blue, and Sample 3 (S3) is green. For all samples, there is minimal change in the impedance prior to week two. Between week two and week three, there is a large increase in the impedance, especially for Sample 11. Sample 11 is seen to have extremely high impedance then the other samples, indicative of a possible discontinuity. After week three, the impedance stays high, with some variation week-to-week, with the exception of Sample 11. With Sample 11, after week 4, the impedance drops, indicating that the discontinuity may have been removed, before it becomes similar to the other samples at week six.

**Table 4.8. Shows impedance value of samples placed over solution.**

| | At 11.755 Hz Frequency | | | | | | | | |
|---|---|---|---|---|---|---|---|---|---|
| | Initial | Week 1 | Week 2 | Week 3 | Week 4 | Week 5 | Week 6 | Week 7 | Week 8 |
| S13 | 461.049 | 453.724 | 399.928 | 1319.824 | 1562.094 | 1189.593 | 1477.784 | 1118.198 | 1589.780 |
| S14 | 460.102 | 457.200 | 451.895 | 1613.614 | 1616.688 | 1391.858 | 1597.735 | 1485.627 | 1648.127 |
| S15 | 450.980 | 425.605 | 405.229 | 1562.588 | 1389.323 | 1297.319 | 1296.941 | 1580.588 | 1245.706 |
| S5 | 450.057 | 416.991 | 416.755 | 1096.000 | 1506.528 | 1460.124 | 1611.307 | 1651.211 | 1418.213 |

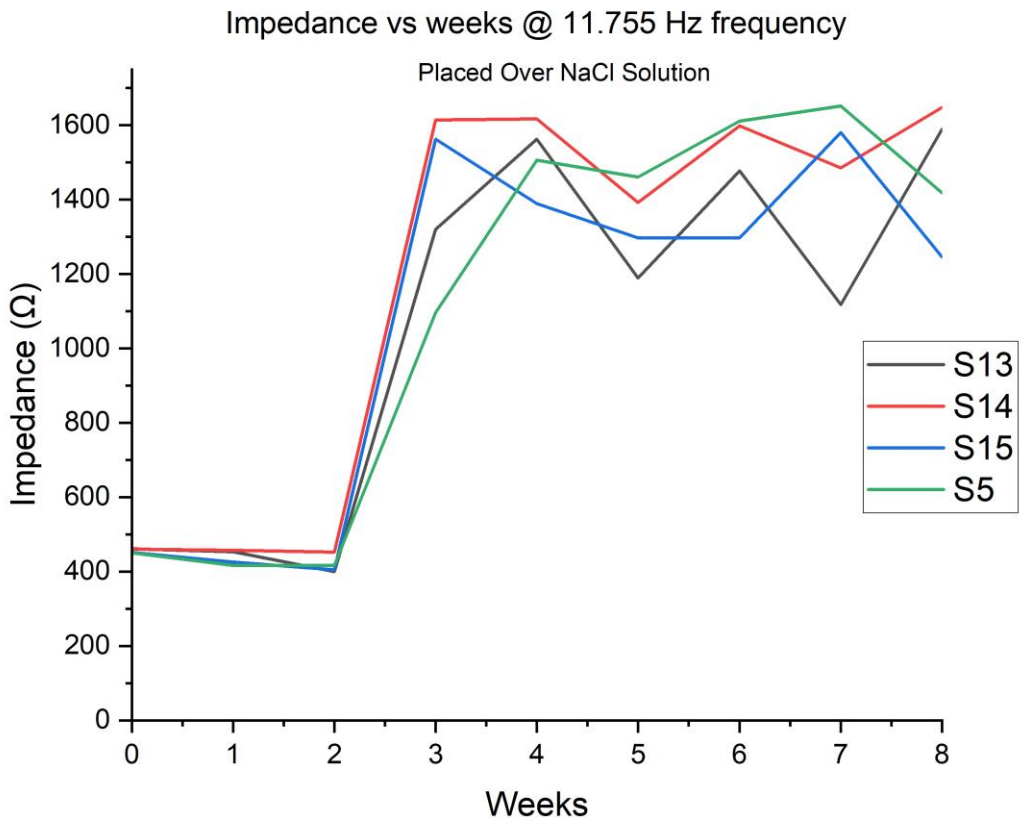


*Figure 4.26. shows impedance value of samples placed over water.*

From Table 4.8 and Figure 4.26, the impedance recorded for the various samples placed over NaCl solution is shown as recorded for each week. Figure 4.26 shows the impedance on the y-axis and weeks on the x-axis, with each sample represented by a different color. Sample 13 (S13) is black, Sample 14 (S14) is red, Sample 15 (S15) is blue, and Sample 5 (S5) is green. For all samples, there is minimal change in the impedance prior to week two. Between week two and

week three, there is a large increase in the impedance. After week three, the impedance stays high, with some variation week-to-week.

**Table 4.9 Shows impedance value of samples buried under wet dirt. Test done with sample out of dirt.**

| | At 11.755 Hz Frequency | | | | | | | | |
|---|---|---|---|---|---|---|---|---|---|
| | Initial | Week 1 | Week 2 | Week 3 | Week4 | Week 5 | Week 6 | Week 7 | Week 8 |
| S7 | 456.624 | 1597.965 | 956.327 | 18459.352 | 17459.352 | 1123.415 | 1223.415 | 3763.283 | 4763.283 |
| S8 | 450.834 | 1604.211 | 1324.249 | 1967.051 | 2256.070 | 1629.874 | 1631.163 | 1614.485 | 1619.726 |
| S9 | 459.980 | 1605.721 | 1519.962 | 1998.726 | 2005.901 | 1308.377 | 1269.810 | 1530.614 | 1445.590 |
| S4 | 440.794 | 1578.867 | 1562.861 | 1891.458 | 2078.134 | 1392.981 | 1446.907 | 1629.437 | 1626.690 |

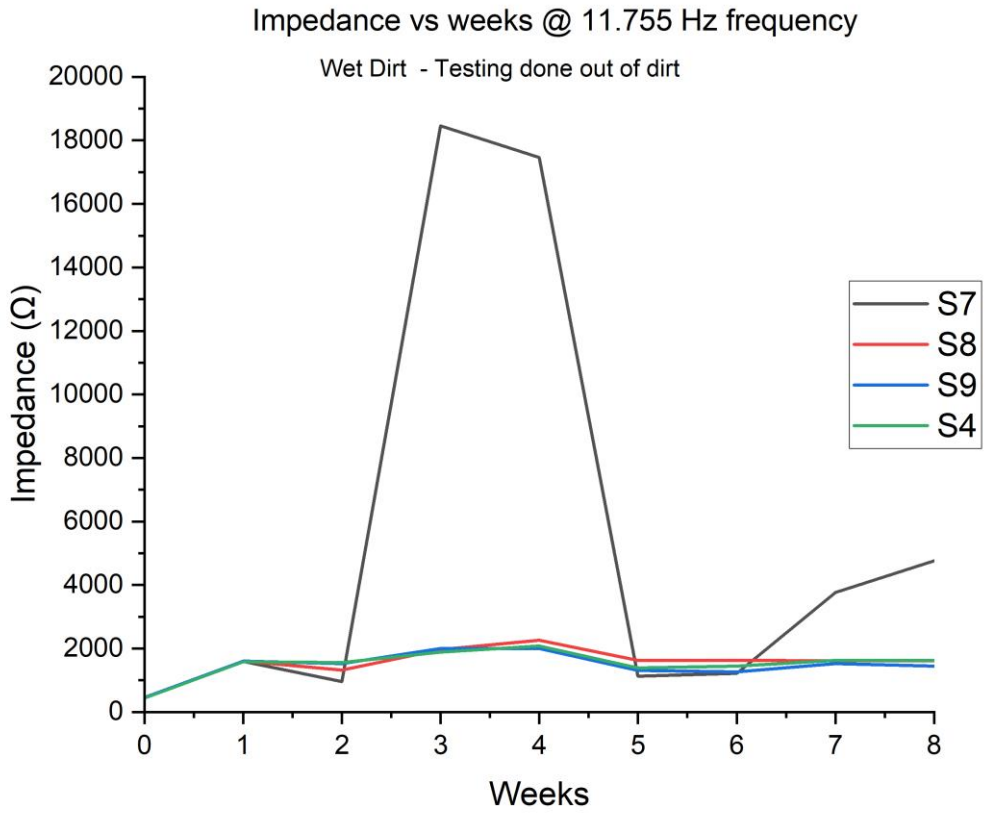


*Figure 4.27. shows impedance value of samples buried under wet dirt. Test done with sample out of dirt*

From Table 4.9 and Figure 4.27, the impedance recorded for samples buried under wet dirt was done while samples were exposed to air at the time of testing. Figure 4.27 shows the impedance on the y-axis and weeks on the x-axis, with each sample represented by a different color. Sample

7 (S7) is black, Sample 8 (S8) is red, Sample 9 (S9) is blue, and Sample 4 (S4) is green. For all samples, there is minimal change in the impedance prior to week two. Between week two and week three, there is a large increase in the impedance, especially for Sample 7. Sample 7 is seen to have extremely high impedance then the other samples, indicative of a possible discontinuity. After week three, the impedance stays high, with some variation week-to-week, with the exception of Sample 7. With Sample 7, after week 4, the impedance drops, indicating that the discontinuity may have been removed, before it becomes similar to the other samples at week five, before increasing after week six.

**Table 4.10. Shows impedance value of samples buried under wet dirt. Test done with sample in wet dirt.**

| | At 11.755 Hz Frequency | | | | | | | | |
|---|---|---|---|---|---|---|---|---|---|
| | Initial | Week 1 | Week 2 | Week 3 | Week 4 | Week 5 | Week 6 | Week 7 | Week 8 |
| S7 | 456.624 | 1448.928 | 1026.603 | 17656.36 | 16656.359 | 946.307 | 446.3073 | 3763.283 | 3863.283 |
| S8 | 450.834 | 1569.615 | 1914.691 | 1910.909 | 1950.843 | 1454.876 | 1054.335 | 1553.998 | 1625.563 |
| S9 | 459.980 | 1543.048 | 1967.526 | 1945.095 | 1953.708 | 1143.834 | 1011.232 | 1475.545 | 1158.375 |
| S4 | 440.794 | 1578.867 | 1862.324 | 1891.458 | 1999.133 | 1392.985 | 1446.907 | 1629.437 | 1626.688 |

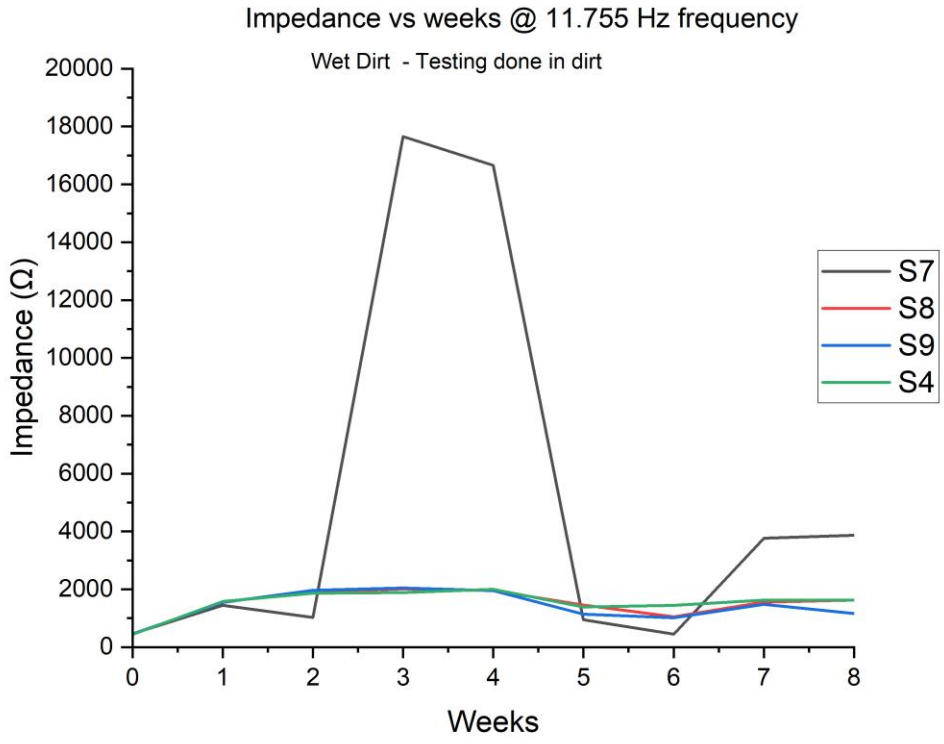


*Figure 4.28. shows impedance value of samples buried under wet dirt. Test done with sample in wet dirt*

From Table 4.10 and Figure 4.28, the impedance recorded for samples buried under wet dirt environment was done while samples were buried under the wet dirt time of testing. Figure 4.28 shows the impedance on the y-axis and weeks on the x-axis, with each sample represented by a different color. Sample 7 (S7) is black, Sample 8 (S8) is red, Sample 9 (S9) is blue, and Sample 4 (S4) is green. For all samples, there is minimal change in the impedance prior to week two. Between week two and week three, there is a large increase in the impedance, especially for Sample 7. Sample 7 is seen to have extremely high impedance then the other samples, indicative of a possible discontinuity. After week three, the impedance stays high, with some variation week-to-week, with the exception of Sample 7. With Sample 7, after week 4, the impedance drops, indicating that the discontinuity may have been removed, before it becomes similar to the

other samples at week five before increasing after week six. The environment does have a slight effect, with the samples in the environment having impedance readings roughly 200 Ω less than the impedance readings taken in air.

## 4.5 Corrosion of the metal pipe.

Figures 4.29 through 4.33 show of images of metal pipe exposed to one of two corrosive environments. From the results of the metal coupons, the two most corrosive environments were determined to be the immersed then dried environment and the wet dirt environment. Figures 4.29 through 4.31 show images of samples used in the immersion and dried environment, while Figures 4.32 through 4.33 show images of samples used in the wet dirt environment.

Figure 4.29 below shows external corrosion of sample placed in immersed and dried environment. Looking at this figure, one can see dark brown coloration with distinct orange-reddish spots.

*Figure 4.29. showing image of external corrosion of the three-metal pipe after the 8 weeks period.*

Figure 4.30 below shows the side of one pipe from the immersed and dried environment. External corrosion of sample is clear, with mostly dark brown discoloration and with orange-reddish spots clearly present on the sides.

*Figure 4.30. showing a closer look at the external corrosion of the metal pipe after the 8 weeks period.*

Figure 4.31 below shows internal corrosion of sample placed in immersed and dried environment. As with the external images, a dark brown discoloration appears around and inside the pipe hole. On the cut end of the pipe, there are also distinct orange-reddish spots. When looking inside the pipe, once can see a long line of the same orange-reddish color along the bottom of the pipe, which occurred from the water sitting and corroding before evaporating.

*Figure 4.31. showing a closer look at the internal corrosion of the metal pipe after the 8 weeks period.*

Figure 4.32 shows the external corrosion of samples. When looking at Figure 4.32, one should notice the distinct removal of material on the bottom (left) side of the pipe, with other patchy spots of corrosion closer the top of the pipe. In addition, the red-orange discoloration of rust is also present.

*Figure 4.32. show metal buried under wet dirt wearing due to corrosion.*

Figure 4.33 shows the internal corrosion of one of the pipes buried under wet dirt. There is some color change inside the pipe, although not as distinctly clear as the immersed then dried sample. Around the cut edge, though, there is the distinct appearance of the formation of small holes (right side, center), as well as the presence of the red-orange color of rust.

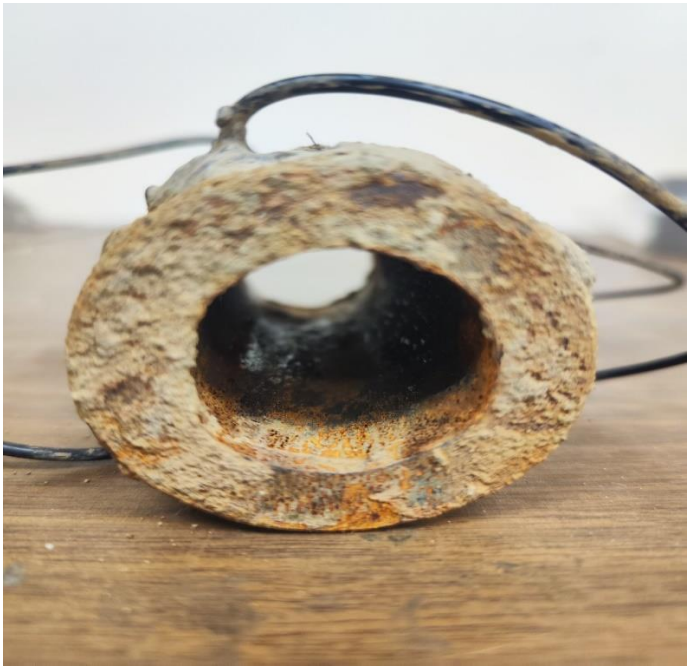

*Figure 4.33. shows internal corrosion of metal buried under wet dirt.*

### 4.5.1 Impedance measurement for Metal Pipe.

As already mentioned in Chapter 1, the purpose of the metal pipe corrosion in this project was to determine if impedance measurement will be affected by the metal orientation. Figure 4.34 through Figure 4. 37 show graphs of impedance vs weeks plotted for the metal pipe.

**Table 4.11 weekly impedance values for samples immersed and dried, values used to plot figure 4.34. Connection done across pipe.**

| | At 54.622 Hz frequency | | | | | | | | |
|---|---|---|---|---|---|---|---|---|---|
| | initial | Week 1 | Week 2 | Week 3 | Week 4 | Week 5 | Week 6 | Week 7 | Week 8 |
| S7 | 83.710 | 458.984 | 1486.347 | 1586.347 | 1773.375 | 1639.547 | 1447.969 | 1339.547 | 927.969 |
| S8 | 78.540 | 447.3733 | 1428.986 | 1528.986 | 1747.969 | 1647.969 | 1462.938 | 1242.969 | 877.047 |
| S9 | 85.960 | 487.7334 | 1479.188 | 1579.188 | 1729.547 | 1639.547 | 1399.047 | 1379.188 | 924.969 |

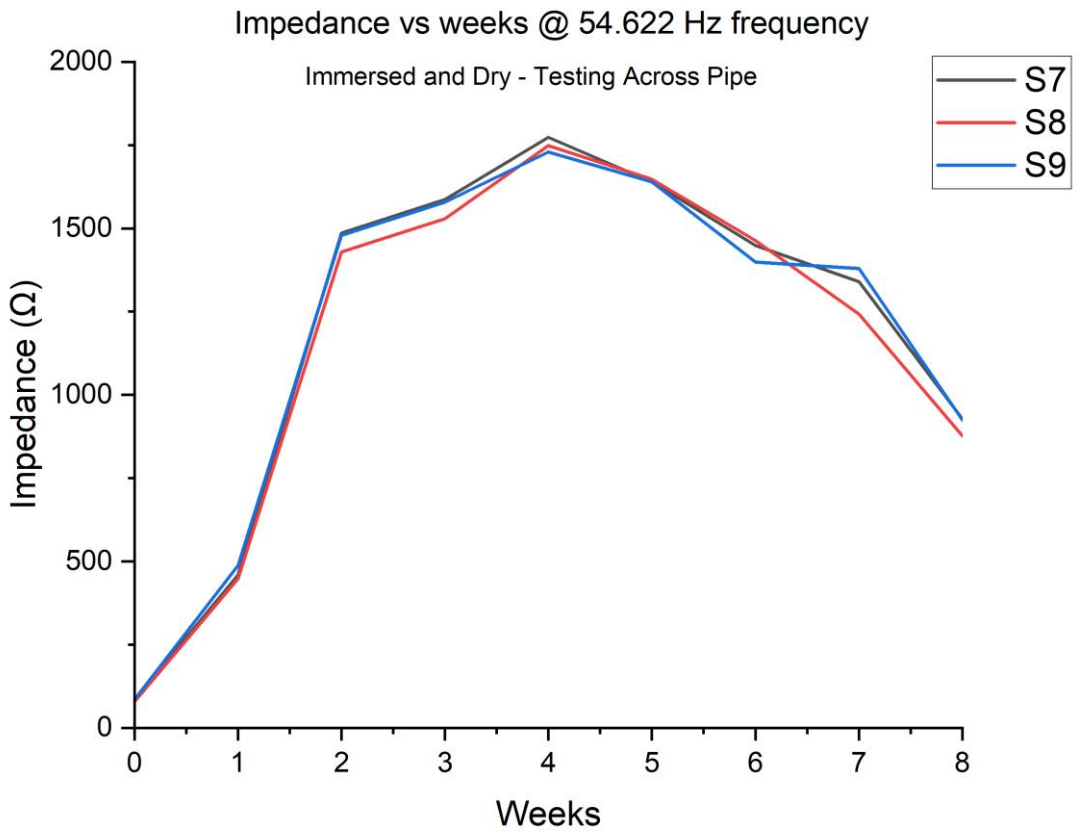


*Figure 4.34. Graph of impedance vs weeks for samples immersed and dried. Connection done across pipe.*

From Table 4.11 and Figure 4.34, the impedance recorded for the various samples from the immersed and dried environment is shown as recorded for each week. Table 4.11 and Figure 4.34 were created from testing done with the wire connected across the length of the pipe. Figure 4.34 shows the impedance on the y-axis and weeks on the x-axis, with each sample represented

by a different color. Sample 7 (S7) is black, Sample 8 (S8) is red, and Sample 9 (S9) is blue. From the beginning, there is an increase in impedance until week four, followed by a gradual decrease.

**Table 4.12. Weekly impedance vales for samples immersed and dried, values used to plot figure 4.35. Connection done around pipe.**

| | At 54.622 Hz frequency | | | | | | | | |
|---|---|---|---|---|---|---|---|---|---|
| | initial | Week 1 | Week 2 | Week 3 | Week 4 | Week 5 | Week 6 | Week 7 | Week 8 |
| S7 | 79.046 | 459.745 | 1456.265 | 1536.135 | 1736.374 | 1621.875 | 1415.965 | 1139.547 | 916.768 |
| S8 | 79.445 | 444.237 | 1443.986 | 1532.563 | 1724.851 | 1672.880 | 1426.938 | 1247.969 | 877.047 |
| S9 | 78.254 | 486.763 | 1442.752 | 1542.416 | 1752.615 | 1682.675 | 1400.047 | 1279.188 | 924.969 |

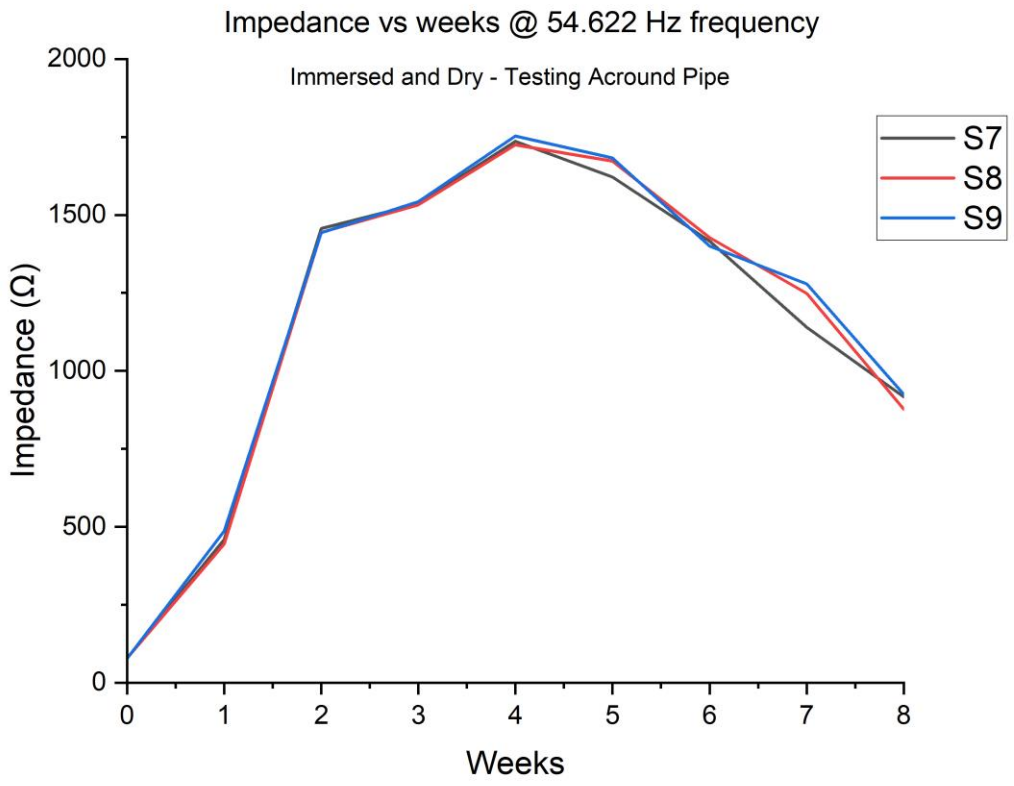


*Figure 4.35. Graph of impedance vs weeks for samples immersed and dried. Connection done around pipe.*

From Table 4.12 and Figure 4.35, the impedance recorded for the various samples from the immersed and dried environment is shown as recorded for each week. Table 4.12 and Figure 4.35 were created from testing with the wire connected around the pipe. Figure 4.35 shows the

impedance on the y-axis and weeks on the x-axis, with each sample represented by a different color. Sample 7 (S7) is black, Sample 8 (S8) is red, and Sample 9 (S9) is blue. From the beginning, there is an increase in impedance until week four, followed by a gradual decrease. When comparing across the pipe with around the pipe, the impedance measurements across the pipe are roughly 100 Ω higher than around the pipe, indicating orientation does not have a large impact on impedance.

**Table 4.13. Weekly impedance vales for samples buried wet dirt, values used to plot figure 4.36. Connection done across pipe.**

| | At 54.622 Hz frequency | | | | | | | | |
|---|---|---|---|---|---|---|---|---|---|
| | initial | Week 1 | Week 2 | Week 3 | Week 4 | Week 5 | Week 6 | Week 7 | Week 8 |
| S4 | 78.814 | 498.845 | 1585.618 | 1679.517 | 1872.735 | 1710.754 | 1533.969 | 1381.465 | 961.828 |
| S5 | 79.408 | 597.536 | 1579.987 | 1677.257 | 1883.310 | 1701.965 | 1534.938 | 1373.975 | 968.369 |
| S6 | 79.129 | 511.013 | 1587.568 | 1676.584 | 1878.615 | 1708.658 | 1537.688 | 1377.755 | 953.349 |

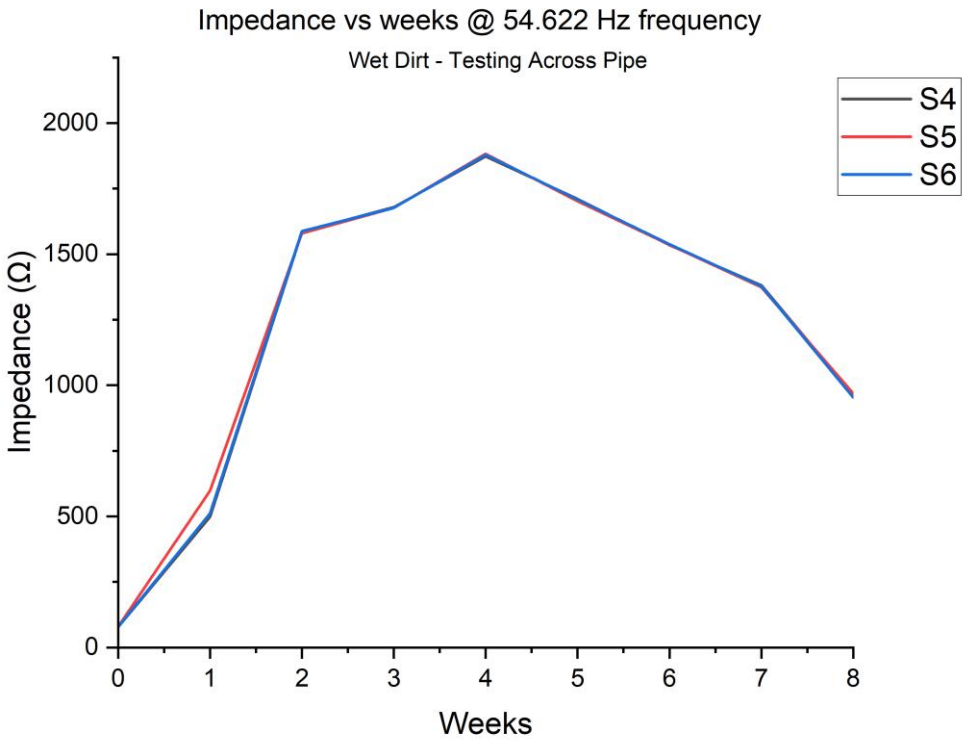


*Figure 4.36. Graph of impedance vs weeks for samples buried in wet dirt. Connection done across pipe.*

From Table 4.13 and Figure 4.36, the impedance recorded for samples buried under wet dirt was done while samples were exposed to air at the time of testing. Table 4.13 and Figure 4.36 were created from testing with the wire connected across the length of the pipe. Figure 4.36 shows the impedance on the y-axis and weeks on the x-axis, with each sample represented by a different color. Sample 4 (S4) is black, Sample 5 (S5) is red, and Sample 6 (S6) is blue. From the beginning, there is an increase in impedance until week four, followed by a gradual decrease.

**Table 4.14. Weekly impedance vales for samples buried wet dirt, values used to plot figure 4.37. Connection done around pipe.**

| | At 54.622 Hz frequency | | | | | | | | |
|---|---|---|---|---|---|---|---|---|---|
| | initial | Week 1 | Week 2 | Week 3 | Week 4 | Week 5 | Week 6 | Week 7 | Week 8 |
| S4 | 78.141 | 499.9785 | 1545.427 | 1659.517 | 1873.735 | 1713.875 | 1523.969 | 1390.547 | 962.767 |
| S5 | 78.410 | 517.7536 | 1544.57 | 1663.257 | 1885.31 | 1699.988 | 1534.938 | 1343.969 | 974.046 |
| S6 | 85.0908 | 501.0127 | 1544.176 | 1654.584 | 1846.615 | 1702.466 | 1507.688 | 1327.475 | 941.968 |

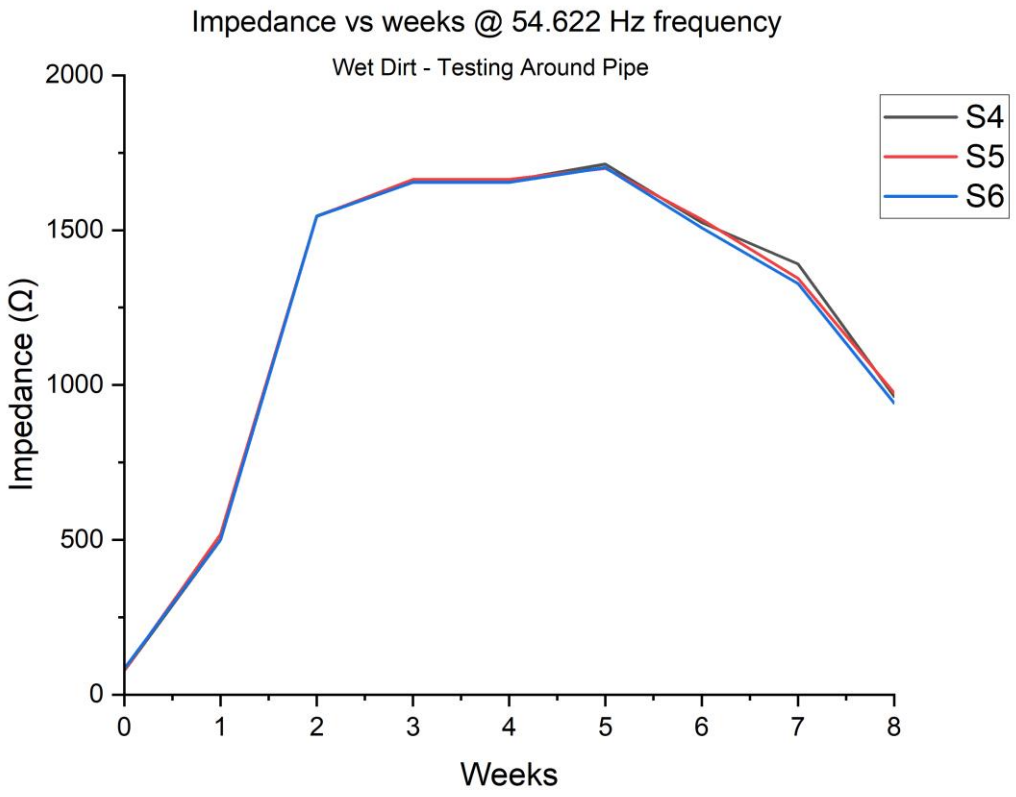


*Figure 4.37. Graph of impedance vs weeks for samples buried in wet dirt. Connection done around pipe.*

Table 4.14 and Figure 4.37 show the impedance recorded for samples buried under wet dirt, which was collected with the samples exposed to air at the time of testing. Table 4.14 and Figure 4.37 were created from testing with the wire connected across the length of the pipe. Figure 4.37 shows the impedance on the y-axis and weeks on the x-axis, with each sample represented by a different color. Sample 4 (S4) is black, Sample 5 (S5) is red, and Sample 6 (S6) is blue. From the beginning, there is an increase in impedance until week four, followed by a gradual decrease. When comparing across the pipe with around the pipe, the impedance measurements across the pipe are less than 50 Ω higher than around the pipe, indicating orientation does not have a large impact on impedance.

## 4.6 Discussion

Table 4.1 through Table 4.4 show the initial and final weight of samples measured and their respective weight loss. This weight loss method applied only to the metal coupons used for the four different environments. The results shown in Table 4.1 occur because of an iron oxide, likely $Fe_2O_3$, formed during corrosion, which is eventually lost to solution, as it does not strongly adhere to the metal surface when in water. In addition, in the immersion solution, small, black material was seen collecting on the bottom of the container, indicative of the formation of FeO, a different type of iron oxide. The results in Table 4.2 are because of formation of an iron oxide as a result of corrosion. This iron oxide, likely $Fe_2O_3$, forms very large crystalline structures as compared to the base iron metal when exposed to air. As it grows in thickness, it easily flakes off, leading to mass loss. The results in Table 4.3 shows that not much material was lost due to corrosion even though corrosion occurred. As with the immersed then dried, $Fe_2O_3$ formed, as indicated by the red rust formation. However, as this oxide could only grow as the water below it evaporated, its effect was quite minimal to cause loss of material. The results in Table 4.4 could be similar to the results in the immersion environment, where FeO formed instead of $Fe_2O_3$. These stayed attached to the surface, instead of falling off, unlike the immersion environment. In addition, the adherence of dirt particle on the metal samples in this environment that were not removed during cleaning, could have affected the weight loss. Between the formation and adherence of FeO and the adherence of the dirt, minimal weight loss occurred. This is further confirmed by the presence of pitting, which does not cause a great amount of weight loss to begin with but is a very destructive form of corrosion.

When looking at Figure 4.2, the samples immersed in the NaCl solution and especially as compared to Figure 4.1, as mentioned previously, the oxide appeared to be in powdered form on the metal surface, as well as no physical deformation occurring. This is because the initial oxide formed on the metal surface is lost to the solution, revealing a new surface for new oxide formation, which is also eventually lost to the solution. The oxide does not remain on the surface, as it is weakly adhered to the metal, and confirms the weight loss results seen previously. Figure 4.3 shows images of the metal coupons immersed in NaCl solution and then dried. Here, the weak oxide that formed on the surface of the metals, as shown in the reddish color, easily flakes off, as previously mentioned. That flaking can take a decent amount of metal with it, resulting in the weight loss seen in Table 4.2. Figure 4.4 shows the images of metal coupons placed over NaCl solution. Not much brown or reddish discoloration is seen, which demonstrates that there was less formation of an oxide on the metal surface as compared to the metal coupons immersed in NaCl solution and then dried. This is further confirmed by looking at Table 4.3, where the weight loss is minimal. As previously mentioned, the only real way to get corrosion in this environment was for the water in NaCl solution to evaporate and condense on the metal, with the reaction being minimal. Figure 4.5 shows the images of the metal coupons buried in wet dirt after 8 weeks. Here, the metal surface is mostly covered with the dirt mix, where images of the oxide formed cannot be seen. Between the formation of an oxide, which is likely still attached, and the dirt that adhered to the surface, even after gently cleaning, the images demonstrate why there was a minimal weight loss with these samples, as shown in Table 4.4.

### 4.6.1 Keyence Imaging of samples immersed in NaCl solution

Figure 4.6 through Figure 4.9 shows images of Samples 16, 17, and 18, which are 0.25-inches in size, and Sample 5, which is 0.5-inches in size. As already described in Section 4.2.2, the real images are to the left and the surface profilometry images are to the right, with the before and after corrosion at the top and bottom, respectively. Looking at the before corrosion images for all surfaces, one can see indentation from machining which correlated to the surface profilometry. Generally, the surface profilometry imaging of the samples before corrosion showed a shade of blue, green, yellow, and red coloration with few dark blue spots. The red color indicate height whereas the deep blue color depicted depth. The dark blue spots present in the before corrosion images showed small indentations from manufacturing.

Figure 4.6, which are images from Sample 16, the infrared surface imaging after corrosion shows a great color change. The gray color before corrosion was largely removed, with brownish and reddish colors present, along with white spots. Looking at the surface profilometry, the whitish spots correlate with raised (red) spots, indicating the presence of a likely build-up of salts. The reddish colors correlate with greens and yellows, also indicating height, which could be the presence of an attached oxide. Where the brownish color is present correlates with light and dark blues, which indicate depth, which is likely the lack of an attached oxide. This lack of attached oxide is further detailed in the presence of several dark blue spots, especially in the left bottom corner, which shows as cluster of pitting. When looking at Sample 17 (Figure 4.7), the surface profilometry image after corrosion does not show the same behavior as in Sample 16, demonstrating that corrosion is dependent on sample as much as environment. As with Sample 16, there are indentations from manufacturing, as shown in the image before corrosion. When

looking after corrosion, the surface shows the same reddish coloration as Sample 16, scattered across the entire surface, with numerous red spots, indicating a raised feature, and numerous light and dark blue spots, indicating pitting. When compared to Sample 16, the pitting is more scattered across the entire surface, instead of clustered, while the raised red spots do not coincide with white spots, meaning it is not likely salt residuals causing the raised spots, but instead, the formation of rust. Comparing Sample 18 (Figure 4.8) with Samples 16 and 17, one can see more machining indentations along the surface prior to corrosion. After, corrosion, the same reddish color appears on sample 18, with numerous raised spots (indicated in red) and depressed spots (indicated in blue). The raised spots provide the accumulation of rust building up from the surface prior to flaking. After corrosion, Figure 4.8 shows some pitting, indicated in blue. When comparing the three 0.25-inch specimens, one can see that pitting is common across all three surfaces, with some clustering and some scattered. When looking at the 0.5-inch specimen, in Figure 4.9, some interesting surface changes occurred. Prior to corrosion, the image revealed a surface with numerous indentations, shown by the red surface, indicating height, with greens and blue indicating depth. After corrosion, the height present was reduced, with only a few red spots, while the surface developed many dark blue spots, which were much smaller in size than the indentations prior to corrosion. This change between surfaces, along with the color change present, demonstrated that corrosion did occur on the 0.5-inch specimen as well, with pitting also occurring. The reduction in size of the indentations also shows that corrosion was occurring across the entire surface, removing metal from the surface and smoothing out the indentations, further confirming the weight loss features from Table 4.1.

### 4.6.2 Keyence Imaging of samples immersed and dried

Figure 4.10 through Figure 4.13 shows images of Samples 10, 11, and 12, which are 0.25-inches in size, and Sample 3, which is 0.5-inches in size. Just as in the case of samples immersed in NaCl solution, the surface profilometry imaging of the samples before corrosion also show a shade of blue, green, yellow, and red coloration with few dark blue spots or none. For all four specimens before corrosion, the dark blue indicated small indentations on the sample surfaces from manufacturing. In Figures 4.10 - 4.12, evidence of corrosion was present after the exposure. In Figure 4.10 for Sample 10, a large spot on the bottom right of the indication is yellow, orange, and red, indicating height, while most of the surface is blue, indicating that the surface is lower than the high point. The large portion at the bottom of the image is likely a rust spot, where the rust has not flaked from the surface, while the remaining portion of the surface has had the rust flake off. Beside the rust flake, there are also dark blue spots, indicating depth into the specimen, and showing that the surface has undergone pitting. In Figure 4.11 for Sample 11, the top left corner has a high concentration of red, indicating height. Looking at the micrograph, one can see the reddish color indicative of rust formation, so the red likely means that the rust has not flaked from the surface. Towards the bottom of this image, one can see a good portion of blue formation, indicating depth, or the lack of a rust covering. Further towards the bottom of the image, there is a cluster of dark blue, indicating further depth and indicative of pitting, this time in a cluster. In Figure 4.12 for Sample 12, the entire micrograph image appears to be reddish, indicating the formation of rust. When looking at the surface profilometry image, though, one can see a large blue section, with even deeper blues within the image, indicating depth. Most of the surface is covered in red, indicating the height increasing, likely due to rust formation.

However, the deep blue indicates depth, and damage. While the micrograph shows the entire image covered in rust, the degrading section, with deep blue present indicating pits, is also covered in red, indicating that this is also covered with rust as well. This large section could have resulted from the degradation of the surface by the NaCl that remains on the surface after the samples were pulled out of the solution and allowed to dry under normal room conditions. The Cl continues to react with, and degrade the metal, creating a metal chloride that is loosely adhered on the surface. When the surface was cleaned, these scales came off, allowing the deformation or irregularity on the surface to be seen. In Figure 4.13 showing Sample 3, which is 0.5 inches, the surface behaved similarly to Sample 11 (Figure 4.11), with metal surfaced covered with some reds, oranges, and yellows indicating height, and attached rust, as well as light blue, dark blue, and very dark blue, indicating the presence of the original metal with pits forming. For all samples in the immersed then dried specimens, the presence of rust occurred, indicated as reds and height, as well as the formation of pits, indicated by blues and depth. Regardless of specimen or thickness, rust was clearly present, places without rust were clearly present, indicating that the rust had flaked off, and pits were clearly forming beneath the rust that had flaked off.

### 4.6.3 Keyence Imaging of samples placed over NaCl solution.

Figure 4.14 through Figure 4.17 present images of Samples 13, 14, and 15, which are 0.25 inches, and Sample 5, which is 0.5 inches, which were placed over NaCl solution. Looking at all four samples, there is evidence of indentation from manufacturing prior to corrosion, indicated by the

dark blues that typically form in small lines. For all four samples, there is also evidence of rust formation, as indicated by the reds and oranges that indicate height and show up as reddish-brown spots on the micrographs. The number and size of the rust spots vary across the four surfaces, but all surfaces demonstrate that corrosion is happening, although in a minor way as compared to the previous two environments. There is also evidence of pitting on all four surfaces, as indicated by dark blue spots. These are not just indentations from machining, as they lack the linear nature seen in the machining marks. Looking at Sample 5 (Figure 4.17), the most pitting was present on this surface, while Samples 11-13 (Figures 4.14, 4.15, and 4.16) showed considerably less pitting, although it was still present. For all four samples, the amount of corrosion, in both the presence of pitting and rust formation, was less than either of the two previous environments, because of the minimum contact of samples with corrosive environment. The samples were placed over NaCl and covered. The metal only encounters the corrosive environment when water from NaCl solution evaporated, and generally, only the water would be evaporating. The water is trapped by the covering and hence condenses back to liquid form, which eventually falls onto the metal, but the corrosive ions needed to truly damage the surface were not present, even when the water fell on the metal after condensation. Given that the experiment was in room temperature of about 27$^{o}$C, there were lower amounts of evaporation, hence less water on metal surface and less corrosion occurring overall, as demonstrated in Table 4.3 which showed minimal weight loss for these samples.

### 4.6.4 Keyence Imaging of samples placed in wet dirt

Figure 4.18 through Figure 4.21 present images of Samples 7, 8, and 9, which are 0.25 inches, and Sample 4, which is 0.5 inches, which were buried under wet dirt. As with all previous samples, prior to corrosion, there were indentations, usually in a linear formation, from machining defects. After corrosion, samples exposed to this environment showed the formation of large pits, indicated by dark blue, with the pits larger and more populous than the other environments. Rust formation or the accumulation of dirt on the surface, indicated by the reds and oranges indicating height, were also present across all four surfaces. It is more than likely the accumulation of dirt, as compared to rust formation, as the micrographs all show more of a brown color than the rust reddish color. As for the large pit formation, this means that this environment was more locally aggressive than the other environments. However, looking at the weight loss in Table 4.4, there was minimal weight loss. For pitting corrosion, this is not unexpected, as one of the detrimental side effects of pitting is that it is not usually detected until it causes catastrophic failure. For pitting, the $O_2$ and other corrosive agents, even chloride ions, present in the soil were in continuous contact with the metal. Any oxides that formed were likely weakly attached and may have fallen off into the dirt. With the continuous contact with the metal, the corrosive ions were able to continually react with the surface, creating the high number of pitting on the surface.

When setting up the wet dirt environment, the dirt was collected form the Environmental Science lab, where it had been stored for three years, with all of the water allowed to evaporate; this left behind any minerals or salts present in the dirt when it was first collected. There was likely no, or minimal, organic matter or microbes present to create an acidic environment, due to the long-

term storage of the dirt. For use in this experiment, enough water, but no added NaCl, was added to create wet dirt that could be molded. Since the dirt likely did have minerals and salts remaining, even though the water was completely removed, it was able to emulate the underground corrosion process. In underground corrosion, the primary factor is the presence of concentrations of sulfates or chlorides or both in the soil, with enough water present to support the electrochemical reactions [104]. In addition to the presence of corrosion ions, moisture, pH, and oxygen concentration all contribute to corrosion. For this research, these were not tested because the interest was not to determined factors causing corrosion, but to corrode the metal and test for the presence of corrosion using the microsensor.

### 4.6.5 Impedance measurement for immersed environment.

Table 4.5, Table 4.6, Figure 4.23, and Figure 4.24 show the impedance recorded for samples immersed in NaCl solution. A graph of impedance's magnitude is plotted against weeks. Samples 16, 17, and 18, all 0.25-inch in size, are showing a maximum impedance recorded at a frequency of about 11.755Hz from the figures mentioned. Sample 1, which is 0.5-inch in size, is also showing a maximum impedance at a frequency of about 11.755Hz.

One key interest was to investigate if the environment affected the impedance measurement. Therefore, for this environment, two different sets of testing were performed for each of the samples involved each week in this environment. Firstly, impedance was measured while the samples remained immersed in the NaCl solution, and then, testing was done while the same samples were taken out of the NaCl solution and exposed to air. Table 4.5 and Figure 4.23 show

testing done for samples while they were still immersed in NaCl solution. Table 4.6 and Figure 4.24 depict values of impedance obtained for testing done for samples while they were taken out of the NaCl solution and exposed to air. It is observed that in both scenarios, where testing was done whether samples were immersed or exposed to air, the impedance values were closely related. It is generally seen that impedance increases drastically at week 3 and peaked at week 4, then drops at week 5, and fluctuates after. The rise and fall in impedance values after week 5 onwards could be because of relative loss of oxide on metal surface. As the oxide flakes off, opening up more fresh metal, the impedance begins to drop. As the oxide builds back up, the impedance begins to increase. Since rust is a large crystal, as it grows from the metal surface, it does become weakly adhered and easy to flake off, thereby supporting this idea that the removal of the flakes decrease impedance reading and the reformation of the rust increases impedance readings.

In other to make a comparison with the two scenarios, the average magnitude and standard deviation in week 4 was calculated, since that is where the highest impedance was present. For the testing done while samples were in solution, the average magnitude and standard deviation was 1609.889 ± 5.81 Ω. For testing done with samples exposed to air, the average magnitude and standard deviation was 1519.088 ± 192. 40881 Ω. The average magnitude and standard values revealed minimal differences in impedance, whether measurement was done in solution or in air and that the microsensor was able to detect impedance well.

When you compare the impedance values of Sample 1, which is 0.5-inch in size, to the impedance values of Samples 16, 17 and 18, which are all 0.25-inch in size, as shown in Table 4.5 and Figure 4.23, it is obvious that the values are closely related. Consider, for example, in Table 4.5, the

impedance value for Sample 1 is 1610.519 Ω, whereas the impedance values for Samples 16, 17, and 18 are 1606.373 Ω, 1617.834 Ω, and 1604.828 Ω respectively for week 4. Again, for week 5, Sample 1 has an impedance value of 1223.736 Ω, whereas impedance values for Samples 16, 17, and 18 are 1325.073 Ω, 1443.110 Ω, and 1313.405 Ω. Considering the closeness of the values, it could be argued that the thickness of the metal coupon had minimal effect on the impedance value for this particular environment, as both 0.5-inch and 0.25-inch sized metal are showing similarity in impedance measured.

### 4.6.6 Impedance measurement for immersed and dry environment.

Table 4.7 and Figure 4.25 show the impedance recorded for samples immersed then dried. Figure 4.25 presented Sample 10, 11, and 12 (0.25-inches), and 3 (0.5 inches), which all show a maximum impedance value recorded at a frequency of 11.755Hz, matching the previous environment. Sample 11 (0.25 inches) is an outlier value on the graph, with a large impedance measurement of 6835 Ω. The error might be due to a couple of reasons. One reason could be resonance; resonance occurs where the frequency of the applied wave equals the natural frequency of system, resulting in a significant error [129]. The other reason could be as a result of interaction between the characteristic impedance of the transmission lines and the propagating signal or wavelength. Standing waves or reflection waves can impact impedance variation [130]. Lastly, it might be due physical fault or damage, buildup of oxide around the connection, or massive pitting within the coupon, which was not detected by Keyence system

[131]. Since the large impedance reading could be the result of a discontinuity, the presence of a non-conductive oxide that eventually flakes off or a pit, which is similar to a hole in the metal, that eventually corrodes away could be the cause of the discontinuity.

It is generally seen that impedance increased drastically at week 3 and peaked at week 4, then gradually decreased for the subsequent weeks. The average impedance magnitude and standard deviation calculated for samples in this environment was 1842.241 ± 46.16321 Ω. It should be noted that sample 11 was excluded from this calculation, given that its values are outliers. Impedance values from Samples 10, 12, and 3 were used for calculating the average magnitude and standard deviation.

When comparing the impedance values of Sample 3, which is 0.5-inch in size, to the impedance values of Samples 10 and 12, which are 0.25-inch in size, and shown in Table 4.7 and Figure 4.25, it is obvious that the values are closely related. Consider, for example, Table 4.5, the impedance value for sample 3 is 1807.446 Ω, whereas impedance values for Samples 10 and 12 are 1824.666 Ω and 1894.610 Ω for week 4, respectively. Again, for week 5, Sample 3 has and impedance value of 1678.722 Ω, whereas impedance values for Samples 10 and 12 are 1696.264 Ω and 1752.958 Ω, respectively. Again, as in the case of the previous environment, considering the closeness of the values, it could be argued that the thickness of the metal coupons had minimal effect on the impedance values for this particular environment, as both 0.5-inch and 0.25-inch sized metal are showing similarity in impedance measured.

### 4.6.7 Impedance measurement for samples placed over solution environment.

Table 4.8 and Figure 4.26 shows the impedance recorded for samples placed over the NaCl solution. A graph of impedance's magnitude is plotted against weeks. Samples 13, 14, and 15, all 0.25-inch in size, are showing a maximum impedance recorded at a frequency of about 11.755Hz. Sample 5, which is 0.5-inch in size, is showing a maximum impedance at a frequency of about 11.755Hz. As with the previous environment, there was a drastic increase in impedance between weeks 2 and 3 and then peaks at week 4. There was variation in impedance values for the subsequent weeks, as seen in a zig zag form on Figure 4.26. This zig zag pattern could be as a result of buildup and loss of oxide on metal surface, which affected the impedance measurement. The average impedance magnitude and standard deviation calculated for samples in this environment was 1518.658 ± 97.24753 Ω.

Comparing the impedance values of Sample 5, which is 0.5-inch in size, to the impedance values of Samples 13, 14 and 15, which are all 0.25-inch in size, as shown in Table 4.8 and Figure 4.26, it is obvious that the values are closely related. The Impedance value for Sample 5 is 1506.528 Ω, whereas impedance values for Samples 13, 14, and 15 are 1562.094 Ω, 1616.688 Ω, and 1389.323 Ω for week 4, respectively. As in the case of the previous environments, considering the closeness of the values, it could be argued that the thickness of the metal coupons had minimal effect on the impedance values for this particular environment, as both 0.5-inch and 0.25-inch sized metal are showing similarity in impedance measured.

### 4.6.8 Impedance measurement for samples buried under wet dirt environment.

Table 4.9, Table 4.10, Figure 4.27, and Figure 4.28 show the impedance recorded for samples buried under wet dirt. To determine whether the dirt will interfere with the impedance reading, the impedance was recorded while the samples were in dirt and then again when exposed to air. Table 4.9 and Figure 4.27 show values of impedance obtained for testing done for samples that were exposed to air at the time of testing. Table 4.10 and Figure 4.28 show values of impedance obtained for testing done for samples that were buried under wet dirt at the time of testing.

Sample 7 in the wet dirt environment did demonstrate a very high impedance reading, similar to Sample 11 in the immersed and dried environment. As with Sample 11, the reasons for this error might be the same. The resonance [129], transmission line [130], and physical fault or damage [131] might be the leading cause of the error in measurement. While the reason for the discontinuity would need to be further examined, to ensure similar discontinuities could be explained, that is beyond the scope of this research. With that been said, it is observed that in both scenarios, whether the samples were buried or exposed to air during testing, the impedance values were closely related. It is generally seen the impedance increases peaked at week 4.

Again, making comparisons between the two scenarios, the average magnitude and standard deviation in week 4, where the highest impedance occurred, was calculated. For the testing done while samples were buried in dirt, the average magnitude and standard deviation was 1967.895 ± 27.09109 Ω. For testing done with samples exposed to air, the average magnitude and standard deviation was 2113.368 ± 128.7526 Ω. The average magnitude and standard values revealed

minimal changes in the impedance measurement in either scenario, and that the microsensor was able to pick up the impedance well in either environment.

Comparing the impedance values of Sample 4, which is 0.5-inch in size, to the impedance values of Samples 8 and 9, which are all 0.25-inch in size, and shown in Table 4.9 and Figure 4.27, it is obvious that the values are closely related. Consider, for example, Table 4.9, the impedance value for Sample 4 is 2078.134 Ω, whereas the impedance values for Samples 8 and 9 are 2256.070 Ω and 2005.901 Ω for week 4, respectively. Again, for week 5, Sample 4's impedance value is 1392.981 Ω, whereas the impedance values for Samples 7, 8, and 9 are 1629.874, 1308.377 Ω, and 1313.405 Ω, respectively. Considering the closeness of the values with respect to each week, it could be argued that the thickness of the metal coupons had minimal effect on the impedance value for this particular environment, as both 0.5-inch and 0.25-inch sized metal are showing similarity in impedance measured.

### 4.6.9 Comparison of Impedance Readings

When looking at the impedance readings of the four different environments, disregarding the outliers, one can see that the highest average impedance reading over the entire exposure time occurs in the wet dirt environment, whether that is outside the dirt in the air (1509.67 ± 53.31 Ω) or under the wet dirt (1478.38 ± 64.26 Ω). This is followed by the specimens immersed in the NaCl solution and then dried (1366.94 ± 346.53 Ω). The other two environments, the immersed and over the NaCl solution have roughly the same impedance values, with the impedance of the immersed in solution of 1085.78 ± 35.95 Ω, the impedance of the immersed out of solution of

1058.98 ± 86.23 Ω, and the impedance of the specimens above the NaCl solution of 1100.95 ± 60.55 Ω. It is because of these differences in behavior, with impedances starting at roughly 500 Ω higher for the wet dirt and 300 Ω higher for the immersed then dried as compared to the immersed and over NaCl solution specimens, that the wet dirt and immersed then dried environments were chosen to continue the corrosion testing of the metal pipe.

### 4.6.10 Corrosion of the metal pipe.

When looking at Figures 4.29 – 4.32, there are obvious signs of corrosion, specifically the formation of the iron oxide ($Fe_2O_3$) on the surface. Again, reddish brown coloration indicates the presence of corrosion. As with the coupons immersed then dried, one can see distinctive red-orange spots, likely indicating the potential for pitting (although not able to be scanned due to size constraints) in Figure 4.29. In Figure 4.30, a closer look at the external corrosion of the metal pipe is shown. The red-orange spots are clearly present, as is a dark reddish-brown color covering the entire surface, demonstrating expansive external corrosion. Figure 4.31 shows the bottom of the inside of the pipe, where water is usually collected and held for a longer time period, before it finally dries, after being pulled from the NaCl solution. Due to the long contact created between the metal and the corrosive agent, extensive corrosion damage is seen at the bottom of the inside of the pipe within the eight weeks. Figure 4.32 shows the pipes that were placed in wet dirt and the degradation of the metal due to corrosion. When the dirt was thoroughly cleaned from the metal, one can see that the surface of metal is uneven and heavily degraded in parts, showing definitive signs of corrosion. When looking at the internal diameter of the pipe

buried in wet dirt as shown in Figure 4.33, there is evidence of corrosion of the internal diameter of the pipe, although maybe less than the external portion of the pipe. When comparing the external surfaces of the pipes between immersed then dried and under wet dirt, the pipe under wet dirt is more obviously degraded, although the pipe immersed then dried shows potentially more pitting corrosion. When comparing the internal surfaces of the pipes, the pipe immersed then dried appears to show more internal corrosion, likely because of the collection of NaCl solution that took time to dry, as compared to the pipe under wet dirt. The pipe under wet dirt does show some internal corrosion, but much less than the external, and with fewer likely pits forming.

### 4.6.11 Impedance measurement for Metal Pipe.

As already discussed above, the metal pipe was only exposed to two environments namely, the immersed and dried and buried under wet dirt, with the wire leads connected across the pipe length and also around the metal pipe. As part of this set of experiments, the orientation of the wires and its effect on impedance readings was important to determine. After the frequency sweep from 1 Hz to 1k Hz, it was observed that the frequency at which we obtained the highest impedance values was 54.622 Hz. When looking at the frequency for the metal pipe, at 54.622 Hz compared to the 11.755 Hz frequency for the metal coupons, the environment where the highest frequency was determined was in air at room temperature, so the environment could not have affected the frequency. Instead, the reason for the difference in frequency may be as result of the type of the samples involved. The metal coupon was rectangular in shape, with a

small amount of material as compared to the pipe. In addition to a much heavier item, the pipe also had hole running through the middle. While the signal would be sent through the metal coupon or around the pipe, with the pipe, more material could have affected the frequency.

For samples immersed and dried, Table 4.11 and Figure 4.34 show testing done across the pipe, while Table 4.12 and Figure 4.35 represent testing done around the pipe. A general trend is seen where impedance increases drastically during week 2 and gradually peaks at week 4 for both readings, and impedance then begins to drop during the subsequent weeks. Since week 4 had the highest impedance values, the average magnitude and standard deviation was calculated for that week to make our comparison of testing done across pipe and around pipe. For the three samples used in this environment, the average magnitude and standard deviation in week 4 for testing done across the pipe was 1750.297 ± 22.00655 Ω. For the three samples used in this environment, the average magnitude and standard deviation in week 4 for testing done around the pipe was 1737.947 ± 13.94865 Ω. The values obtained are closely related and so it may be concluded that the wire positioning had little effect on impedance value recorded.

For the wet dirt, just as above, testing was done across the pipe and then around the pipe. In this case, impedance was measured while samples remain buried under dirt. Table 4.13 and Figure 4.36 show testing done across pipe. Table 4.14 and Figure 4.37 show testing done around pipe. For the three samples used in this environment, the average magnitude and standard deviation in week 4 for testing done across the pipe was 1878.22± 5.298554 Ω. For the three samples used in this environment, the average magnitude and standard deviation in week 4 for testing done around the pipe was 1868.553± 19.86109 Ω. The values obtained are closely related and so it may be concluded that the wire positioning had little effect on impedance value recorded.

Comparing the two environments, the wet dirt environment recorded the highest impedance value, regardless of wire orientation, at 1272.29 ± 20.02 Ω for the period of study, as compared to the immersed then dried, at1192.90 ± 29.95 Ω for the period of study. This difference in impedance suggests that the metal in the wet dirt was more corroded than in the immersed then dried environment. However, the difference is relatively small. When looking at the images (Figure 4.13-4.14 for wet dirt and Figures 4.11-4.12 for immersed then dried), and comparing the appearance of corrosion, the slight differences in impedance can be suggested. For the wet dirt, the outside of the pipes appears to be much more corroded than the outside of the pipes for the immersed then dried, which would lead to higher impedance readings. When looking at the inner portion of the pipe, the immersed then dried appears more corroded than the wet dirt, causing this impedance reading to increase, approaching the value of the wet dirt. Overall, impedance reading show that corrosion can be detected whether it is the more extreme external corrosion of the wet dirt pipes, or the apparent pitting both externally and internally of the immersed then dried pipe.

# 5 Chapter 5.

## 5.1 Conclusion

This work, being the first phase of the project to develop a Bluetooth enabled 3D microcontroller to be used for corrosion detection in oil and gas pipeline, presents evidence of the microsensor's ability to detect signs of corrosion. 4140 steels, which are normally used for oil and gas pipeline construction use, was used and the presence of corrosion was measured by the change in impedance. After analysis, it was determined that the microcontroller was able to detect corrosion at lower frequencies better than higher frequencies.

The following were also identified as outcomes of the experiment:

1. The microcontroller can detect corrosion by predicting the change in electromechanical properties, which, in this case, was the weekly change in impedance measured.
2. 0.5-inch size metal coupons had approximately the same impedance values as 0.25-inch size metal coupons, as recorded by the microsensor. The closeness of impedance values suggests the thickness of the metal does not affect impedance measurement of the microsensor.
3. From the experiment using the metal pipe, it was found that the impedance measurement was not affected by the wire orientation, comparing along the pipe length with across the pipe diameter.
4. The wet dirt environment corroded the samples the most, followed by immersed then dried, immersion in the NaCl solution, and placed over NaCl solution. This was seen with

the Keyence imaging revealing more pitting in samples and the sensor recording the highest impedance value for the wet dirt environment.

## 5.2 Recommendations

I recommend that further research be conducted on how metal orientation affects impedance measurement, because this experiment focused on just two points, either along the metal pipe length or around the pipe diameter. I would also recommend investigating why the highest impedance for metal coupon was recorded at 11.755Hz, while it was recorded at 54.622Hz for metal pipe. Specifically, would the size of the metal pipe, with respect to outer diameter, inner diameter, or wall thickness affect the frequency, meaning each pipe would have its own value. Lastly, I also suggest more work needs to be done to understand the causes of discontinuities, to avoid issues with impedance readings.

# 6 References.


1. Dhawan, S. K., Bhandari, H., Ruhi, G., Bisht, B. M. S., & Sambyal, P. (2020). Corrosion Preventive Materials and Corrosion Testing.

2. Farh, H. M. H., Seghier, M. E. A. B., & Zayed, T. (2022). A comprehensive review of corrosion protection and control techniques for metallic pipelines. *Engineering Failure Analysis*, 106885.

3. Bardal, E., & Drugli, J. M. (2004). Corrosion detection and diagnosis. *Materials science and engineering*, *3.*

4. Yamashita, M., Miyuki, H., Matsuda, Y., Nagano, H., & Misawa, T. (1994). The long term growth of the protective rust layer formed on weathering steel by atmospheric corrosion during a quarter of a century. *Corrosion science*, *36*(2), 283-299.

5. Shaw, B., & Kelly, R. (2006). What is corrosion?. *The Electrochemical Society Interface*, *15*(1), 24.

6. Stern, M., & Geary, A. L. (1957). Electrochemical polarization: I. A theoretical analysis of the shape of polarization curves. *Journal of the electrochemical society*, *104*(1), 56.

7. Singh R. (2013). Pipeline Integrity Handbook: Risk Management and Evaluation. Gulf Professional Publishing, Houston, TX, pp. 320.

8. Natarajan K.A. NPTEL Web Course, Lecture 1: Corrosion: Introduction, Definitions and Types, Advances in Corrosion Engineering.

9. Koch, G., Varney, j., Thompson, N., Moghissi, O., Gould, M., Payer, J. (2016) NACE s International Measures of Prevention, Application and Economics of Corrosion Technology (IMPACT), 1, 3-6.

10. Beyer, J., Trannum, H. C., Bakke, T., Hodson, P. V., & Collier, T. K. (2016). Environmental effects of the Deepwater Horizon oil spill: a review. *Marine pollution bulletin*, *110*(1), 28-51.

11. Liu, Y., Weisberg, R. H., Hu, C., & Zheng, L. (2011). Tracking the Deepwater Horizon oil spill: A modeling perspective. *Eos, Transactions American Geophysical Union*, *92*(6), 45-46.

12. Shaw, B., & Kelly, R. (2006). What is corrosion?. *The Electrochemical Society Interface*, *15*(1), 24.

13. Fontana, M. G., & Mitra, M. S. (1953). The Eight Forms of Corrosion & the Corrective Measures.

14. Serrano, J., & Penalver, J. (1992, March). Control of Erosion-Corrosion in Flowlines of Wells in Northern Monagas. In *SPE Latin America and Caribbean Petroleum Engineering Conference* (pp. SPE-23651). SPE.

15. Zhang, X. G. (2011). Galvanic corrosion. *Uhlig's Corrosion Handbook*, *51*, 123.

16. P.R. Roberge, Handbook of corrosion engineering, McGraw-Hill2000.

17. Y. Sun, S. Nesic, A parametric study and modeling on localized CO2 corrosion in horizontal wet gas flow, CORROSION 2004, DOI (2004).

18. B.O. Oyelami, A. Asere, Mathematical modelling: An application to corrosion in a petroleum industry, National Mathematical Centre, DOI (2005) 48-56.

19. A. Samimi, Causes of Increased Corrosion in Oil and Gas Pipelines in the Middle East, Int. J. Basic Appl. Sci. Indonesia (2012) 572–577.

20. S. Nešić, Key issues related to modelling of internal corrosion of oil and gas pipelines – A review, Corros. Sci. 49 (2007) 4308–4338.

21 L. Gray, B. Anderson, M. Danysh, P. Tremaine, Mechanism of carbon steel corrosion in brines containing dissolved carbon dioxide at pH 4, corrosion/89, paper no. 464, Houston, TX: NACE International, DOI (1989)

22. S. Nesic, J. Postlethwaite, S. Olsen, An electrochemical model for prediction of CO 2 corrosion, S. Nesic, J. Postlethwaite, and S. Olsen, Paper, DOI (1995).

23 L.G. Gray, B.G. Anderson, M.J. Danysh, P.R. Tremaine, Effect of pH and temperature on the mechanism of carbon steel corrosion by aqueous carbon dioxide, Corrosion/90, paper, 40 (1990).

24 A. Hedayati, A. Samimi, Evaluating salt Concentration and Exiting Sewage Electrical Directing of Isfahan Oil Refinery Company for Application in Green Environment, Int. J. Innovat. Appl. Studies 4 (2013) 672.

25. M. Ko, B. Ingham, N. Laycock, D. Williams, In situ synchrotron X-ray diffraction study of the effect of chromium additions to the steel and solution on CO2 corrosion of pipeline steels, Corros. Sci. 80 (2014) 237–246.

26. J. Heuer, J.F. Stubbins, An XPS characterization of FeCO3 films from CO2 corrosion, Corros. Sci. 41 (1999) 1231–1243.

27. U. Lotz, T. Sydberger, CO2 corrosion of carbon steel and 13Cr steel in particle-laden fluid, Corrosion 44 (1988) 800–809.

28. D. Lopez, T. Perez, S. Simison, The influence of microstructure and chemical composition of carbon and low alloy steels in CO2 corrosion. A state-of-the-art appraisal, Mater. Des. 24 (2003) 561–575.

29. C. De Waard, D. Milliams, Carbonic acid corrosion of steel, Corrosion 31 (1975) 177–181.

30. A. Mustafa, B. Ari-Wahjoedi, M. Ismail, Inhibition of CO 2 corrosion of X52 steel by imidazoline-based inhibitor in high pressure CO 2-water environment, J. Mater. Eng. Perform. 22 (2013) 1748–1755.

31. S. Nešić, Key issues related to modelling of internal corrosion of oil and gas pipelines – A review, Corros. Sci. 49 (2007) 4308–4338.

32. S. Nesic, K.-L.J. Lee, V. Ruzic, A mechanistic model of iron carbonate film growth and the effect on CO2 corrosion of mild steel, CORROSION/2002, paper, 2237 (2002).

32. Y.T. Al-Janabi, H.A. Al-Ajwad, Corrosivity and Corrosion Inhibition of Wet-Sour Crude Oil Wells, CORROSION 2015, NACE International, 2015

33. A. El-Sherik, H. Ajwad, Sour Corrosion: A Review of Current Gaps and Challenges, Mater. Perform. 57 (2018) 48–50.

33. I. Obot, M.M. Solomon, S.A. Umoren, R. Suleiman, M. Elanany, N.M. Alanazi, A.A. Sorour, Progress in the development of sour corrosion inhibitors: Past, present, and future perspectives, Journal of Industrial and Engineering Chemistry, DOI (2019).

34. J. Tang, Y. Shao, J. Guo, T. Zhang, G. Meng, F. Wang, The effect of H2S concentration on the corrosion behavior of carbon steel at 90 C, Corros. Sci. 52 (2010) 2050–2058.

35. Z.Y. Liu, X.Z. Wang, R.K. Liu, C.W. Du, X.G. Li, Electrochemical and Sulfide Stress Corrosion Cracking Behaviors of Tubing Steels in a H2S/CO2 Annular Environment, J. Mater. Eng. Perform. 23 (2014) 1279–1287.

36. K. Videm, A. Dugstad, Corrosion of carbon steel in an aqueous carbon dioxide environment Part 1, Mater. Performance; (United States) 28 (1989).

37. Energy Institute (2008) Guidance for corrosion management in oil and gas production and processing. Annual Report, London

38. Nalli K (2010) Corrosion and its mitigation in the oil and gas industry. An overview. PM-Pipeliner Report

39. Johansson E, Pettersson R, Alfonsson E, Weisang-Hoinard F (2010) Specialty stainless for solving corrosion problems in the oil and gas industry. Offshore World 40

40. Smith L (1999) Control of corrosion in oil and gas production tubing. British Corro J 34(4):247

41. de Waard C, Lotz U (1994) Prediction of CO2 corrosion of carbon steel. EFC publication number 13. The Institute of Materials, London

42. Mannan S, Patel S (2008) A new high strength corrosion resistant alloy for oil and gas applications. Paper presented at NACE Corrosion, New Orleans

43. Craig BD (1995) Selection guidelines for corrosion resistant alloys in the oil and gas industry. NiDI Tech Series 10073:1–8

44. Miksic BM, Kharshan MA, Furman AY (2005). Proceeding of 10th European Symposium of Corrosion and scale inhibitors

45. Kharshan M, Furman A (1998) Incorporating vapor corrosion inhibitors (VCI) in oil and gas pipeline additive formulations. NACE, Corrosion 98(236)

46. Rajeev P, Surendranathan AO, Murthy CSN (2012) Corrosion mitigation of the oil well steels using organic inhibitors – a review. J Mater Environ Sci 3(5):856–869

47. NACE-SP0169-2013, Control of external corrosion on underground or submerged metallic piping systems, Houston, TX: NACE, DOI (2002).

48. 48. Nestleroth, J. B. (2006). Pipeline in-line inspection challenges to ndt. Insight-Non-Destructive Testing and Condition Monitoring, 48(9), 524-524.

49. T. Crosby, J. Wolodko, H. Tsaprailis, Gap Analysis of Canadian Pipeline Coatings: A Review Study, NACE International Corrosion Conference Proceedings, NACE International, 2016, pp. 1.

50. Accessed, 5th September 2023, DOI. http://www.united-steel.com/productshow/fbe-coated-pipe.html

51. Shiwei WG, Gritis N, Jackson A, Singh P (2005) Advanced onshore and offshore pipeline coating technologies. 2005 China international oil and gas technology conference and expo, Shangai, China

52. Lazzari L, Pedeferri P (2006) Cathodic protection, 1st edition. McGraw Hill, New York

53. Guyer JP (2009), An introduction to cathodic protection. Continuing Education and Development Inc., New York

54. Lazzari L, Pedeferri P (2006) Cathodic protection, 1st edition. McGraw Hill, New York

55. Baeckmann WV (1997) Handbook of cathodic corrosion protection, 3rd edition. McGraw Hill, New York

56. https://www.pipelineprotection.co.uk/services/cathodic-protection/ (Accessed, September 5, 2023)

57.https://www.utelectrode.com/article/what-is-an-impressed-current-cathodic-protection-system-.html (Accessed, September 5, 2023)

58. Canadian Association of Petroleum Producers (2009) Best management practices for the mitigation of internal corrosion in oil effluent pipeline systems. Annual report. Annual report. CAPP, Calgary

59. Varela, F., Yongjun Tan, M., & Forsyth, M. (2015). An overview of major methods for inspecting and monitoring external corrosion of on-shore transportation pipelines. *Corrosion Engineering, Science and Technology*, *50*(3), 226-235.

60. Adriman, R., Ibrahim, I. B. M., Huzni, S., Fonna, S., & Ariffin, A. K. (2022). Improving half-cell potential survey through computational inverse analysis for quantitative corrosion profiling. *Case Studies in Construction Materials*, *16*, e00854.

61. D. Hevle and A. Kowalski: 'Close-interval survey techniques', in 'ASM Handbook', (ed. S. D. Cramer), 13C. Rev. edn, 84–88; 2006, Ohio, USA, ASM International.

62. A. Kowalski: 'The close interval potential survey (CIS/CIPS) method for detecting corrosion in underground pipelines', in 'Underground pipeline corrosion', (ed. M. E. Orazem), 227–246; 2014, Cambridge, Woodhead Publishing.

63. ISO: 'Petroleum and natural gas industries – cathodic protection of pipeline transportation systems', Part 1, on-land pipelines'; 2003. Geneva, Switzerland, ISO. [15589-1:2003(E)].

64. NACE: 'The use of coupons for cathodic protection monitoring applications'; 2004, NACE, [RP0104:2004] Houston, TX, USA

65. C. D. Stears, R. M. Degerstedt, O. C. Moghissi and L. Bone III: 'Field program on the use of coupons to monitor cathodic protection of an underground pipeline', Proc. Corrosion 97, New Orleans, Louisiana, March 1997, NACE international, Paper 564, 1–2; 1997

66. B. N. Popov and S. P. Kumaraguru: 'Cathodic protection of pipelines', in 'Handbook of environmental degradation of materials', 2nd edn, 771–798; 2012, Oxford, William Andrew Publishing.

67. D. Eyre: 'The Pearson survey method for detecting corrosion in underground pipelines', in 'Underground pipeline corrosion', (ed. M. E. Orazem), 247–254; 2014, Cambridge, Woodhead Publishing.

68. S. Shawki: ‘Above ground coating integrity assessment: experience with SUMED pipelines’, in ‘Integrity of pipelines transporting hydrocarbons’, (ed. G. Bolzon), 311–322; 2011, Biskra, Algeria, Springer

69. Z. Masilela and J. Pereira: ‘Using the direct current voltage gradient technology as a quality control tool during construction of new pipelines’, Eng. Fail. Anal., 1998, 5, (2), 99–104.

70. J. Cordell and H. Vanzant: ‘Pipeline pigging handbook’ in ‘In-line inspection pigging’, (ed. J. Cordell and H. Vanzant), 3rd edn, 8.1–8.15; 2003, Houston, TX, USA, Clarion Technical Publishers.

71. S. Brockhaus, M. Ginten, S. Klein, M. Teckert, O. Stawicki, D. Oevermann, S. Meyer and D. Storey: ‘In-line inspection (ILI) methods for detecting corrosion in underground pipelines’, in ‘Underground pipeline corrosion’, (ed. M. E. Orazem), 255–285; 2014, Cambridge, Woodhead Publishing.

72. Y. Bai and Q. Bai: ‘Subsea pipeline integrity and risk management’ in ‘Pipeline inspection and subsea repair’, (ed. Y. Bai and Q. Bai), 73–99; 2014, Boston, Gulf Professional Publishing.

73. T. Bubenik: ‘Electromagnetic methods for detecting corrosion in underground pipelines: magnetic flux leakage (MFL)’, in ‘Underground pipeline corrosion’, (ed. M. E. Orazem), 215–226; 2014, Cambridge, Woodhead Publishing

74. Khan, A., Qurashi, A., Badeghaish, W., Noui-Mehidi, M. N., & Aziz, M. A. (2020). Frontiers and challenges in electrochemical corrosion monitoring; surface and downhole applications. *Sensors*, *20*(22), 6583.

75. ASTM, Standard test method for corrosion potentials of uncoated reinforcing steel in concrete, C876-09, 2009

76. Millard, S., & Sadowski, L. (2009). Novel method for linear polarisation resistance corrosion measurement. *e-Journal of Nondestructive Testing & Ultrasonics*, *14*.

77. Saarenketo, T. (2009). NDT transportation. *Ground penetrating radar: theory and applications*, 395-444.

78. W.-L. Lai, T. Kind, M. Stoppel, H. Wiggenhauser, Measurement of accelerated steel corrosion in concrete using ground penetrating radar and modified half-cell potential method, J. Infrastruct. Syst. 19 (2) (2013) 205–220.

78. Paetsch, O., Baum, D., Prohaska, S., Ehrig, K., Meinel, D., & Ebell, G. (2015, June). 3D corrosion detection in time-dependent CT images of concrete. In *Proceedings of the Digital Industrial Radiology and Computed Tomography Conference, Ghent, Belgium* (pp. 22-25).

79 D. Eisenmann, F. Margetan, C.-P.T. Chiou, R. Roberts, S. Wendt, Ground penetrating radar applied to rebar corrosion inspection, in: AIP Conf. Proc., American Institute of Physics, 2013.

80. Dinh, K., Zayed, T., Romero, F., & Tarussov, A. (2015). Method for analyzing time-series GPR data of concrete bridge decks. *Journal of Bridge Engineering*, *20*(6), 04014086.

81. Dinh, K., Zayed, T., Romero, F., & Tarussov, A. (2015). Method for analyzing time-series GPR data of concrete bridge decks. *Journal of Bridge Engineering*, *20*(6), 04014086.

82. Cole, P. T., & Watson, J. R. (2006). Acoustic emission for corrosion detection. *Advanced Materials Research*, *13*, 231-236.

83. Miller, S.D., O'Brien, J., Keck, D.L. (1998) Proceedings of 7th European Conference For Non-Destructive Testing, Copenhagen.

84. Alleyne, D. N., Lowe, M. J. S., & Cawley, P. (1998). The reflection of guided waves from circumferential notches in pipes.

85. Carandente, R., & Cawley, P. (2012). The effect of complex defect profiles on the reflection of the fundamental torsional mode in pipes. *Ndt & E International*, *46*, 41-47.

86. Agilent Technologies 2008. ‘‘A Data Sheet of Agilent E4980A Precision LCR Meter, USA,’’ Available at: http://cp.literature. agilent.com/litweb/pdf/5989-4435EN.pdf (accessed on March 20, 2008)

87. Peairs, D.M., Park, G. and Inman, D.J. 2004b. ‘‘Improving Accessibility of the Impedance-based Structural Health Monitoring Method,’’ Journal Intelligent Material Systems and Structures, 15:129 139.

88. Prazak, M., & Barton, K. (1967). The estimation of corrosion velocity by measuring polarization resistance. *Corrosion Science*, *7*(3), 159-163.

89. Epelboin, I., Keddam, M., & Takenouti, H. (1972). Use of impedance measurements for the determination of the instant rate of metal corrosion. *Journal of Applied Electrochemistry*, *2*(1), 71-79.

90. Liang, Chen, Fan Ping Sun, and Craig A. Rogers. "Coupled electro-mechanical analysis of adaptive material systems-determination of the actuator power consumption and system energy transfer." Journal of intelligent material systems and structures 8.4 (1997): 335-343.

91. Park, Gyuhae, Harley H. Cudney, and Daniel J. Inman. "Feasibility of using impedance-based damage assessment for pipeline structures." Earthquake engineering & structural dynamics 30.10 (2001): 1463-1474.

92. Thoriya, Amit, Tarak Vora, and Pius Nyanzi. "Pipeline corrosion assessment using electromechanical impedance technique." Materials Today: Proceedings 56 (2022): 2334-2341.

93. Park, Seunghee, and Sun-Kyu Park. "Quantitative corrosion monitoring using wireless electromechanical impedance measurements." Research in Nondestructive Evaluation 21.3 (2010): 184-192.

94. Talakokula, Visalakshi, Suresh Bhalla, and Ashok Gupta. "Corrosion assessment of reinforced concrete structures based on equivalent structural parameters using electro-mechanical impedance technique." Journal of Intelligent Material Systems and Structures 25.4 (2014): 484-500.

95. Martowicz, Adam, et al. "Application of electromechanical impedance-based SHM for damage detection in bolted pipeline connection." Nondestructive Testing and Evaluation 31.1 (2016): 17-44.

96. Zhu, Hongping, et al. "Mechanical impedance-based technique for steel structural corrosion damage detection." Measurement 88 (2016): 353-359.

97. Na, Wongi S. "Possibility of detecting wall thickness loss using a PZT based structural health monitoring method for metal based pipeline facilities." Ndt & E International 88 (2017): 42-50.

98. Na, Wongi S., and Jongdae Baek. "Impedance based health monitoring technique with probabilistic neural network for possible wall thinning detection of metal structures." Journal of Sensors 2017 (2017).

99. Li, Weijie, et al. "An electromechanical impedance-instrumented corrosion-measuring probe." Journal of Intelligent Material Systems and Structures 30.14 (2019): 2135-2146.

100. Zuo, Chunyuan, et al. "Crack detection in pipelines using multiple electromechanical impedance sensors." Smart Materials and Structures 26.10 (2017): 104004.

101. Reddypogu, Sandeep Sagar, and Mallika Alapati. "Numerical investigation on EMI signatures in pipes with varied damage levels." Materials Today: Proceedings 45 (2021): 3452-3457.

102. Khante, S. N., and Nidhi Jain. "Erosion identification and assessment of a steel pipeline using EMI technique." Green Buildings and Sustainable Engineering. Springer, Singapore, 2019. 347-355.

103. Raju, Jayalakshmi, Suresh Bhalla, and Talakokula Visalakshi. "Pipeline corrosion assessment using piezo-sensors in reusable non-bonded configuration." NDT & E International 111 (2020): 102220.

104. https://blog.belzona.com/why-you-should-be-concerned-about-pitting-corrosion-and-the-proven-solutions-to-combat-it/ (Accessed, September 17, 2023).

104. https://hocktools.wordpress.com/2011/10/24/rust-part-1/ (Accessed, 17th September 2023).

105. https://fishertank.com/2015/06/19/tools-for-storage-tank-pros-think-tank-round-up/ (Accessed, September 18, 2023).

106. https://www.stinstruments.com/applications/coatings/corrosion-of-reinforced-concrete/ (Accessed, September 18, 2023).

107. https://www.researchgate.net/figure/Damage-of-varying-intensity-a-damage-of-concrete-and-steel-corrosion-of-rebars-and_fig5_338373093 (Accessed, September 18, 2023).

108. https://www.researchgate.net/figure/Pitting-corrosion-on-carbon-steel-39-Note-that-this-is-not-piping-from-the-SRS-waste_fig6_268370729 (Accessed, September 19, 2023)

109. https://www.ampp.org/technical-research/impact/corrosion-basics/group-1/crevice-corrosion (Accessed, September 19, 2023)

110. https://www.h2xengineering.com/blogs/erosion-corrosion/ (Accessed, September 19, 2023)

111. https://www.ampp.org/technical-research/impact/corrosion-basics/group-1/galvanic-corrosion (Accessed, September 19, 2023)

112. https://blog.eplane.com/aircraft-corrosion-filiform-pitting-other-corrosion-types/ (Accessed, September 20, 2023)

113. https://www.azom.com/article.aspx?ArticleID=102 (Accessed, September 20, 2023)

114. https://www.metalsupermarkets.com/grade-guide-4140-steel , (Accessed, September 20, 2023)

115. https://www.xometry.com/resources/materials/4140-alloy-steel/ (Accessed, September 20, 2023)

116 Hsissou, R. (2021). Review on epoxy polymers and its composites as a potential anticorrosive coatings for carbon steel in 3.5% NaCl solution: Computational approaches. *Journal of Molecular Liquids*, *336*, 116307.

117. https://www.findthisbest.com/best-electrical-wire/26-awg (Accessed, September 20, 2023)

118. https://www.keyence.com/landing/lpc/3d-scanner-vr.jsp (Accessed, September 20, 2023)

119. https://wiki.analog.com/resources/eval/user-guides/eval-ad5940/tools (Accessed, September 20, 2023)

120. Alamri, A. H. (2020). Localized corrosion and mitigation approach of steel materials used in oil and gas pipelines–An overview. *Engineering failure analysis*, *116*, 104735.

121. https://cortec-me.com/protection-of-cased-pipeline-crossings/ (Accessed, September 20, 2023)

122. Popoola, L. T., Grema, A. S., Latinwo, G. K., Gutti, B., & Balogun, A. S. (2013). Corrosion problems during oil and gas production and its mitigation. *International Journal of Industrial Chemistry*, *4*, 1-15.

123.https://www.pipelineprotection.co.uk/services/cathodic-protection/ (Accessed, September 18,2023)

124.https://www.utelectrode.com/article/what-is-an-impressed-current-cathodic-protection-system-.html (Accessed, September 18,2023)

125..https://geoscopelocating.com.au/how-ground-penetrating-radar-works-to-find-underground-utilities/ (Accessed, September 18,2023)

126.https://medium.com/@sareen.aarya6/acoustic-emission-testing-compared-with-other-ndt-methods-989d56799230 (Accessed, September 18,2023)

127.https://www.linshangtech.com/tech/how-to-use-an-ultrasonic-thickness-gauge-tech1472.html (Accessed, September 18,2023)

128. https://www.cosasco.com/product/atmospheric-er-corrosion-sensor-610 (Accessed, September 18,2023)

129. Wilkinson, M. B., & Outram, M. (2009). Principles of pressure transducers, resonance, damping and frequency response. *Anaesthesia & Intensive Care Medicine*, *10*(2), 102-105.

130. Grbic, A., & Eleftheriades, G. V. (2005). Practical limitations of subwavelength resolution using negative-refractive-index transmission-line lenses. *IEEE transactions on antennas and propagation*, *53*(10), 3201-3209.

131. Chawla, S. K., Anguish, T., & Payer, J. H. (1990). Microsensors for corrosion control. Materials Performance;(USA), 29(5).

132. J. Van der Spiegel, 1. Leuks, S. Yoder, C. More, J. Mckeon, "Integrated Electrochemical Sensors," Proc. Symp. Sensor Science and Technology, eds. B. Schumm, C.C. Liu, R.A. Powers, E.B. Yeager, vol. 87-15 (The Electrochem. Soc., 1987), p. 31.